

**CENTRO DE INVESTIGACIÓN CIENTÍFICA Y DE EDUCACIÓN
SUPERIOR DE ENSENADA, BAJA CALIFORNIA**



**SCIENCE POSTGRADUATE PROGRAM IN
ELECTRONICS AND TELECOMMUNICATIONS**

**Inter-Cell Interference Management via Coordinated Multi-Point
Transmission-Reception (CoMP) associated with the LTE-Advanced Systems**

Dissertation

submitted in partial fulfillment of the requirements for the degree of

Doctor in Sciences

Presented by:

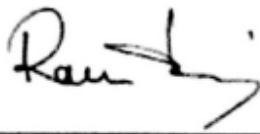
Leonardo Fabio Yepes Arbeláez

Ensenada, Baja California, México,

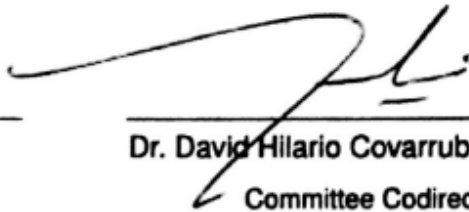
2014

Thesis defended by
Leonardo Fabio Yepes Arbeláez

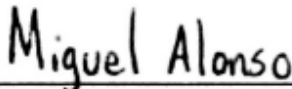
and approved by the following committee



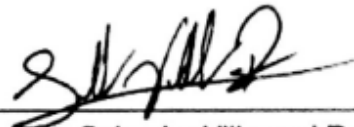
Dr. Ramon Antonio Ferrús Ferré
Committee Codirector



Dr. David Hilario Covarrubias Rosales
Committee Codirector



Dr. Miguel Angel Alonso Arévalo
Committee Member



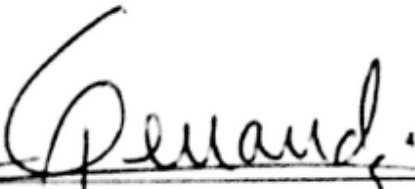
Dr. Salvador Villarreal Reyes
Committee Member



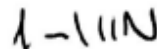
Dr. Vitaly Kober
Committee Member



Dr. Enrique Stevens Navarro
Committee Member



Dr. César Cruz Hernández
Postgraduate Coordinator
in Electronics and Telecommunications



Dr. Jesús Favela Vara
Director of
Graduate Studies

December, 2014

Resumen de la tesis que presenta **Leonardo Fabio Yepes Arbeláez** como requisito parcial para la obtención del grado de Doctor en Ciencias en Electrónica y Telecomunicaciones con orientación en Telecomunicaciones.

Gestión de Interferencia Inter-Celular con Esquemas de Múltiples-Puntos de Transmisión-Recepción Coordinados (CoMP) en Sistemas LTE-Advanced

Resumen elaborado por:

Leonardo Fabio Yepes Arbeláez

Las redes de comunicaciones móviles celulares han manifestado un crecimiento sorprendente tanto en el número de usuarios, como en la prestación de servicios, esto debido en esencia a la inserción social de esta tecnología. En la última década, este crecimiento ha llevado a un incremento del consumo de energía en un 20% por año. Por lo tanto, es necesario proponer nuevas estrategias que logren reducir la huella de carbono, hasta en un 50% en los siguientes 10 años.

Con el fin de atender esta problemática global, en este trabajo se proponen y analizan soluciones amigables con el medio ambiente (environment-friendly), las cuales están vinculadas con las técnicas de gestión de la interferencia inter-celular empleando la tecnología de múltiples puntos de transmisión-recepción coordinados (CoMP), empleando sistemas de antenas avanzados que buscan conseguir una mejor utilización de los recursos radio, y por consiguiente, mejorar el consumo energético de estos sistemas.

En esta tesis, las técnicas analizadas se encuentran distribuidas en dos partes. En la primera parte, se aborda la síntesis de los agrupamientos de antenas, presentes en las estaciones base de la red celular. La síntesis tiene como objetivo reducir no solo el consumo energético sino también el costo y el tamaño del sistema de radiación. En la segunda parte, la métrica de eficiencia energética fue incorporada con el fin de valorar el consumo energético en toda la red celular optimizada empleando la tecnología CoMP basada en la coordinación de las fuentes radiantes o beamforming. Esto permite un aumento significativo de la eficiencia energética, superiores a la unidad en [bit/Hz/Joule]. Además el incremento depende del número de antenas por estación base y la relación señal-a-ruido del sistema. De este modo, en este trabajo se ha contribuido al estado del arte de los sistemas móviles celulares con nuevas metodologías de síntesis y gestión de recursos de radiación desde un punto de vista de redes verdes.

Palabras Clave: **Coordinación de Estaciones Base, Escasez en Agrupamientos de Antenas, Interferencia Inter-celular, Algoritmos de Eficiencia Energética.**

Abstract of the thesis presented by **Leonardo Fabio Yepes Arbeláez** as a partial fulfillment of the requirements of the degree of Doctor in Sciences in Electronics and Telecommunications with orientation in Telecommunications.

Inter-Cell Interference Management via Coordinated Multi-Point Transmission-Reception (CoMP) associated with the LTE-Advanced Systems

Abstract elaborated by:

Leonardo Fabio Yepes Arbeláez

The mobile wireless communication networks have manifested a significant growth in terms of the number of users as well as offered services, given that this technology has a high insertion into the society. In the last decade, this growth has carried out an energy consumption increasing, up to 20% per year. Therefore, it is necessary to propose new network strategies capable of reducing the carbon footprint, down to 50% in the next 10 years.

Aiming to resolve this global problematic, in this work I conducted an environment-friendly solution, which is linked to the inter-cellular interference management using the coordinated multi-point (CoMP) transmission schemes, which involve the use of advanced antenna systems that seek to achieve a better radio resource management, and consequently, improve the energy consumption of these systems.

In this thesis, the techniques analyzed are distributed in two parts. In the first part, I initially addressed the antenna array synthesis, which is present in the base stations that conform the cellular network. The synthesis aims to reduce not only the energy consumption but also the cost and physical size of the radiation system. In the second part, the energy efficiency metric was incorporated in order to assess the energy consumption on the entire cellular network optimized with the CoMP technology based on the coordinated beamforming scheme. It leads a considerable increase of the energy efficiency, greater than the unit in [bit/Hz/Joule]. Moreover, the increase depends on the antenna elements per base stations and the signal-to-noise ratio of the entire system. In this way, in this research I contributed to the state-of-the-art with new methodologies to synthesize and to manage the radiation resources applied to the mobile wireless communication networks from a green network point of view.

Keywords: Base Station Coordination, Sparseness on Antenna Arrays, Inter-Cell Interference, Energy Efficiency Algorithms.

*To my beloved parents,
José Leonardo and Ana Cecilia*

My dreams are come true with their greatness and support,

I will always be grateful...

To my adorable son, Nicolás

Now, we have started the pathway where our lives converge,

i love you my little boy...

Acknowledgements

First and foremost, i would like to express my endless gratitude to my advisors, Dr. David Covarrubias and Dr. Ramon Ferrús. Their advice and guidance was essential in the good development of my doctoral and personal education. To them, my respect and admiration.

I would personally like to thank to the members of my thesis committee, Dr. Enrique Stevens Navarro, Dr. Salvador Villarreal Reyes, Dr. Vitaly Kober and Dr. Miguel Angel Alonso Arévalo. Their continuous feedback and constructive criticism were fundamental to find the properly direction to this final research product. A special thanks to Dr. Miguel A. Alonso and their family, whom i consider a mentor. To him, my resounding respect.

Special thanks to all the buddies and partners that I made during these four years spent in the realization of this work, Dr. Guillermo “Memo” Galaviz, Dr. Armando Arce, Dr. Angel Andrade, Dr. Jose G. Arceo, Dr. Alejandro Galaviz, Dr. Ruben Garcia, Dr. Roberto Conte, Dr. Horacio Soto, Ramon Muraoka, Leopoldo “Polillo” Garza, Carlos Martinez, Adrian Hernández, Fabian Mendoza, Eduardo Velázquez Wong and family, Dr. Ramon Agustí, Dr. Jordi Perez Romero, Dr. Anna Umbert,

Alessandro Raschella, Katerina Koutlia and so many others to list.

To my whole family, especially to my brothers, Alvaro Yepes and Yaneth Torres, to my aunts, Angela Rosa Arbeláez and Ana Pastorita Arbeláez, and to my goddaughter, Ana Maria Torres. To them, thanks and I hope to see them back soon, I love them.

I would like to manifest a specially feeling of gratitude to the Mexican people and Government, specially, this work was possible thanks to the support of the Mexican Council for Science and Technology (CONACyT) under scholarship number 256336. I would also like to thank the Research and Higher Education Center of Ensenada (CICESE), the Department of Electronics and Telecommunications, the Universitat Politècnica de Catalunya (UPC) and their Department of Signal Theory and Communications for the support they provided during the development of this research.

Content

	Page
Resumen en español	i
Abstract	ii
Dedicatory	iii
Acknowledgements	iv
List of Figures	ix
List of Tables	xii
List of Acronyms	xiii
1. Introduction	1
1.1 Motivation and Scope of Work	1
1.2 Problem Statement	3
1.2.1 Coordinated Multi-Point Transmission (CoMP) technology platform	4
1.2.2 CoMP based on Coordinated Beamforming scheme	6
1.2.3 Synthesis of Antenna Arrays with sparseness characteristics	7
1.3 Aim of Thesis	9
1.4 Thesis Outline	9
1.5 Main Outcomes and contributions of this thesis	11
I Antenna Array Design	13
2. Synthesis of sparse linear antenna arrays	14
2.1 Synthesis of sparse antenna arrays using the Matrix Pencil Method (MPM)	15

	Page
2.1.1	16
2.1.2	19
2.1.3	23
2.2	27
2.3	34
2.3.1	36
2.3.2	40
2.4	45
3. Hybrid sparse antenna array synthesis	47
3.1	48
3.2	52
3.2.1	53
3.2.2	57
3.2.3	58
3.2.4	60
3.3	61
3.3.1	61
3.3.2	64
3.3.3	65
3.4	66
3.4.1	67
3.4.2	69
3.5	71
II Interference Management	73
4. Coordinated multi-point (CoMP) transmission-reception via coordinated beamforming (CB)	74
4.1	75
4.1.1	75
4.2	77

	Page
4.2.1	Downlink system model 79
4.2.2	Imperfect radio channel estimation 83
4.2.3	Performance assessment under multi-cell environment with imperfect CSI 86
4.3	CoMP using downlink coordinated beamforming (CB) 88
4.3.1	Coordinated beamforming description and system model . . 90
4.3.2	Numerical assessment 94
4.4	Conclusions 97
5.	Energy efficiency optimization applied to CoMP-CB 99
5.1	Coordinated Beamforming formulation under the energy efficiency criterion 100
5.1.1	System model for CoMP-CB with energy efficiency criterion 100
5.1.2	Multi-cell multi-user precoding optimization 103
5.1.3	Energy Efficient Maximization Algorithm 108
5.1.4	Algorithm Analysis - Computational complexity analysis . . . 111
5.1.5	Numerical analysis and assessment 113
5.2	Conclusions 117
6.	Conclusions and future work 118
6.1	Summary of main contributions and conclusions 118
6.1.1	Antenna array design 118
6.1.2	Interference management 120
6.2	Future research work and recommendations 121
	List of References 123
A.	First appendix 129
A.1	Sequential solver for the Maximization of $\mathcal{L}(\mathbf{a}, \sigma^2)$ 129
B.	Second Appendix 131
B.1	Proof of Theorem 1, introduced in section 5.1.3 for the energy effi- ciency maximization algorithm. 131

List of Figures

Figure		Page
1	LTE evolution in order to incorporate new technology areas, Astely <i>et al.</i> (2013).	3
2	Technological components associated with 3GPP LTE-Advanced, in order to exploit the system capacity defined by the boundaries of the Shannon criteria.	4
3	Layout structure and organization of this thesis.	10
4	Singular value spectrum of the broadside Chebyshev pattern.	21
5	Reconstruction of the desired pattern by nonuniform arrays with 12 and 13 elements.	22
6	Desired shaped-beam pattern with 16 elements and the patterns reconstructed by the MPM- and FB-MPM-based methods, both with 13 elements.	25
7	Distributions of the poles associated with the MPM and FB-MPM synthesis methodologies.	25
8	Radiation patterns of the reference and a set representative BCS arrays. . . .	33
9	Geometric representation of the independent compression regions for the formulation of two-dimensional array factor synthesis.	37
10	Singular value spectrum of the original 10 elements broadside Chebyshev pattern.	41
11	Beam pattern with 46 elements using the proposed ICR method. The PSLL = -17.9 dB and the MLW = 0.236.	42

List of Figures (continuation)

Figure		Page
12	Singular value spectrum of the original 20 elements broadside Chebyshev pattern.	43
13	Beam pattern with 78 elements using the proposed ICR method. The PSLL= -19.6 dB and the MLW = 0.067 along the u -axis, MLW = 0.138 along the v -axis.	43
14	Singular value spectrum of the original 10 elements shaped-beam pattern.	44
15	Beam pattern with 46 elements using the proposed ICR method for shaped-beam pattern synthesis. The PSLL= -26.3 dB and the MLW = 0.856.	45
16	Narrow-beam pattern with 24 antenna elements for each of the evaluated techniques.	62
17	Graphical representation of the normalized amplitude current and excitation phase versus element locations for the narrow-beam pattern with 24 antenna elements, synthesized by means of (a) FB-MPM, (b) BCS, (c) Caratelli's Approach and (d) Proposed Approach.	63
18	Flat-Top beam pattern synthesized with 22 antenna elements for each of the evaluated techniques.	64
19	Square-Cosecant beam pattern synthesized with 29 antenna elements for each of the evaluated techniques.	65
20	Beam pattern with 46 elements using the ICR method based on HSLAS. The PSLL= -17.5 dB and the MLW = 0.234.	68
21	Shaped-beam pattern synthesized with 24 antenna elements for each of the evaluated techniques.	69
22	Graphical representation of the excitation phase versus element locations for the shaped-beam pattern with 24 antenna elements, synthesized by means of FB-MPM and HSLAS.	70
23	Beam pattern with 224 elements using the ICR method for shaped-beam pattern synthesis. The PSLL= -20 dB and the MLW = 0.856.	70
24	Mobile cellular system considered and the definition of CoMP cluster, Marsch and Fettweis (2011).	76
25	Concept of intra-cell beamforming, Marsch and Fettweis (2011).	77

List of Figures (continuation)

Figure		Page
26	Non-cooperative transmission and PMI/CQI feedback concept considered, Marsch and Fettweis (2011).	80
27	SINR estimation error reported by Thiele <i>et al.</i> (2009).	87
28	CDF of system sum capacity reported by Qiang <i>et al.</i> (2010).	95
29	Cumulative distribution function of capacity in one cell reported by Qiang <i>et al.</i> (2010).	96
30	Simulation platform to assessment a coordinated base station scheme, with $K = 3$.	114
31	Energy efficiency performance of Algorithm 1, for $M_j = 4, N_{j,k} = 2, d_{j,k} = 1, \forall j, k$.	115
32	Sum rate performance of Algorithm 1, for $M_j = 4, N_{j,k} = 2, d_{j,k} = 1, \forall j, k$.	115
33	Energy efficiency performance of Algorithm 1, for $N_{j,k} = 2, d_{j,k} = 1, \forall j, k$.	116

List of Tables

Table		Page
1	Locations and amplitudes of the reconstructed nonuniformly spaced array and the uniformly spaced Chebyshev array	22
2	Element locations and amplitudes reconstructed by the FB-MPM synthesis method in Fig. 6.	26
3	Comparison between planar array specifications reported by Yang <i>et al.</i> (2011) Vs. ICR Method based on MPM.	41
4	Comparison between planar array specifications reported by Yepes <i>et al.</i> (2013) Vs. ICR Method based on HSLAS.	68
5	Simulation assumptions to analyze a multi-cell environment with imperfect CSI.	87
6	Simulation assumptions to analyze a CoMP-CB based on the SLNR metric. . .	95

List of Acronyms

3D-MIMO 3D Multiple-Input-Multiple-Output

3GPP 3rd Generation Partnership Project

AAF Auxiliary Array Factor

AP Access Point

AWGN Additive White Gaussian Noise

BCS Bayesian Compressive Sampling

BLER Block Error Rate

BS Base Station

CB Coordinated Beamforming

CDF Cumulative Distribution Function

CoMP Coordinated Multi-Point Transmission-Reception

CQI Channel Quality Indicator

CSI Channel State Information

CSIR Channel State Indicator at the Receiver

CTR Current Taper Ratio

DFT Discrete Fourier-Transform

EE Energy Efficiency

FB-MPM Forward-Backward Matrix Pencil Method

HARQ Hybrid Automatic Repeat Request

HSLAS Hybrid Sparse Linear Array Synthesis

ICI Inter-Cell Interference

ICIN Inter-Cell Interference Nulling

ICR Independent Compression Regions

ICT Information and Communication Technologies

IID Independently and Identically Distributed

IRC Interference Rejection Combining

ITU International Telecommunication Union

ISI Inter-symbol interference

JP Joint Processing

KKT Karush-Kuhn-Tucker

LSE Least Square Error

LTE Long Term Evolution

MAC Multiple Access Channel

MLW Main-Lobe Width

MMSE Minimum Mean Square Error

MPM Matrix Pencil Method

MRC Maximal Ratio Combining

MU-MIMO Multi-User MIMO

OFDMA Orthogonal Frequency Division Multiple Access

PAPC Per-Antenna Power Constraint

POM Phase Optimization Method

PMI Precoding Matrix Indicator

PSLL Peak Side-Lobe Level

QoS Quality of Service

RI Rank Indicator

RVM Relevance Vector Machine

SINR Signal-to-Interference-plus-Noise Ratio

SLL Side-Lobe Level

SLNR Signal-to-leakage-plus-Noise Ratio

SNR Signal-to-Noise Ratio

SVD Singular Value Decomposition

TDD Time Division Duplex

UE User Equipment

ZF Zero-Forcing

Introduction

This chapter gives an introduction of the research background. First, are presented the driving factors that motivated the research conducted in this thesis. In the next sections, the problem statement is briefly outlined in order to introduce the aim of thesis. Finally, the thesis outline and the main outcomes are shown.

1.1 Motivation and Scope of Work

Mobile communication networks present a really tremendous growth, this is due to the social insertion of this technology. The International Telecommunication Union (ITU) has reported that at the end of 2013 the number of subscribers associated with mobile cellular networks around the world was of 4,100 millions, practically this amount equals to the number of inhabitants of the planet earth, in ITU (2014). The ITU has estimated that at the end of 2018 the number of subscribers will increase up to 4,900 millions. However, this growth in number of subscribers and also of mobile data traffic implies, at least, an energy consumption increase of 20% per year. Due to this high energy consumption, it is adequate to pose new strategies to significantly

reduce the carbon footprint down to 50% in the next 10 years.

In the last decade the attention for environment-friendly solutions has drastically increased. Especially due to the debate concerning climate change, nowadays every emerging technology is scrutinously evaluated on its carbon footprint. This is also the case for information and communication technologies (ICT). It is estimated that ICT is accountable for 2 – 4% of the worldwide carbon emissions and a significant part of these emissions, about one sixth, is attributed to telecommunication networks, Vereecken *et al.* (2011).

Different research efforts are being aimed toward optimization strategies that allow to reduce the power consumption of telecommunication equipment. Particularly, mobile communication networks under the standard Long Term Evolution (LTE), that was defined by 3rd Generation Partnership Project (3GPP), have incorporated the concept of network Energy Efficiency (EE) and the use of Multi-Antenna technologies, such as Coordinated Multi-Point transmission (CoMP) and 3D Multiple-Input-Multiple-Output (3D-MIMO),¹ on the Releases 12 and 13, as an environment-friendly evolution, as shown in Fig. 1, in order to reduce the carbon footprint.

Motivated by the possibility to develop a strategy that allows to reduce this carbon footprint associated with the LTE-Advanced standard, this thesis is focused in two main aspects:

1. The antenna array synthesis with sparseness² characteristics.
2. Employment of coordinated multi-point transmission technology as an interfer-

¹3D-MIMO is defined as the incorporation of the vertical or elevation angle in the antenna beam-forming techniques.

²Sparseness on antenna arrays is related to the procedure to reduce the number of antenna array elements but preserving the original radiation pattern.

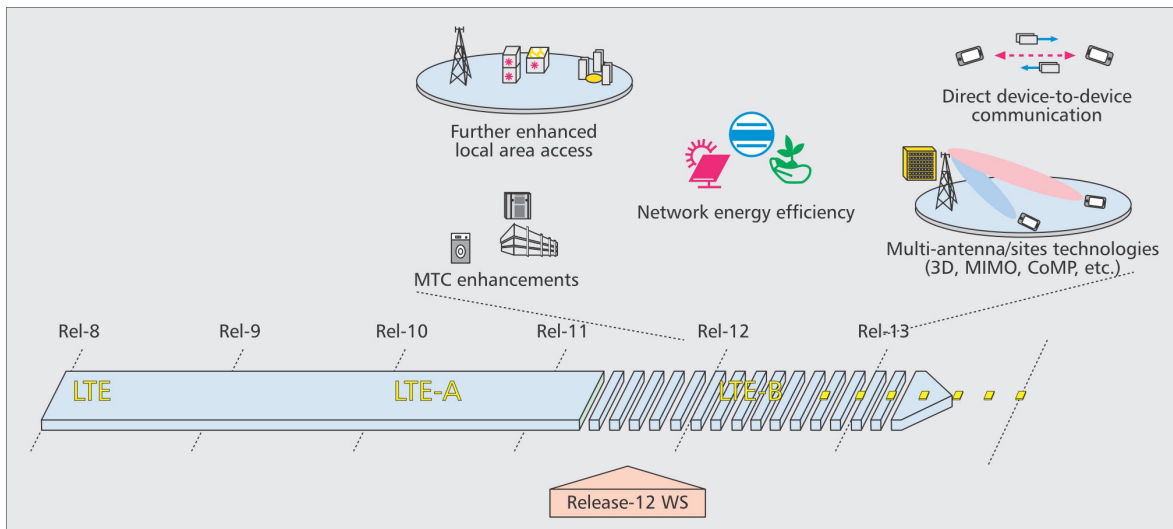


Figure 1. LTE evolution in order to incorporate new technology areas, Astely et al. (2013).

ence management scheme with energy efficiency characteristics.

The first aspect is aimed to reduce the number of antenna array elements from a previously synthesized antenna array, with a desired radiation pattern, and therefore reduce size, cost and energy consumption. The second aspect is focused in CoMP technology as a mechanism for the inter-cellular interference management, which is able to increase the users cell-edge throughput, but incorporating an energy efficiency measure for each cell. Accordingly, both aspects work jointly in order to increase the energy efficiency of the entire mobile cellular system.

1.2 Problem Statement

The deployment of next generation mobile broadband systems, based on the 3GPP LTE radio access technology, should be able to incorporate new mechanisms in order to optimize the energy efficiency of the entire system architecture. For this reason, the major step in this evolution of LTE, also referred to as “Release 12 and Beyond”

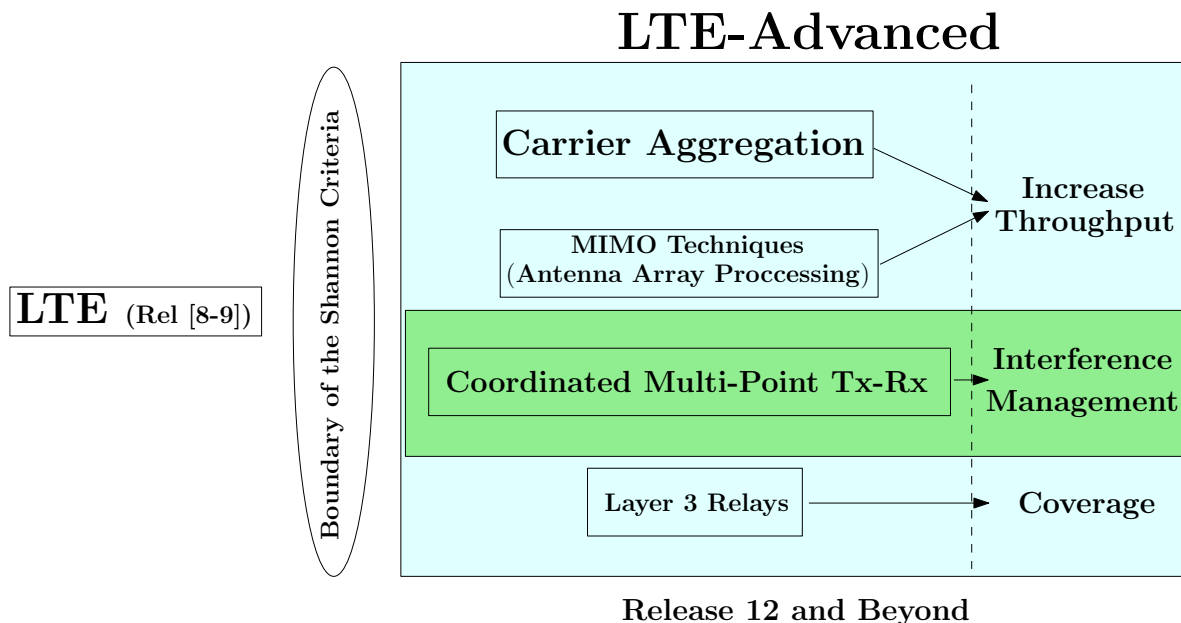


Figure 2. Technological components associated with 3GPP LTE-Advanced, in order to exploit the system capacity defined by the boundaries of the Shannon criteria.

(LTE-B), is carried out with the resource management politics from a environment-friendly perspective.

With this goal in mind, it was necessary to define which of the four technological components on 3GPP LTE, shown in Fig. 2, is able to fulfill this requirement. From the experiences associated in CICESE Wireless Communication Group, derivative of several doctoral thesis on this research area, it was determined that the most adequate technological component to be incorporated as an energy efficiency measure was the Coordinated Multi-Point (CoMP) Transmission scheme.

1.2.1 Coordinated Multi-Point Transmission (CoMP) technology platform

Given that other technological platforms require of the deployment of new equipment, it is known from theory, Marsch and Fettweis (2011), that interference can be over-

come and even exploited if coordination or cooperation between cells is introduced. For this reason, CoMP schemes has been as a key technology of LTE-Advanced due to its requirements of a fairly small change of mobile network infrastructure, and may lead to more homogeneous quality of service (QoS) distribution over the area, particularly important on cell-edge environments, Marsch and Fettweis (2011).

The term CoMP may refer to multitude of schemes. All of them have in common that intra- or inter-cell interference is somehow taken into account or even exploited to enhance data rates and/or fairness. The CoMP schemes can be classified according to the extent of cooperation (or information exchange) taking place between cells, as follows:

- **Joint signal processing:** In this scheme, user data or (partially) processed transmit or receive signals are exchanged among base stations. One here considers non-coherent and coherent schemes, where the latter aim at aligning the phases of signals transmitted from or received at different antennas. As might expect, this requires precise synchronization between all involved entities.
- **Interference coordination or Coordinated Beamforming:** In order to relax the compromise among cooperation, data exchange and synchronization, this scheme uses a limited data exchange between cells for the purpose of multi-cell cooperative scheduling, multi-cell interference-aware link adaptation or multi-cell interference-aware precoding or beamforming.

In order to compare the CoMP benefits, is appropriate to define a Non-cooperative or interference aware transceiver schemes, in which the base stations or terminals adjust their transmit or receive strategy according to some knowledge on interference.

This does not require explicit information exchange between cells, but the estimation of interference must be enabled through appropriate reference signal design. This class of schemes includes single-cell multi-user signal processing.

Given that the Coordinated Beamforming schemes, represents a suitable mechanism to achieve an interference management based on the energy efficiency measure, a brief description of this CoMP scheme is displayed follows.

1.2.2 CoMP based on Coordinated Beamforming scheme

From the downlink interference coordination perspective, the base stations exchange channel state information (CSI) in order to adjust their transmission strategies, so that the generated extent of inter-cell interference is reduced. The coordinated beamforming (CB) offers a fair balance between ensuring a reasonable load on the backhaul links and attaining the performance gains using cooperation. The shared CSI is used by the base stations to design individual precoding matrices (or beamforming vectors for single-stream transmission) to transmit exclusively to users within their own cell.

There are several CB's approaches in the literature. For example, Qiang *et al.* (2010) propose a CB scheme in downlink CoMP which exploits the signal leakage information to other cells to design the precoding vector, but does not necessarily maximize sum-rates³. On the other hand Zhang *et al.* (2011) propose an iterative distributed solution to design precoding matrices for multi-cell systems, which will maximize the

³The sum-rate, system throughput or aggregate throughput, is the sum of the data rates that are delivered to all terminals in a network.

sum-rate at high signal-to-noise ratio (SNR), using a discrete power control. An interesting CB approach is suggested by Kim *et al.* (2013), where it is proposed a low-complexity minimum mean square error (MMSE) transmit filter design under a practical per-antenna power constraint (PAPC). The PAPC opens the possibility to define a new constraint directed towards the energy efficiency measure, which is posteriorly proposed by He *et al.* (2014) considering a new criterion of weighted sum energy efficiency and satisfies heterogeneous requirements from different kinds of cells. Another parallel proposal, regarding to energy efficiency measure, is developed by Li *et al.* (2014), where the energy efficiency is maximized for multi-cell multi-antenna downlink network with coordination and meanwhile ensures the minimal data rate requirement of each user. Given that the above cooperative transmission strategies are highly dependent on the quality of the CSI fed back by the users, most of the literature on multi-cell cooperation assumes that full CSI is available at the transmitters.

1.2.3 Synthesis of Antenna Arrays with sparseness characteristics

On the other hand, an important aspect, before continuing with the CoMP energy efficiency strategy, is related to the synthesis of antenna arrays that allow the reliability of the entire wireless system with minimum power consumption. In this way, new phased antenna arrays synthesis methods are required to achieve arrays with sparseness characteristics with the purpose of reducing the total number of antenna array elements. In the context of sparse antenna arrays design, there are effective proposals such as the Matrix Pencil Method (MPM) developed by Liu *et al.* (2008) and then improved with the Forward-Backward MPM, also proposed by Liu *et al.* (2010), where a non-iterative procedure is used to synthesize a nonuniform linear

array with a reduced number of elements. Another recent approach is the Bayesian Compressive Sampling (BCS) method proposed by Oliveri and Massa (2011), where the design of maximally-sparse linear arrays is introduced by employing a probabilistic formulation of the array synthesis. However, such formulation deals with symmetric purely-real arrangements, and its extension to complex synthesis, is not efficient because of the real-valued nature of the solver itself Oliveri and Massa (2011). In order to overcome this limitation, Oliveri *et al.* (2012) proposed an enhancement to the BCS approach capable of synthesizing linear arrays with complex reference pattern. Another approach has been introduced as a deterministic synthesis technique, developed by Caratelli and Viganó (2011), where a non-uniform array design method is developed based on the concept of the auxiliary array factor (AAF) function, providing an optimal array element density and excitation tapering distributions useful to mimic a desired radiation pattern.

In this thesis seeking to contribute to the state-of-the-art, an antenna array synthesis method with sparseness characteristics is first formulated using the concept of independent compression regions (ICR). In order to use the non-iterative matrix pencil method (MPM) and the iterative Bayesian compressive sampling (BCS) method, both of these techniques have been previously used for the compression of linear arrays, but now will be applied them in the context of two-dimensional arrays. Besides, as an advance to the previous process, a new hybrid technique is introduced, which is based on the combination of two methods. The first method is a deterministic synthesis algorithm is used to resolve the non-uniform amplitude excitations and the antenna element locations. The second method is an iterative optimization scheme that computes the phase of the excitation currents. This approach is proven valid to

properly match diverse beam patterns with sparse linear arrays. On the other hand, a CoMP based on coordinated beamforming is presented, which is defined as the weighted sum of the energy efficiencies of multiple cells. Given that the energy efficiency optimization problem is non-convex, it is transformed into a parameterized polynomial form optimization problem, by which a solution in closed form is achieved through a two-layer optimization.

1.3 Aim of Thesis

Energy efficiency optimization of wireless systems has become urgently important due to its impact on the global carbon footprint. For this reason, this thesis is aimed at designing and assessing the inter-cell interference management, via coordinated multi-point transmission using a coordinated beamforming, as mechanism to optimize energy efficiency over LTE-Advanced systems. Besides, using sparseness properties over the antenna array synthesis, we will develop a new methodology to reduce the power consumption on the radiation system employed by the beamforming.

1.4 Thesis Outline

The main sections of this thesis, which span Chapters 2 to 5, comprise a description of the relevant aspects of synthesis of antenna arrays, pointed to reduce power consumption, and the mechanisms to optimize the energy efficiency, over a multi-cellular multi-user LTE-Advanced wireless communication system, using coordinated multi-point transmission technology under a coordinated beamforming scheme.

A short summary of each of the core sections of this thesis, as well as its relation to

the publications listed in Section 1.5, can be found in the subsections below.

A schematic diagram that represents the complete thesis structure is shown in Fig. 3.

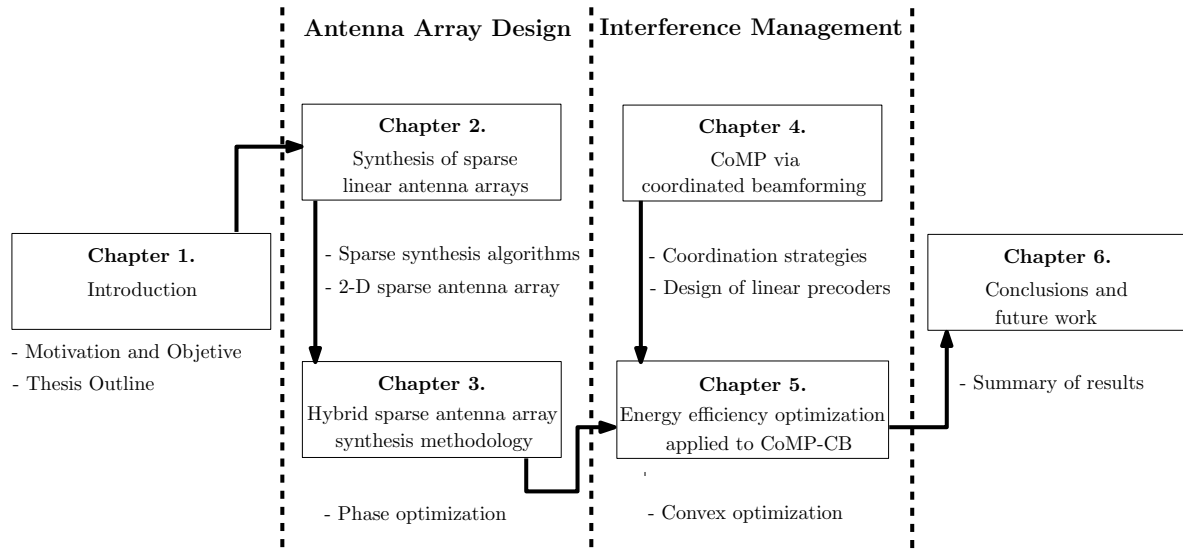


Figure 3. Layout structure and organization of this thesis.

Chapter 2: Synthesis of sparse linear antenna arrays

This chapter describes the non-iterative matrix pencil method (MPM) and the iterative Bayesian compressive sampling method, which are the most significant methodologies inside of the sparse antenna array synthesis procedures. Besides, a new procedure to synthesize two-dimensional antenna arrays is introduced as a contribution to the state-of-the-art.

Chapter 3: Hybrid sparse antenna array synthesis methodology

From the study of methodologies associated with the synthesis of sparse antenna arrays, this chapter introduces a new hybrid sparse antenna array synthesis methodology, intended to resolve the drawbacks regards to current phases and locations of

antenna elements. Also as a contribution to the state-of-the-art.

Chapter 4: Coordinated multi-point transmission using coordinated beamforming (CoMP-CB)

This chapter introduces the coordinated multi-point transmission technology as a countermeasure against inter-cellular interference involved on the entire LTE-Advanced mobile system. Specifically, the chapter describes the state-of-the-art in relation to the coordinated beamforming scheme and the techniques to design linear precoders or beamformers to increase the network data rate.

Chapter 5: Energy Efficiency Optimization applied to CoMP-CB

This chapter is focused on the design of precoders that optimize the energy efficiency measure of multiple cells, when they operate with a coordinated scheme based on coordinated beamforming. To achieve this criterion, is proposed to use the block coordinated monotonic method jointly with the parallel projection method into convex sets, in order to increase the convergence of the algorithm.

Chapter 6: Conclusions and Future Work

The final chapter, outlines the most relevant contributions regards to the current research and propose some potential follow-up research activities.

1.5 Main Outcomes and contributions of this thesis

Derivative of this research work, the main outcomes were published in the following journals and conference:

- Arce, A., Yepes, L. F., Covarrubias, D. H., and Panduro, M. A. (2012). A new approach in the simplification of a multiple-beam forming network based on corps using compressive arrays. *International Journal of Antennas and Propagation*, 2012: p. 8
- Yepes, L. F., Covarrubias, D. H., Alonso, M. A., and Arceo, J. G. (2013). Synthesis of two-dimensional antenna array using independent compression regions. *IEEE Transactions on Antennas and Propagation*, 61(1): p. 449–453
- Yepes, L. F., Covarrubias, D. H., Alonso, M. A., and Ferrus, R. (2014b). Hybrid sparse linear array synthesis applied to phased antenna arrays. *IEEE Antennas and Wireless Propagation Letters*, 13: p. 185–188
- Yepes, L. F., Covarrubias, D. H., Alonso, M. A., and Arceo, J. G. (2014a). Corrections to synthesis of two-dimensional antenna array using independent compression regions. *IEEE Transactions on Antennas and Propagation*, 62(8): p. 4436
- Yepes, L. F., Covarrubias, D. H., Alonso, M. A., and Ferrus, R. (2014c). Hybrid sparse two-dimensional antenna array synthesis using independent compression regions. In *2014 Loughborough Antennas and Propagation Conference (LAPC)*, Burleigh Court International Conference Centre, Loughborough University, United Kingdom

PART I

ANTENNA ARRAY DESIGN

Chapter 2

Synthesis of sparse linear antenna arrays

A good deal of attention that has been devoted in the past, and in the recent literature, to the problem of synthesizing arbitrary far-field radiation beam pattern, subject to given far-field constraints, by using the minimal number of antenna array elements. The problem is of particular interest in many applications where the weight and size of antennas are extremely limited, such as complex arrays radar, satellite communications and mobile cellular technology, Prisco and D'Urso (2011). Given the above, this chapter seeks to contribute to the state-of-the-art by introducing two new proposals focused to resolve this problematic, on the one hand, the Matrix Pencil Method (MPM), which belongs to Dolph-Chebyshev and Taylor methods, is considered as a deterministic methodology. On the other hand, Bayesian Compressive Sampling (BCS) is presented as a stochastic procedure. Both procedures belong to the tools and algorithms already proposed in the open literature.

2.1 Synthesis of sparse antenna arrays using the Matrix Pencil Method (MPM)

Matrix pencil methodology focuses on the problem of reducing the total number of elements for linear antenna arrays. The problem can be described as follows, Liu *et al.* (2008). Let a linear array be composed of M identical antenna elements. The array factor is given by

$$F_M(\theta) = \sum_{i=1}^M R_i \exp(jkd_i \cos(\theta)) \quad (1)$$

where R_i is the complex excitation coefficient of the i th element located at $x = d_i$ along the linear array direction x , and $k = (2\pi/\lambda)n$ is the spatial wavenumber. The objective is to synthesize a new linear antenna array, that has the minimum number of elements, while maintaining the same desired pattern as $F_M(\theta)$ with a small tolerance. That is, it is necessary to find a solution to the following problem:

$$\begin{cases} \min Q \\ \text{Const.} \left\{ \min_{\{R'_i, d'_i\}_{i=1, \dots, Q}} \left\| F_M(\theta) - \sum_{i=1}^Q R'_i \exp(jkd'_i \cos(\theta)) \right\|_L \right\} \leq \epsilon \end{cases} \quad (2)$$

where R'_i and d'_i ($i = 1, \dots, Q \leq M$) are the complex excitations and locations for Q antenna elements, and $L = 2$ if the least square error (LSE) is used.

To resolve this problem, the method use two steps. In the first step, the singular value decomposition (SVD) technique is used to obtain the low rank approximation in LSE of the Hankel matrix constructed by the desired pattern samples. The lower-rank matrix data actually corresponds to the approximated pattern that consists of a smaller number of antenna elements. Hence, the first step allows to determine

how many array elements are required, in a given approximation tolerance, for a desired pattern before the distributions of excitation elements are determined. After the required number of elements is determined, the second step is to apply the matrix pencil method (MPM) to rearrange the excitation and location distributions for the new antenna array with the reduced number of elements.

2.1.1 Estimation of the minimum number of antenna elements

The array factor is described by (1). Let $u = \cos(\theta)$ and $w_i = kd_i$, thus (1) can be written as

$$F_M(\cos^{-1}(u)) = \sum_{i=1}^M R_i \exp(jw_i u). \quad (3)$$

Equation (3) is in the form of a sum of exponentials. The problem described in (2) is to use as few exponentials (or antenna elements) as possible to approximate the original pattern function F_M within a desired tolerance. For this reason, it is well known, Liu *et al.* (2008), that the matrix pencil method has been proven to be useful for dealing with this class of problems. The method of determining the minimum value of Q in (2) is described as follows.

First, the objective antenna beam pattern is sampled in uniform steps of u from $u = -1$ to $u = +1$. Let

$$u_n = n\Delta = \frac{n}{N}, n = -N, \dots, 0, \dots, N \quad (4)$$

where the number of samples is $(2N + 1)$. If

$$f_M(n) = F_M(\cos^{-1}(n\Delta)) = \sum_{i=1}^M R_i z_i^n \quad (5)$$

where $z_i = \exp(jw_i\Delta)$. According to the Nyquist sampling theorem, the condition that $\Delta \leq \lambda/(2d_{\max})$ must be satisfied, where $d_{\max} = \max\{d_i\}$. For instance, $\Delta \leq 1/(M-1)$ for the M -element array with a uniform spacing of $\lambda/2$. In other words, $(2M-1)$ sampling points are adequate to describe the pattern of the M -element uniformly spaced array.

Then, a Hankel matrix is constructed from the sampled pattern data to arrive at

$$[\mathbf{Y}] = \begin{bmatrix} y(0) & y(1) & \cdots & y(L) \\ y(1) & y(2) & \cdots & y(L+1) \\ \vdots & \vdots & & \vdots \\ y(2N-L) & y(2N-L+1) & \cdots & y(2N) \end{bmatrix}_{(2N-L+1) \times (L+1)} \quad (6)$$

where $y(n) = f_M(n-N)$. The parameters $\{N, L\}$ are chosen such that $2N-L \geq M$, and $L+1 \geq M$. For instance, it is possible to set $N = L = M$, as the minimum number of samples while maintaining the best performance. Then the singular value decomposition (SVD) of matrix $[\mathbf{Y}]$ is carried out as

$$[\mathbf{Y}] = [\mathbf{U}] [\mathbf{\Sigma}] [\mathbf{V}]^H \quad (7)$$

where $[\mathbf{U}] \in \mathbb{C}^{(2N-L+1) \times (2N-L+1)}$ and $[\mathbf{V}] \in \mathbb{C}^{(L+1) \times (L+1)}$ are unitary matrices. $[\mathbf{\Sigma}] = \text{diag}\{\sigma_1, \sigma_2, \dots, \sigma_M, \dots, \sigma_P; \sigma_1 \geq \sigma_2 \geq \dots \geq \sigma_P\}$ with $\{\sigma_i\}$ being the ordered singular values of $[\mathbf{Y}]$, and $P = \min\{2N-L+1, L+1\}$.

The rank of the Hankel matrix $[\mathbf{Y}]$ and the number of nonzero singular values would

be equal to the number of exponentials. In general, there should be M nonzero singular values for the M -element array antenna. Thus the non-principal values can be discarded to obtain a low rank approximation of $[\mathbf{Y}]$, which corresponds to a new antenna array with fewer elements. A typical method is to set these non-principal singular values equal to zero. That is

$$[\mathbf{Y}_Q] = [\mathbf{U}] [\boldsymbol{\Sigma}_Q] [\mathbf{V}]^H \quad (8)$$

where $[\boldsymbol{\Sigma}_Q] = \text{diag} \{ \sigma_1, \sigma_2, \dots, \sigma_Q, 0, \dots, 0 \}$ and $Q \leq M$. It has been proven that among all the matrices with rank of Q , $[\mathbf{Y}_Q]$ has the minimum approximation error in Frobenius norm, Liu *et al.* (2008), i.e., mathematically

$$\|[\mathbf{Y}] - [\mathbf{Y}_Q]\|_F = \min_{\text{rank}([\mathbf{X}])=Q} \|[\mathbf{Y}] - [\mathbf{X}]\|_F = \sqrt{\sum_{i=Q+1}^M \sigma_i^2}. \quad (9)$$

From (9), the approximation error decreases monotonously as Q , the number of antenna elements, increases. The final error goes to zero when $Q = M$. This means that the radiation pattern of the new array can always achieve a good approximation of the original pattern. In practical synthesis problem, the minimum value of Q is chosen as follows:

$$Q = \min \left\{ q; \left| \frac{\sqrt{\sum_{i=Q+1}^P \sigma_i^2}}{\sqrt{\sum_{i=1}^q \sigma_i^2}} \right| < \epsilon \right\} \quad (10)$$

where ϵ is a small positive number. The choice of ϵ depends on how accurately the reconstructed pattern approximates the original radiation pattern.

2.1.2 Rearrangement of excitations and locations of antenna elements

Once the low rank matrix $[\mathbf{Y}_Q]$ is available, the parameters $\{z'_i\}$ corresponding to the locations of the new Q array elements can be obtained by solving the following generalized eigenvalue problem:

$$([\mathbf{Y}_{Q,f}] - z' [\mathbf{Y}_{Q,l}])\bar{v}' = 0 \quad (11)$$

where $[\mathbf{Y}_{Q,f}] \in \mathbb{C}^{(2N-L+1) \times L}$ is obtained from $[\mathbf{Y}_Q]$ by deleting the first column, and $[\mathbf{Y}_{Q,l}] \in \mathbb{C}^{(2N-L+1) \times L}$ is obtained from $[\mathbf{Y}_Q]$ by deleting the last column. The parameters z'_i would be equal to the nonzero eigenvalues z' . However, a more computationally effective method than using (11) is to find the eigenvalues of the following matrix:

$$\left\{ ([\mathbf{V}_{Q,b}]^H [\mathbf{V}_{Q,b}])^{-1} ([\mathbf{V}_{Q,t}]^H [\mathbf{V}_{Q,b}]) - z' \right\} \quad (12)$$

where $[\mathbf{V}_{Q,t}] \in \mathbb{C}^{L \times Q}$ (resp., $[\mathbf{V}_{Q,b}] \in \mathbb{C}^{L \times Q}$) is obtained by removing the top (resp., bottom) row of $[\mathbf{V}_Q] \in \mathbb{C}^{(L+1) \times Q}$ which contains only Q dominant left-singular vectors of $[\mathbf{V}]$ in (8).

From (12), only the inverse of a $(Q \times Q)$ matrix and the eigenvalues of a $(Q \times Q)$ matrix are required in this method. Thus, (12) is more computationally effective than directly using (11). Once the z'_i 's are obtained, the locations of antenna elements are given by

$$d'_i = \frac{1}{jk\Delta} \ln(z'_i). \quad (13)$$

The source locations d'_i may turn out to be complex if $|z'_i| \neq 1$. Hence, an approximate

method is to take only the real parts as the estimated of d'_i s. Thus the estimated excitations and locations are given as

$$\hat{d}'_i = \frac{1}{jk\Delta} \ln(\hat{z}'_i). \quad (14)$$

$$R'_i = \left([\hat{\mathbf{Z}}]^H [\hat{\mathbf{Z}}] \right)^{-1} [\hat{\mathbf{Z}}] \bar{f}_M \quad (15)$$

where $\hat{z}'_i = \frac{z'_i}{|z'_i|}$, $\bar{f}_M = (f_M(-N), f_M(-N+1), \dots, f_M(N))^T$ and

$$[\hat{\mathbf{Z}}] = \begin{bmatrix} (\hat{z}'_1)^{-N} & (\hat{z}'_2)^{-N} & (\hat{z}'_Q)^{-N} \\ (\hat{z}'_1)^{-N+1} & (\hat{z}'_2)^{-N+1} & (\hat{z}'_Q)^{-N+1} \\ \vdots & \vdots & \vdots \\ (\hat{z}'_1)^N & (\hat{z}'_2)^N & (\hat{z}'_Q)^N \end{bmatrix}_{(2N+1) \times Q} \quad (16)$$

Equation (15) finds the least squares solution of excitation, which makes up the effect of discarding the imaginary parts of d'_i s to some degree. In order to demonstrate the use of this methodology, was conducted the design of a nonuniform array with less antenna elements than that required by a uniformly spaced Chebyshev array will be given. It is supposed that a broadside $T_{19}(x)$ pattern with side-lobe level $SLL = -30[dB]$ is desired. Twenty antenna array elements are spaced at equidistance $d = 0.5\lambda$ in the original Chebyshev array. The number of samples is set to $N = M$.

Fig. 4 represents the singular value spectrum of the Chebyshev pattern samples. It can be seen that the singular values beyond the 12th value decay rapidly. Some

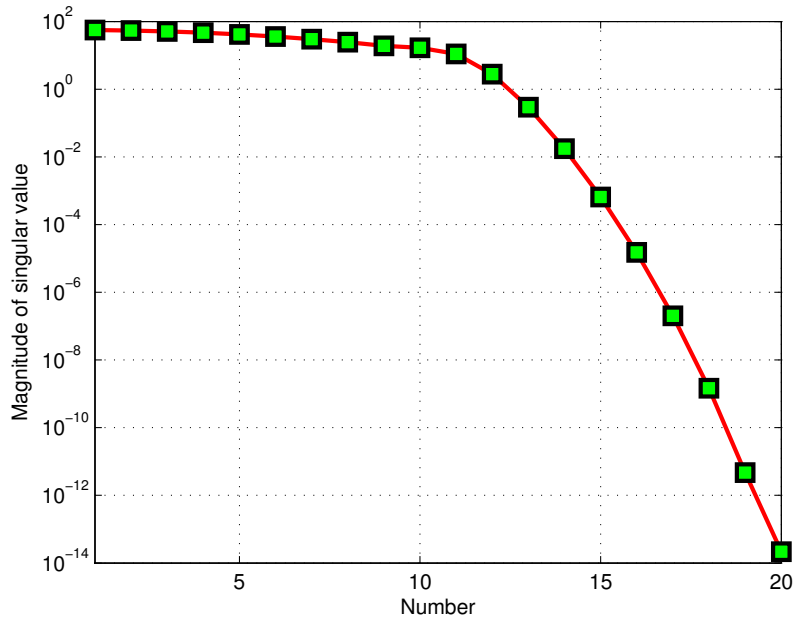


Figure 4. Singular value spectrum of the broadside Chebyshev pattern.

very small singular values can be discarded. Thus the desired pattern can be reconstructed by fewer antenna elements. The criterion to obtain the value of Q at $\epsilon = 10^{-2}$ gives as result a value of $Q = 12$, for $Q = 13$ at $\epsilon = 10^{-3}$. Fig. 5 shows the comparison between reconstructed patterns (using $Q = 12$ and $Q = 13$, respectively) and the desired pattern. As can be seen, 13 nonuniformly spaced antenna elements almost exactly reproduce the desired pattern produced by the 20 uniformly spaced Chebyshev elements. Table 1 shows the corresponding element positions and excitation amplitudes (for $Q = 12$ and $Q = 13$, resp.) and amplitudes of uniformly spaced Chebyshev array.

By using our proposed method, conventional broadside patterns are reproduced by nonuniformly spaced linear arrays with fewer elements than that required in uniformly spaced arrays. The saving in the number of elements can be more than 40%. In addition, most of the synthesis results yield a smaller aperture than the original array.

Table 1. Locations and amplitudes of the reconstructed nonuniformly spaced array and the uniformly spaced Chebyshev array

Chebyshev ($M = 20$)		Nonuniform ($Q = 12$)		Nonuniform ($Q = 13$)	
i	R_i	d'_i/λ	R'_i	d'_i/λ	R'_i
1	1	0.4254	1	0	1
2	0.9701	1.2755	0.9141	0.8206	0.9582
3	0.9124	2.1236	0.7597	1.6381	0.8411
4	0.8310	2.9671	0.5672	2.4481	0.6718
5	0.7315	3.8011	0.3712	3.2432	0.4812
6	0.6203	4.6371	0.2684	4.0071	0.3005
7	0.5046			4.7145	0.2335
8	0.3910				
9	0.2856				
10	0.3256				

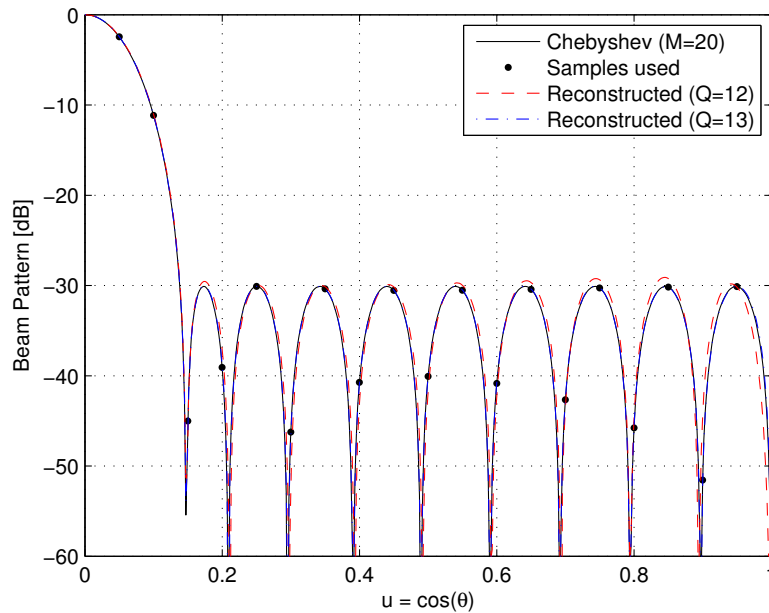


Figure 5. Reconstruction of the desired pattern by nonuniform arrays with 12 and 13 elements.

However, there exists a limitation in this methodology for the synthesis of shaped beam patterns, where the imaginary parts of synthesized element locations at the estimated minimum element number are not always negligible. Under this circum-

stances, Liu *et al.* (2010) have conducted a new proposal called forward-backward matrix pencil method (FB-MPM), which is discussed as follows.

2.1.3 Forward-backward matrix pencil method (FB-MPM)

To resolve the problem mentioned above, Liu *et al.* (2010) have proposed using the forward-backward matrix pencil method (FB-MPM), which places a necessary constraint on the distribution of poles. This constraint is not sufficient but very useful for limiting all poles on the unit circle. To do so, the sampled pattern data is organized into a Hankel-Toeplitz matrix that is given by

$$\mathbf{Y}^{fb} = \begin{bmatrix} \mathbf{y}_0 & \mathbf{y}_1 & \cdots & \mathbf{y}_L \\ \mathbf{y}_L^* & \mathbf{y}_{L-1}^* & \cdots & \mathbf{y}_0^* \end{bmatrix} \quad (17)$$

where $*$ denotes complex conjugate, the pencil parameter L is chosen such that $M \leq L \leq 2N - M$. Consider the matrix pencil

$$\mathbf{Y}_f^{fb} - z\mathbf{Y}_l^{fb} \quad (18)$$

where \mathbf{Y}_f^{fb} is obtained from \mathbf{Y}^{fb} by deleting the first column, and \mathbf{Y}_l^{fb} is obtained from \mathbf{Y}^{fb} by deleting the last column. It can be proven that if $\{z'_i, \mathbf{v}_1\}$ is a pair of generalized eigenvalue and eigenvector of this matrix pencil, $\{(1/z'_i)^*, \mathbf{v}_2\}$ must be another pair of generalized eigenvalue and eigenvector, where $\mathbf{v}_2(k) = \mathbf{v}_1^*(L - k)$. That is, all the eigenvalues (or poles) must be obtained as a pair of $\{z'_i, (1/z'_i)^*\}$. Although this is only a necessary condition for guaranteeing that $|z'_i| = 1$, this constraint is actually locally sufficient for z'_i in the neighborhood of the true value. Using this constraint can improve significantly the estimation accuracy of the poles, which is very important for

extending the MPM-based synthesis method to deal with asymmetric shaped-beam patterns.

Following with the final goal to reduce the number of elements for a desired pattern, the SVD of \mathbf{Y}^{fb} is performed and then find an optimal lower-rank approximation of this matrix by retaining only Q largest singular values, just as Liu *et al.* (2008) did in the MPM-based synthesis method. Denote the lower-rank matrix by \mathbf{Y}_Q^{fb} . It can be shown that \mathbf{Y}_Q^{fb} is not a Hankel-Toeplitz matrix anymore, but still maintains exactly the same vector structure as that of (17) in terms of y_l . Consider the following matrix pencil

$$\mathbf{Y}_{Q,f}^{fb} - z\mathbf{Y}_{Q,l}^{fb} \quad (19)$$

where $\mathbf{Y}_{Q,f}^{fb}$ (resp., $\mathbf{Y}_{Q,l}^{fb}$) is obtained from \mathbf{Y}_Q^{fb} by deleting the first column (resp., deleting the last column). This matrix pencil maintains a similar matrix structure as (18), and the generalized eigenvalues of this pencil would have the same constraint as the eigenvalues of (18). This constraint is very useful for avoiding the poles moving off the unite circle, which will be validated by the next proposed synthesis experiment. Once the eigenvalues (or the poles) are obtained correctly, the positions and excitations of the new elements can be immediately calculated through (13)-(16).

Fig. 6 shows the comparison between MPM- and FB-MPM-based methodologies when an asymmetric shaped-beam pattern is synthesized. The desired pattern was originally synthesized by Marcano and Durán (2000) using a genetic algorithm with 16 equispacing elements. With 13 elements, the FB-MPM synthesis method (with $L = 4N/3$) gives very accurate reconstruction of the original pattern. However, the MPM synthesis method gives poor reconstruction accuracy. The distribution of poles

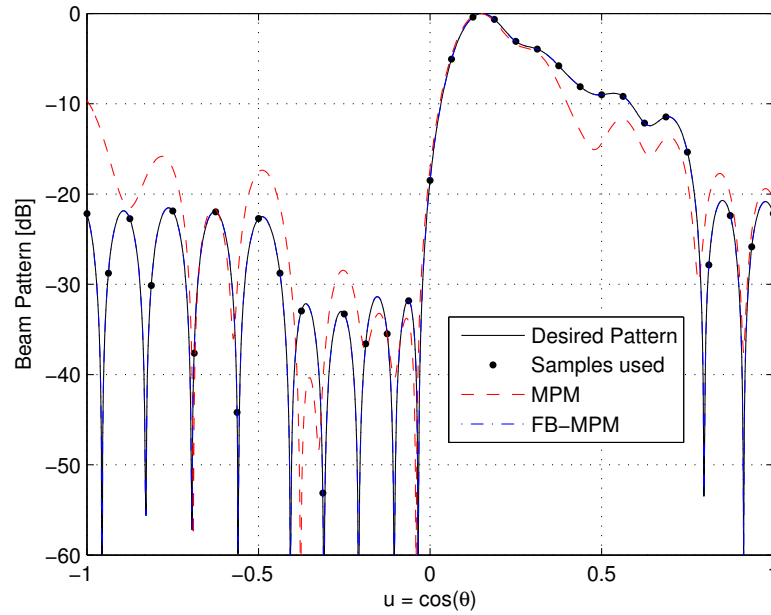


Figure 6. Desired shaped-beam pattern with 16 elements and the patterns reconstructed by the MPM- and FB-MPM-based methods, both with 13 elements.

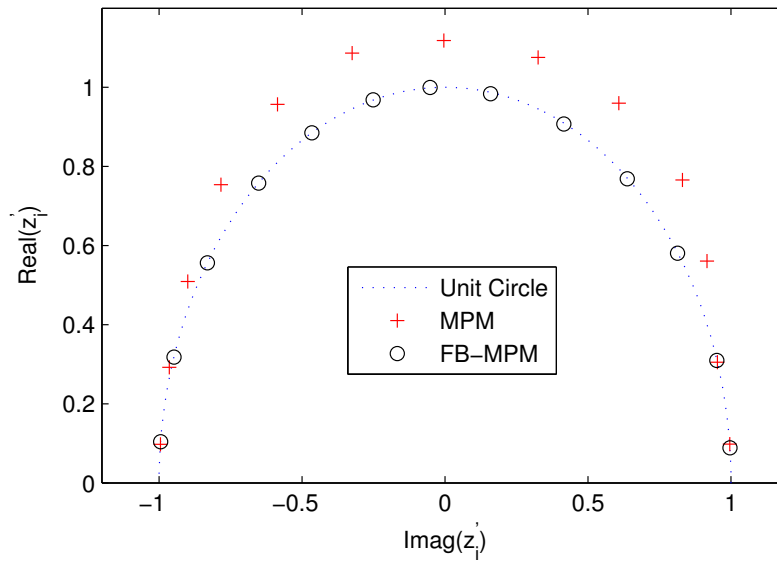


Figure 7. Distributions of the poles associated with the MPM and FB-MPM synthesis methodologies.

Table 2. Element locations and amplitudes reconstructed by the FB-MPM synthesis method in Fig. 6.

i	d'_i/λ	$ R'_i $	$\angle R'_i(^{\circ})$
1	-3.7371	0.33397	67.678
2	-3.1847	0.44635	-12.512
3	-2.5223	0.59718	-43.909
4	-1.8467	0.84712	-82.909
5	-1.2806	1	-141.543
6	-0.7364	0.76353	161.967
7	-0.2049	0.36678	117.061
8	0.5024	0.28782	146.374
9	1.1496	0.34988	122.173
10	1.7895	0.29436	78.679
11	2.4321	0.21135	43.217
12	3.2006	0.09265	81.155
13	3.7720	0.19506	0.751

obtained from these two methods are both shown in Fig. 7. As can be observed, most poles obtained from MPM synthesis method do not lie on the unit circle, while all the poles obtained from FB-MPM method are located exactly on the unit circle. Table 2 shows locations and excitations of the antenna elements reconstructed by the FB-MPM synthesis method. In this case, have saved 18.8% antenna elements. This section has presented a deterministic point of view to the problem of reducing the number of antenna elements. The MPM- and FB-MPM-based synthesis methodologies although achieve a good performance reducing the antenna elements, they have certainly other drawbacks that necessitate to explore their counterpart Bayesian. For this reason, the next section explores the Bayesian point of view to reduce the number of antenna elements, this also constitutes a contribution to the state-of-the-art.

2.2 Bayesian compressive sampling (BCS)

Bayesian compressive sampling (BCS) is a robust and theoretically solid technique to produce sparse models in regression and classification problems. Oliveri and Massa (2011) have proposed this technique for the design of maximally-sparse linear arrays. The method is devoted to find the maximally-sparse array with the highest a-posteriori probability to match a user-defined reference pattern. Towards this end, an efficient BCS solver exploiting a fast relevance vector machine (RVM) algorithm is adopted. To understand this methodology, the next mathematical formulation is developed:

Consider a symmetric linear arrangement of $M = (2N - \chi)$ ($\chi = 0$ if an even number of elements is at hand, $\chi = 1$ otherwise) isotropic elements, $w_n \in \mathbb{R}$ being the real excitation of the n -th element pair ($n = 1, \dots, N$). The synthesis problem is that of finding the set of array weights, such that (a) the radiated pattern is sufficiently close to a given reference one, $E_{\text{Ref}}(u)$, and (b), the number P of active array elements is as small as possible. Towards this end, the BCS formulation considers the following assumptions:

- The reference pattern is approximated in an arbitrary set of K angular positions $u_k, \forall k = 1, \dots, K$, within the visible range ($u_k \in [-1, 1]$).
- The set of P active positions are constrained to a large, but finite, user-chosen set of M (i.e., $M \gg P$) candidate locations not necessarily belonging to a regular lattice.

Mathematically, the problem can be formulated as follows:

Synthesis Problem - Given a set of K samples of the reference pattern, $E_{\text{Ref}} \in \mathbb{R}^K$, and a fidelity factor ϵ find the set of array weights, \mathbf{w} , which is maximally sparse subject to $\|\mathbf{E}_{\text{Ref}} - \mathbf{E}\|_2 \leq \epsilon$.

where $\|\bullet\|_2$ is the ℓ_2 -norm, $\mathbf{E}_{\text{Ref}} \triangleq [E_{\text{Ref}}(u_1), \dots, E_{\text{Ref}}(u_K)]^H$, $\mathbf{w} \triangleq [w_1, \dots, w_N]^H$, $\mathbf{E} \triangleq [E(u_1), \dots, E(u_K)]^H$ whose k -th entry is given by

$$E(u_k) = \sum_{n=1}^N \nu_n w_n \cos\left(2\pi \frac{d_n}{\lambda} u_k\right) \quad (20)$$

where λ being the wavelength, d_n the distance of the n -th location from the array center ($d_1 = 0$ if $\chi = 1$), and ν_n is the Neumann's number defined as $\nu_n = 2 - \chi$ if $n = 1$, and $\nu_n = 2$ otherwise. The synthesized pattern samples \mathbf{E} can be then expressed as

$$\mathbf{E} = \Psi \mathbf{w} \quad (21)$$

where $\Psi \in \mathbb{R}^{K \times N}$ and its (k, n) -th element are given by

$$\Psi(k, n) = \nu_n \cos\left(2\pi \frac{d_n}{\lambda} u_k\right) \quad (22)$$

To recast the problem as a BCS problem, the following three steps are necessary. First, rewrite the ℓ_2 -norm constraint ($\|\mathbf{E}_{\text{Ref}} - \mathbf{E}\|_2 \leq \epsilon$) as

$$\mathbf{E}_{\text{Ref}} - \Psi \mathbf{w} = \mathbf{e} \quad (23)$$

where $\mathbf{e} = [e_1, \dots, e_K]^T$ is a zero mean Gaussian error vector with an user-defined variance σ^2 proportional to the mismatching with the reference pattern (i.e., $\sigma^2 \propto \epsilon$).

Then, \mathbf{E}_{Ref} is modeled through a Gaussian likelihood

$$p(\mathbf{E}_{\text{Ref}} | [\mathbf{w}, \sigma^2]) = \frac{1}{(2\pi\sigma^2)^{\frac{K}{2}}} \exp\left(-\frac{1}{2\sigma^2} \|\mathbf{E}_{\text{Ref}} - \Psi\mathbf{w}\|_2\right) \quad (24)$$

to recast the original problem as the following linear regression one with sparseness constraints (LRSC) it has:

LRSC Problem - Given $\mathbf{E}_{\text{Ref}} \in \mathbb{R}^K$ find \mathbf{w} and σ^2 which maximize the a-posteriori probability $p(\mathbf{w}, \sigma^2 | \mathbf{E}_{\text{Ref}})$ subject to the constraint that \mathbf{w} is maximally-sparse.

Finally, the sparseness of \mathbf{w} is enforced. As regards the Bayesian formulation, such a task is accomplished by introducing a sparseness prior¹ over \mathbf{w} . Hereinafter, the Gaussian hierarchical prior is invoked

$$p(\mathbf{w} | \mathbf{a}) = \frac{\prod_{n=1}^N \sqrt{a_n} \exp\left(-\frac{a_n w_n^2}{2}\right)}{(2\pi)^{\frac{N}{2}}} \quad (25)$$

where $\mathbf{a} \triangleq [a_1, \dots, a_N]$ and $a_n, \forall n = 1, \dots, N$ is the n -th independent hyperparameter controlling the strength of the prior over w_n . To fully specify (25), the hyperpriors over \mathbf{a} [i.e., $p(\mathbf{a})$] and σ^2 [i.e., $p(1/\sigma^2)$] have to be defined. The Gamma distributions are here considered

$$p(\mathbf{a}) = \prod_{n=1}^N G(a_n | \alpha_1, \alpha_2) \quad (26)$$

and

$$p\left(\frac{1}{\sigma^2}\right) = G\left(\frac{1}{\sigma^2} \middle| \alpha_3, \alpha_4\right) \quad (27)$$

¹In Bayesian inference, a prior represents the a-priori knowledge about an unknown quantity in probabilistic terms.

where $\alpha_i, \forall i = 1, \dots, 4$ is the i -th scale prior, $G(a_n | \alpha_1, \alpha_2) (\alpha_2^{\alpha_1} a_n^{\alpha_1 - 1} \exp(-\alpha_2 a) / \Gamma(\alpha_1))$, and $\Gamma(\alpha_1) \triangleq \int_0^{\infty} t^{\alpha_1 - 1} \exp(-t) dt$ is the gamma function. Thanks to (25), (26) and (27), the original synthesis problem can be finally formulated as

BCS Problem - Given $\mathbf{E}_{\text{Ref}} \in \mathbb{R}^K$, find \mathbf{w}_{BCS} , \mathbf{a}_{BCS} and σ_{BCS}^2 which maximize $p([\mathbf{w}, \mathbf{a}, \sigma^2] | \mathbf{E}_{\text{Ref}})$.

In order to determine the desired sparse solution, the relevant vector machine (RVM) method, which theoretically guarantees to solve the BCS problem, is applied. In this way, it is necessary consider that the posterior over all unknowns can be expressed as

$$p([\mathbf{w}, \mathbf{a}, \sigma^2] | \mathbf{E}_{\text{Ref}}) = p(\mathbf{w} | [\mathbf{E}_{\text{Ref}}, \mathbf{a}, \sigma^2]) p([\mathbf{a}, \sigma^2] | \mathbf{E}_{\text{Ref}}). \quad (28)$$

Moreover, because of (24) and (25), the posterior distribution over \mathbf{w}

$$p(\mathbf{w} | [\mathbf{E}_{\text{Ref}}, \mathbf{a}, \sigma^2]) = \frac{1}{(2\pi)^{\frac{N+1}{2}}} \times \exp \left\{ -\frac{(\mathbf{w} - \mu)^H (\Sigma)^{-1} (\mathbf{w} - \mu)}{2} \right\} \quad (29)$$

where the posterior mean and the covariance are given by $\mu = \Sigma \Psi^H \mathbf{E}_{\text{Ref}} / \sigma^2$ and $\Sigma = ((\Psi^T \Psi / \sigma^2) + \mathbf{A})^{-1}$, respectively, being $\mathbf{A} \triangleq \text{diag}(a_1, \dots, a_N)$.

As for the second term on the right-hand side of (28), the delta-function approximation is used to model the hyperparameter posterior

$$p([\mathbf{a}, \sigma^2] | \mathbf{E}_{\text{Ref}}) \approx \delta(\mathbf{a}_{\text{BCS}}, \sigma_{\text{BCS}}^2) \quad (30)$$

where \mathbf{a}_{BCS} and σ_{BCS}^2 are the most probable values, $(\mathbf{a}_{\text{BCS}}, \sigma_{\text{BCS}}^2) = \arg \max_{\mathbf{a}, \sigma^2} \{p([\mathbf{a}, \sigma^2] | \mathbf{E}_{\text{Ref}})\}$, also called hyperparameter posterior modes. In order to determine their values, consider that

$$p([\mathbf{a}, \sigma^2] | \mathbf{E}_{\text{Ref}}) \approx p(\mathbf{E}_{\text{Ref}} | [\mathbf{a}, \sigma^2]) p(\mathbf{a}) p(\sigma^2) \quad (31)$$

and assume uniform scale priors. Then, $p(\sigma^2)$ and $p(\mathbf{a})$ become constant values and the maximization of (31) is equivalent to maximize the term $p(\mathbf{E}_{\text{Ref}} | [\mathbf{a}, \sigma^2])$, whose logarithm is given by

$$\begin{aligned} \mathcal{L}(\mathbf{a}, \sigma^2) &\triangleq \log \{p(\mathbf{E}_{\text{Ref}} | [\mathbf{a}, \sigma^2])\} \\ &= -\frac{1}{2} [N \log(2\pi) + \log(|C|) + \mathbf{E}_{\text{BCS}}^H C^{-1} \mathbf{E}_{\text{BCS}}] \end{aligned} \quad (32)$$

where $C = \sigma^2 I + \Psi A^{-1} \Psi^T$. It is worthwhile to point out that it is not possible to perform the maximization of the “marginal likelihood” (32) in an exact fashion, but a type-II maximum likelihood procedure can be profitably exploited for determining an iterative re-estimation of $(\mathbf{a}_{\text{BCS}}, \sigma_{\text{BCS}}^2)$. Such a technique, whose Matlab implementation is available in `ml_2`, is summarized in the Appendix A.

Finally, by substituting (29) and (30) in (27), is obtained that

$$p([\mathbf{w}, \mathbf{a}, \sigma^2] | \mathbf{E}_{\text{Ref}}) \approx p(\mathbf{w} | [\mathbf{E}_{\text{Ref}}, \mathbf{a}, \sigma^2])_{(\mathbf{a}, \sigma^2) = (\mathbf{a}_{\text{BCS}}, \sigma_{\text{BCS}}^2)}. \quad (33)$$

The posterior over all unknowns results a multivariate Gaussian function (29) only depending on the unknown set \mathbf{w} once $(\mathbf{a}_{\text{BCS}}, \sigma_{\text{BCS}}^2)$ have been determined. Therefore, the value of $\mathbf{w}_{\text{BCS}} = \arg \max_{\mathbf{w}} \{p([\mathbf{w}, \mathbf{a}, \sigma^2] | \mathbf{E}_{\text{Ref}})\}$ turns out to be equal to the posterior mean of $p(\mathbf{w} | [\mathbf{E}_{\text{Ref}}, \mathbf{a}, \sigma^2])_{(\mathbf{a}, \sigma^2) = (\mathbf{a}_{\text{BCS}}, \sigma_{\text{BCS}}^2)}$ given by

$$\mathbf{w}_{\text{BCS}} = \mu_{(\mathbf{a}, \sigma^2) = (\mathbf{a}_{\text{BCS}}, \sigma_{\text{BCS}}^2)}. \quad (34)$$

The algorithmic implementation of the BCS-based pattern synthesis consists of the following steps:

1. **Input Phase** - Set the reference pattern $E_{\text{Ref}}(u)$, the grid of admissible locations $(d_n; \forall n = 1, \dots, N)$, the set of pattern sampling points $(u_k; \forall k = 1, \dots, K)$, the target variance σ^2 of the error term \mathbf{e} , and its initial estimate σ_0^2 for the sequential solver of the RVM algorithm;
2. **Matrix Definition** - Fill the entries of the matrices \mathbf{E}_{Ref} , Ψ , \mathbf{e} and $\hat{\mathbf{E}}_{\text{Ref}} = \mathbf{E}_{\text{Ref}} + \mathbf{e}$;
3. **Hyperparameter Posterior Modes Estimation** - Find $(\mathbf{a}_{\text{BCS}}, \sigma_{\text{BCS}}^2)$ by maximizing (32) as described in the Appendix A;
4. **Array Weights Estimation** - Find \mathbf{w}_{BCS} by (34);
5. **Output Phase** - Return the estimated array weights, \mathbf{w}_{BCS} , the number of active array elements, $P_{\text{BCS}} = -\chi + 2 \|\mathbf{w}_{\text{BCS}}\|_0^2$, and the corresponding hyperparameter modes $(\mathbf{a}_{\text{BCS}}, \sigma_{\text{BCS}}^2)$.

In order to evaluate the “degree of optimality” of the antenna array designs, the following metrics and pattern descriptors are used: the matching error ξ defined as

$$\xi \triangleq \frac{\int_{-1}^1 |E_{\text{Ref}}(u) - E(u)|^2 du}{\int_{-1}^1 |E_{\text{Ref}}(u)|^2 du}, \quad (35)$$

the aperture length L , the mean inter-element spacing $\Delta L = \frac{L}{P} - 1$, and the minimum spacing $\Delta L_{\min} = \min_{p=1, \dots, P-1} \{|d_{p+1} - d_p|\}$.

² $\|\mathbf{x}\|_0$ is the ℓ_0 -norm of \mathbf{x} (i.e., the number of non-zero elements of \mathbf{x}).

To demonstrate the accuracy of this methodology, the synthesis of a non-uniform array matching a Chebyshev pattern is considered. A broadside Chebyshev pattern with $L = 9.5\lambda$ and side-lobe level $SLL = -20[\text{dB}]$ is assumed as reference. Notice that such a pattern can be synthesized through a uniform array with $P_{\text{uniform}} = 20(\lambda/2)$ -spaced elements. The BCS synthesis has been carried out sampling $E_{\text{Ref}}(u)$ at K points ($u_k \in [0, 1]$, $u_k = \frac{(k-1)}{(K-1)}, \forall k = 1, \dots, K$) and assuming the following grid of admissible locations

$$d_n = \frac{L(n-1)}{2(N-1)}, \quad \forall n = 1, \dots, N. \quad (36)$$

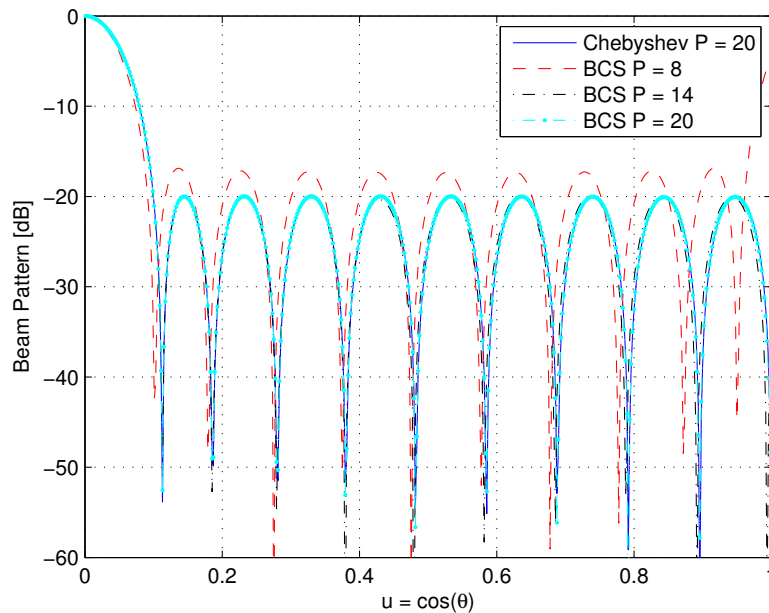


Figure 8. Radiation patterns of the reference and a set representative BCS arrays.

Fig. 8 describes the BCS results versus A Chebyshev ($P = 20$, and $SLL = -20[\text{dB}]$) beam pattern; for values of P_{BCS} equals to 8, 14, 20-elements, respectively. The matching error ξ associated with each number of P_{BCS} is 10^{-1} , 10^{-4} , 10^{-6} , respec-

tively.

The BCS technique has shown, Oliveri and Massa (2011), the following main features:

- BCS favorably compares with state-of-the-art techniques such as the MPM in terms of accuracy, array sparseness and computational burden when matching reference broadside patterns;
- On average the number of active elements in a BCS array turns out to be smaller than the corresponding uniform arrangement still providing a high accuracy in matching the reference pattern (i.e., $\xi \leq 10^{-4}$);
- BCS usually outperforms MPM when dealing with shaped beampatterns.

2.3 Synthesis of two-dimensional antenna array using independent compression regions

For more than sixty years, the problem of synthesis of antenna arrays has been defined in a traditional way, using solutions aimed to determine the antenna array feed and locations of all the antenna elements, in order to achieve a particular gain and side-lobe level (SLL) for a particular radio communication application Balanis (1997). To achieve these goals in the case of two-dimensional antenna arrays (also known as planar antenna arrays), in Bae *et al.* (2005); Panduro *et al.* (2006); Rocha Alicano *et al.* (2007); Amador *et al.* (2009) several methods based on evolutive algorithms were developed; furthermore, in Chen *et al.* (2006, 2007); Liu *et al.* (2008); Oliveri and Massa (2011); Yang *et al.* (2011) the compression methods were directly integrated to the synthesis process. The interest in reducing or compressing the

number of antenna elements stems from the need of reaching the weight, size and cost for antennas required by the communication systems of new generation based on MIMO technology. For example, the case of International Mobile Telecommunications (IMT)-Advanced, with data rates associated of 1 Gbps for fixed wireless and 100 Mbps for wireless users with high mobility, Dahlman *et al.* (2011).

The increase in performance requirements for antenna arrays makes necessary to extend current array synthesis methodologies to the two-dimensional space, creating a new research problem. In this work we propose and analyze a novel synthesis methodology for two-dimensional array antenna based on the Independent Compression Regions (ICR). We incorporate a number of different compression techniques depending on the spectral characteristics of each region and improve the available array amplitude distributions, side lobe control and compression level. The proposed methodology consists of dividing the array in multiple regions allowing the total array factor to be considered as the sum or difference of independent array factors Elliot (2003). For the assessing the ICR approach we propose the non-iterative Matrix Pencil Method (MPM) Liu *et al.* (2008) and the iterative Bayesian Compressive Sampling method (BCS) Oliveri and Massa (2011). The MPM is a technique with low variance in the estimation of the synthesis parameters from a sum of complex exponentials Liu *et al.* (2008), however, it is susceptible to fail due to the possibly complex inter-element distance and the real part approximation may negatively affect the antenna array performance. In Liu *et al.* (2010) proposes a partial solution to this problem using the Forward-Backward Matrix Pencil Method (FBMPM) which applies a necessary constraint on the distribution of poles on the unit circle. In the case of the BCS method, it produces the synthesis of antenna arrays with maximally-sparse antenna elements Oliveri and Massa (2011). For the BCS method the solution is

obtained using the fast Relevance Vector Machines (RVM), allowing the maximum a posteriori probability approach the reference array factor with a minimum number of antenna elements.

2.3.1 Mathematical Formulation

Using as a starting point the two-dimensional array factor, defined by Collin and Zucker (1969), as:

$$AF(u, v) = \sum_{m=-M}^M \sum_{n=-N}^N I_{mn} \exp(jk \cdot (md_x(u - u_0) + nd_y(v - v_0))) \quad (37)$$

where M, N are the dimension of planar array, I_{mn} is the feed, ($u = \sin \theta \cos \phi$, $v = \sin \theta \sin \phi$) are defined as angles of observation, ($u_0 = \sin(\theta_0) \cos(\phi_0)$, $v_0 = \sin(\theta_0) \sin(\phi_0)$) are the main beam direction, (d_x, d_y) are the inter-element uniform distance and $k = \frac{2\pi}{\lambda}$ refers to the free-space wavenumber where λ is the wavelength. The most important restriction is the I_{mn} feed complexity, thus many practical designs use identical feeds that sum one row of radiating elements at a time, the outputs of all linear array are then connected by a feeding network. This reduces feed complexity, volume and cost, but restricts the available array amplitude distributions and side lobe control.

In order to extend the analysis presented by Liu *et al.* (2008) (MPM) and Oliveri and Massa (2011) (BCS) to planar arrays, we decompose the planar array as the product of two linear reference arrays (see Fig. 9). The array factor for a separable two-dimensional antenna array is defined as the product Collin and Zucker (1969):

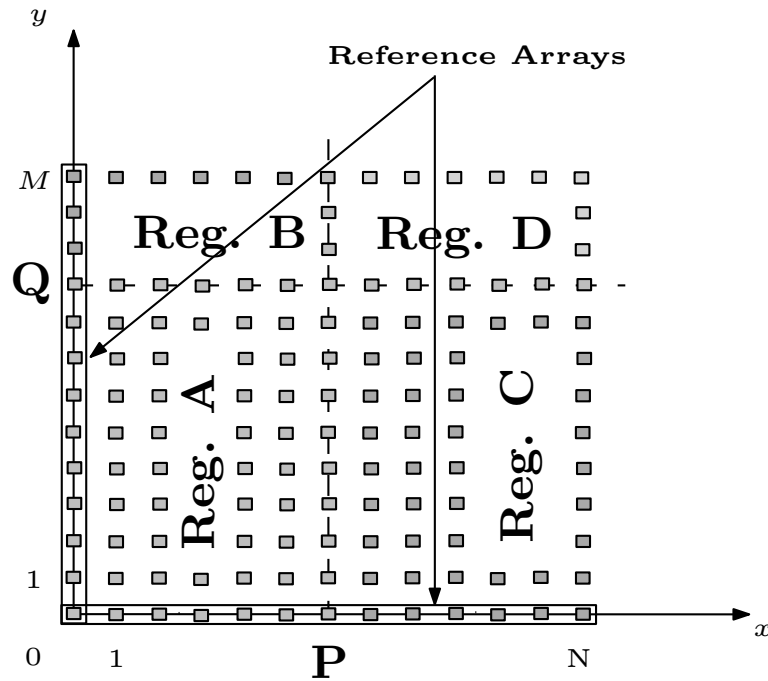


Figure 9. Geometric representation of the independent compression regions for the formulation of two-dimensional array factor synthesis.

$$\begin{aligned}
 AF(u, v) &= \left[\sum_{n=0}^N I_n \exp(jknd_x(u - u_0)) \right] \cdot \left[\sum_{m=0}^M I_m \exp(jkmd_y(v - v_0)) \right] \quad (38) \\
 &= AF(u) \cdot AF(v)
 \end{aligned}$$

where $AF(u)$ and $AF(v)$ represent the array factor associated to the reference array located in x and y , respectively. It has been pointed before that one of the limitations of separable distributions is higher side lobes along the principal planes and much lower ones elsewhere, Kummer (1992). Furthermore in Yang *et al.* (2011) the compression process is only applied to the individual array factors, neglecting other regions inside of the array. To counteract this problem, we propose a novel way of segmenting the array factor into independent regions, see Fig. 9. Due to the charac-

teristics of the compression methods it is convenient to separate (39) into real and imaginary components as proposed by Oliveri *et al.* (2012). A mathematical formulation based on the decomposition of (39) in four independent regions is developed as follows:

$$\begin{aligned}
AF(u) &= I_o + \sum_{n=1}^P I_n \exp(jknd_x(u - u_o)) + \sum_{m=P+1}^N I_m \exp(jknd_x(u - u_o)) \\
&= \left[I_o + \sum_{n=1}^P I_n \cos(knd_x(u - u_o)) + \sum_{n=P+1}^N I_n \cos(knd_x(u - u_o)) \right] \\
&\quad + j \left[\sum_{n=1}^P I_n \sin(knd_x(u - u_o)) + \sum_{n=P+1}^N I_n \sin(knd_x(u - u_o)) \right] \\
&= \mathcal{Re} \{AF(u)\} + j\mathcal{Im} \{AF(u)\}.
\end{aligned} \tag{39}$$

and

$$\begin{aligned}
AF(v) &= I_o + \sum_{m=1}^Q I_m \exp(jkmd_y(v - v_o)) + \sum_{m=Q+1}^M I_m \exp(jkmd_y(v - v_o)) \\
&= \left[I_o + \sum_{m=1}^Q I_m \cos(kmd_y(v - v_o)) + \sum_{m=Q+1}^M I_m \cos(kmd_y(v - v_o)) \right] \\
&\quad + j \left[\sum_{m=1}^Q I_m \sin(kmd_y(v - v_o)) + \sum_{m=Q+1}^M I_m \sin(kmd_y(v - v_o)) \right] \\
&= \mathcal{Re} \{AF(v)\} + j\mathcal{Im} \{AF(v)\}
\end{aligned} \tag{40}$$

In this way, the antenna array factor $AF(u, v)$ can be decomposed as

$$AF(u, v) = \mathcal{Re} \{AF(u, v)\} + j\mathcal{Im} \{AF(u, v)\} \tag{41}$$

where,

$$\mathcal{R}e \{AF(u, v)\} = [\mathcal{R}e \{AF(u)\} \cdot \mathcal{R}e \{AF(v)\}] - [\mathcal{I}m \{AF(u)\} \cdot \mathcal{I}m \{AF(v)\}] \quad (42)$$

and

$$\mathcal{I}m \{AF(u, v)\} = [\mathcal{R}e \{AF(u)\} \cdot \mathcal{I}m \{AF(v)\}] + [\mathcal{I}m \{AF(u)\} \cdot \mathcal{R}e \{AF(v)\}] \quad (43)$$

where Q and P are the region bounds, N and M the number of elements for each reference array. This rectangular geometry can be reduced when a symmetric array is used, as shown in Bae *et al.* (2005).

In order to determine values for P and Q , in Bae *et al.* (2005) propose to calculate these limits in terms of the ratios R/N and Q/N , and their relationship to the level of reduction of the design parameter SLL (RNSLLR), as $\text{RNSLLR [dB]} = \text{MSLL}$, where MSLL is the side lobe level of a reference one-dimensional array. Our proposal is based on the singular value spectrum of each reference array pattern samples. The values are designated with respect to a required fidelity factor ϵ , defined from the least square error (LSE) as:

$$\|AF_{ref}(u, v) - AF_{reduced}(u, v)\|^2 \leq \epsilon \quad (44)$$

The compression process that we employ in this work is based on the techniques proposed by Liu *et al.* (2008) for the MPM and FB-MPM Liu *et al.* (2010). Moreover, in order to address the state-of-art, we applied the BCS method developed by Oliveri

and Massa (2011). Just as in Yang *et al.* (2011), both methods are applied to each of the reference arrays.

Numerical Analysis and Assessment

In this section we will assess the benefits of using independent compression regions in the synthesis of two-dimensional arrays.

2.3.2 Small 2-D arrays

Concerning the first numerical experiment associated to small 2-D arrays, a 10×10 planar array with $\lambda/2$ spacing is considered. Yang *et al.* (2011) use the MPM and obtained better results than those published by Trucco (1999). When using our novel ICR method with the MPM technique we obtained an increase in performance compared with Yang *et al.* (2011), as shown in Table 3. Conversely, when using the ICR method with the BCS approach, we did not reach a compression level above the result reported in Yang *et al.* (2011).

The parameters P and Q are determined with respect to the singular value spectrum shown in Fig. 10, where the first five elements form a high energy cluster necessary for the preservation of the beam pattern characteristics. Therefore, the value of P and Q are directly obtained from the number of elements that constitute this high energy cluster. Once these regions are defined, we applied the MPM once again (with $\epsilon = 10^{-1}$) in region D (see Fig. 9), because this region makes the least contribution over the total beam pattern, allowing a reduction in the total number of elements down to just one. The beam pattern response is shown in Fig. 11, according to the visible region concept defined in Trees (2002).

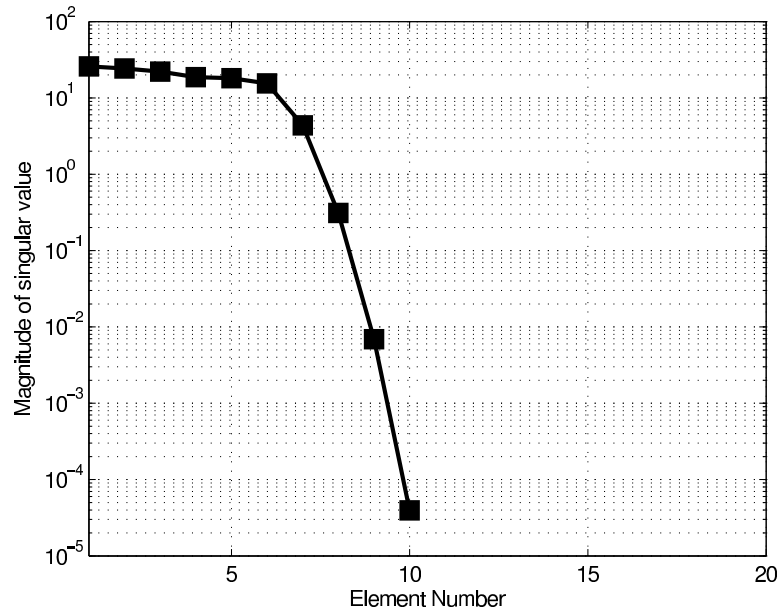


Figure 10. Singular value spectrum of the original 10 elements broadside Chebyshev pattern.

Table 3. Comparison between planar array specifications reported by Yang *et al.* (2011) Vs. ICR Method based on MPM.

Specifications	Yang <i>et al.</i> (2011)	ICR with MPM
Main Lobe Width (MLW) in -6 [dB]	0.237	0.234
Peak Side Lobe Level (PSLL) in [dB]	-17.6	-17.9
Aperture	$22.29\lambda^2$	$22.29\lambda^2$
Current Taper Ratio (CTR)	2.1	2.2
Number of Elements	49	46

Large 2-D arrays

The second numerical experiment proposed is the assessment of large 2-D arrays. Yang *et al.* (2011) propose to optimize 20×10 planar array because the aperture size is much greater than λ (large array criteria). One of the best results reported by Yang *et al.* (2011) was obtained using an array of 84 elements, with a side-lobe peak of -20.0 dB, a MLW = 0.064 along the u -axis, and MLW = 0.134 along the v -axis. Taking as reference the values obtained by Yang *et al.* (2011), we decided to evaluate

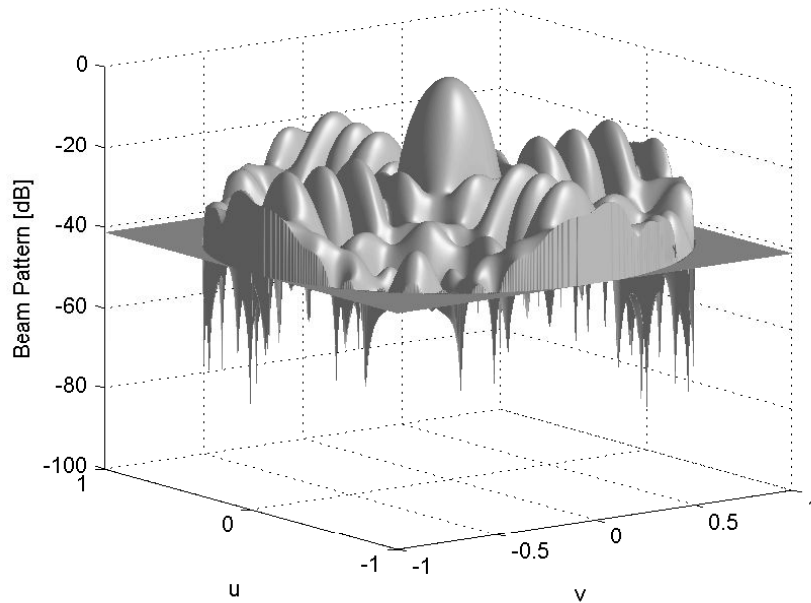


Figure 11. Beam pattern with 46 elements using the proposed ICR method. The PSLL= -17.9 dB and the MLW = 0.236.

the MPM and BCS methods only in the 20 elements linear array. In our numerical evaluation both methods have the same response, however, when the main beam steering is changed ($u_0 \neq 0$ or $v_0 \neq 0$), BCS clearly outperforms MPM.

The parameters Q and P are selected through the singular value spectrum shown in Fig. 12, in a similar way to the previous numerical experiment. In this case $Q = 5$ and $P = 8$. Because the values are near each other, the region D is the most suitable to reapply the reduction. A $\epsilon = 10^{-2}$ was used to reduce by 6 elements the original results obtained by Yang *et al.* (2011), that is down to 78 elements. The ICR beam pattern is shown in Fig. 13. Again the ICR method reduces the number of elements in the synthesis process, providing levels of MLW = 0.067 along the u -axis, MLW = 0.138 along the v -axis and PSLL = -19.6 dB near to the specifications.

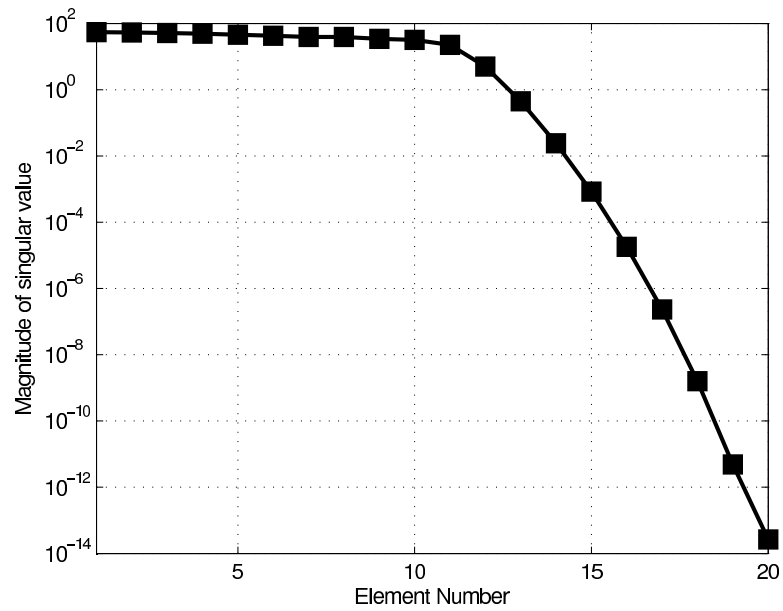


Figure 12. Singular value spectrum of the original 20 elements broadside Chebyshev pattern.

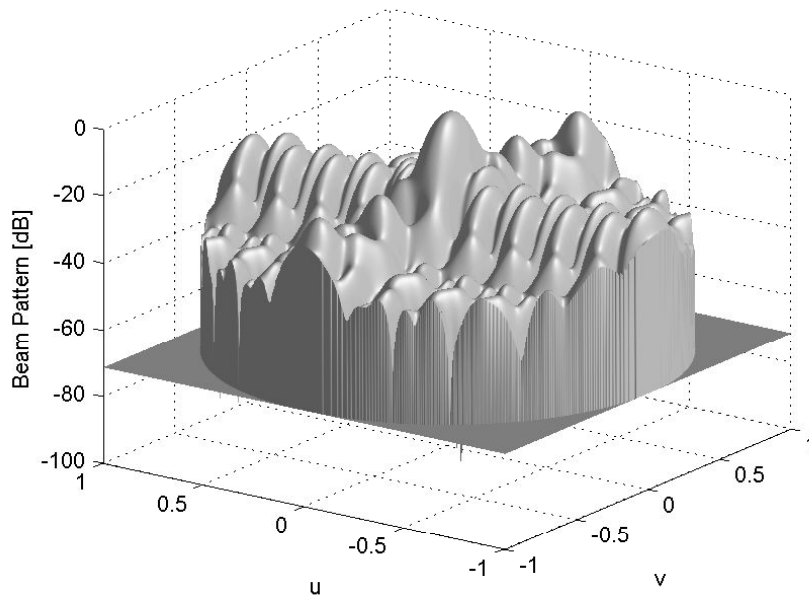


Figure 13. Beam pattern with 78 elements using the proposed ICR method. The PSLL= -19.6 dB and the MLW = 0.067 along the u -axis, MLW = 0.138 along the v -axis.

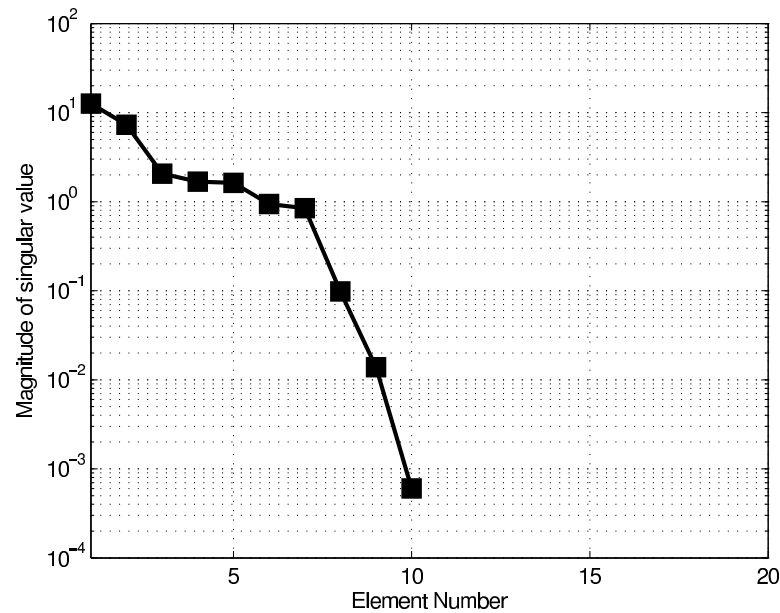


Figure 14. Singular value spectrum of the original 10 elements shaped-beam pattern.

Shaped-beam Arrays

Finally, our proposed method was used to synthesize shaped-beam arrays. Although we evaluated the symmetric and nonsymmetric cases for shaped-beam planar arrays, only the symmetric option will be shown. In Ares and Moreno (1990), a convolutional shaped-beam was synthesized to reduce the Current Taper Ratio (CTR) level. The numerical experiment consists of 10 elements separated $3\lambda/5$ with $MLW = 0.84$, $PSLL = -20$ dB and $CTR = 9$. In order to determine the values of P and Q , in Fig. 14 the singular value spectrum presented a convenient value of 6 for both bounds. When the ICR method was applied to the 2-D shaped-beam pattern, an optimized shaped-beam array with 46 elements was obtained, with $MLW = 0.856$, $PSLL = -26.3$ dB and $CTR = 10.1$, Fig. 15 shows the beam pattern.

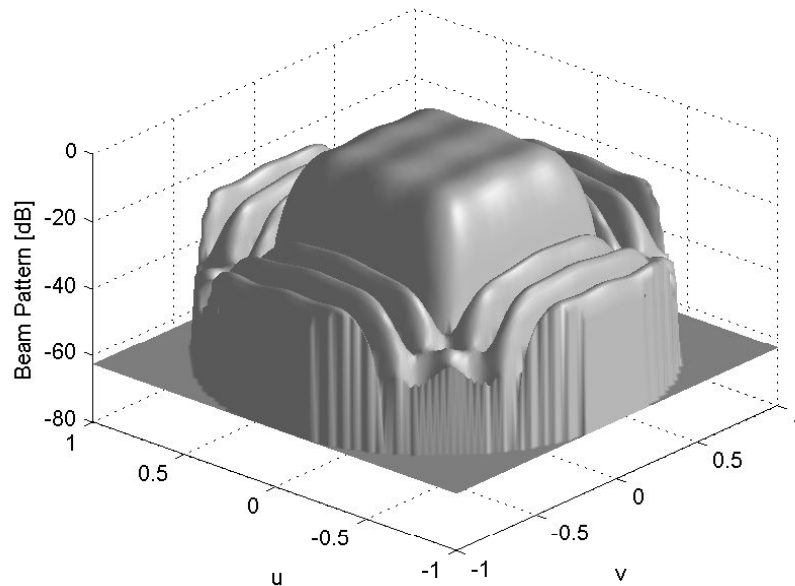


Figure 15. Beam pattern with 46 elements using the proposed ICR method for shaped-beam pattern synthesis. The PSLL= -26.3 dB and the MLW = 0.856.

2.4 Conclusions

We have devised a novel synthesis procedure, applicable to two-dimensional antenna arrays, which introduces independent compression regions (ICR) for reducing the number of antenna elements. The method exploits the best features of one-dimensional compression techniques, namely MPM and BCS. With the ICR method, we are able to increase the compression level of reference arrays with respect to the state-of-the-art procedure reported in Yang *et al.* (2011). In addition, the singular value spectrum was used as a strategy to obtain the appropriate values of the limits of each region, providing an alternative approach to the method proposed in Bae *et al.* (2005).

We have conducted 3 numerical experiments where we show the versatility of our

proposal. The first two numerical experiments present a typical narrow beam response, using the ICR method with the MPM technique we synthesized planar arrays with reduced number of elements preserving all the original specifications. In the last numerical experiment we extended the validation of the ICR method and we show how the BCS and MPM techniques can be simultaneously combined to increase even further the overall compression level.

To further contribute to the state-of-the-art associated with the synthesis of antenna arrays with sparseness characteristics, in the next chapter we introduce a new synthesis methodology, which is focused to resolve the amplitude currents and locations of the antenna array elements with a deterministic approach, and the phase currents are computed using a phase optimization procedure, which makes of this proposal a new hybrid sparse antenna array synthesis approach.

Hybrid sparse antenna array synthesis

In this chapter, motivated by the possibility to solve analytically the optimal element density and excitation tapering distributions, we propose a new synthesis technique based on the combination of two methods. First, a deterministic synthesis algorithm based on Caratelli and Viganó (2011) is adapted to resolve the non-uniform amplitude excitations and element locations. In this way, the array sparseness can be conveniently tuned in order to achieve the design requirements in terms of minimum spacing between the antenna elements, and maximal array aperture size. Then, an iterative optimization method is used to compute the phase of the excitation currents. This optimization allows us to enhance the phase point-matching condition proposed in Caratelli and Viganó (2011). In order to achieve this improvement, we use the phase optimization methodology, developed by Bulatsyk *et al.* (2010) and associated with the antenna theory domain by Semenov (1972). This approach is proven valid to properly match diverse beam patterns (narrow-beam, flat-top and square-cosecant) with sparse linear arrays.

3.1 Deterministic synthesis algorithm to estimate the non-uniform amplitude excitations and element locations

We first consider the array factor relevant to a radiating structure consisting of N antennas deployed over a line, defined as:

$$AF(\vartheta) = \sum_{n=1}^N \bar{A}_n \exp [j (k_o \bar{x}_n \sin \vartheta + \bar{\alpha}_n)] \quad (45)$$

where k_o is the propagation constant in free space, and $\bar{I}_n = \bar{A}_n \exp(j\bar{\alpha}_n)$ the excitation coefficient of the n -th array element located at $x = \bar{x}_n$. As it can be readily inferred, the expression in (45) may be regarded as the Riemann's sum approximating the auxiliary array factor function, defined below:

$$F_A(\vartheta) = \int_0^{q_{\max}} A(q) \exp \{j [2\pi \xi(q) \sin \vartheta + \alpha(q)]\} dq \quad (46)$$

where $\xi(q)$, $A(q)$ and $\alpha(q)$ denote the continuous normalized positioning, amplitude and phase distributions, respectively, generalizing the discrete quantities $\frac{k_o \bar{x}_n}{2\pi}$, \bar{A}_n and $\bar{\alpha}_n$ appearing in (45). Similarly, q is the continuous version of the index n relevant to the general antenna element forming the array, and ranging from 0 to the maximum value q_{\max} (typically specified to be the unity for the purpose of normalization). After setting for shortness $\psi = 2\pi \sin \vartheta$, the auxiliary array factor function can be written as:

$$F_A(\psi) = \sum_{m=1}^M F_{A_m}(\vartheta) \quad (47)$$

with

$$F_{A_m}(\vartheta) = \int_{q_{m-1}}^{q_m} A_m(q) \exp \{j [\psi \xi_m(q) + \alpha_m(q)]\} dq \quad (48)$$

being the contribution pertinent to the m -th interval $[q_{m-1}, q_m]$. In each interval, the positioning, amplitude and phase functions are assumed to be linearized according to the following expression:

$$\chi_m(q) = \hat{\chi}_{m-1} + \frac{q - q_{m-1}}{\Delta q} \widehat{\Delta \chi}_m \quad (49)$$

where $\hat{\chi}_m = \chi(q_m)$, $\widehat{\Delta \chi}_m = \hat{\chi}_m - \hat{\chi}_{m-1}$ for $\chi = \xi, A, \alpha$ and $\Delta q = q_m - q_{m-1} = \frac{q_{\max}}{M}$.

As it is obvious, the larger the number M of intervals which the domain $[0, q_{\max}]$ is divided into, the better the accuracy of the described discretization procedure on the array tapering functions. Heuristically, M can be selected to be νN with $\nu \gg 1$.

Under the mentioned assumptions, the general term $F_{A_m}(\psi)$ can be evaluated in a closed form as follows:

$$F_{A_m}(\psi) = \frac{\Delta q}{\left(\psi \widehat{\Delta \xi}_m + \widehat{\Delta \alpha}_m\right)^2} \times \left[\exp \left[j \left(\psi \hat{\xi}_m + \hat{\alpha}_m \right) \right] \left\{ \left[1 - j \left(\psi \widehat{\Delta \xi}_m + \widehat{\Delta \alpha}_m \right) \right] \times \right. \right. \\ \left. \left. \hat{A}_m - \hat{A}_{m-1} \right\} - \exp \left[j \left(\psi \hat{\xi}_{m-1} + \hat{\alpha}_{m-1} \right) \right] \times \left\{ \hat{A}_m - \left[1 + j \left(\psi \widehat{\Delta \xi}_m + \widehat{\Delta \alpha}_m \right) \right] \right. \right. \\ \left. \left. \hat{A}_{m-1} \right\} \right]. \quad (50)$$

In order to achieve a fully analytical formulation useful to mimic a given objective array factor mask $F_{\text{Obj}}(\psi)$ in a deterministic way, it is convenient to directly carry out the synthesis procedure in the domain of the Fourier transform $\mathcal{F}\{\cdot\}$ with respect to the variable ψ . By making judicious use of the shift property of the operator $\mathcal{F}\{\cdot\}$,

one can readily obtain, after mathematical manipulations:

$$\begin{aligned}\tilde{F}_{A_m}(H) &= \mathcal{F}\{F_{A_m}(\psi)\} = \int_{-\infty}^{\infty} F_{A_m}(\psi) \exp(j\psi H) d\psi \\ &= \left| \tilde{F}_{A_m}(H) \right| \exp\left(j \arg\left\{ \tilde{F}_{A_m}(H) \right\}\right)\end{aligned}\quad (51)$$

where:

$$\begin{aligned}\left| \tilde{F}_{A_m}(H) \right| &= 2\pi\Delta q \frac{\hat{A}_{m-1}(H + \hat{\xi}_m) - \hat{A}_m(H + \hat{\xi}_{m-1})}{\widehat{\Delta\xi}_m^2} \\ &\quad \cdot P_{\widehat{\Delta\xi}_m}\left(H + \hat{\xi}_{m-\frac{1}{2}}\right); \end{aligned}\quad (52)$$

$$\begin{aligned}\arg\left\{ \tilde{F}_{A_m}(H) \right\} &= \left[\hat{\alpha}_{m-1} - \frac{\widehat{\Delta\alpha}_m}{\widehat{\Delta\xi}_m} (H + \hat{\xi}_{m-1}) \right] \\ &\quad \cdot P_{\widehat{\Delta\xi}_m}\left(H + \hat{\xi}_{m-\frac{1}{2}}\right), \end{aligned}\quad (53)$$

where $P_{\Delta}(H)$ denote the pulse distribution having width Δ and centered at the origin $H = 0$. It is to be pointed out that, by virtue of the said piecewise linearization of the normalized positioning, amplitude and phase functions, each term $F_{A_m}(\psi)$ in (47), (48) is Fourier-transformed into a function with compact support centered at $H = -\hat{\xi}_{m-\frac{1}{2}} = -\frac{(\hat{\xi}_{m-1} + \hat{\xi}_m)}{2} = -\left(\hat{\xi}_{m-1} + \frac{\widehat{\Delta\xi}_m}{2}\right)$ and having width $\widehat{\Delta\xi}_m$. Upon noticing that the supports of the modulated-pulse functions $\tilde{F}_{A_m}(H)$ are not overlapping, it is straightforward to show that the following equality holds true:

$$\left| \tilde{F}_A(H) \right| = \left| \sum_{m=1}^M \tilde{F}_{A_m}(H) \right| = \sum_{m=1}^M \left| \tilde{F}_{A_m}(H) \right|. \quad (54)$$

A similar property is featured by the argument of the Fourier-transformed auxiliary function, namely:

$$\arg \left\{ \tilde{F}_A(H) \right\} = \arg \left\{ \sum_{m=1}^M \tilde{F}_{A_m}(H) \right\} = \sum_{m=1}^M \arg \left\{ \tilde{F}_{A_m}(H) \right\}. \quad (55)$$

The array synthesis is carried out by enforcing $\tilde{F}_A(H) = \tilde{F}_{\text{Obj}}(H)$ or, equivalently, $\tilde{F}_{A_m}(H) = \tilde{F}_{\text{Obj}}(H)$ within each interval $H \in [-\hat{\xi}_m, -\hat{\xi}_{m-1}]$ for $m = 1, 2, \dots, M$. So, by making use of (52), we have defined a calculation procedure consisting of three stages. In the first stage, the continuous element location function $\xi(q)$ is calculated, for each evaluation segment q_m , employing the integral equation defined in Caratelli and Viganó (2011), as:

$$\int_{\xi(q_{m-1})}^{\xi(q_m)} \left| \tilde{F}_{\text{Obj}}(-H) \right| dH = \pi(q_m - q_{m-1})(A(q_{m-1}) + A(q_m)) \quad (56)$$

where $\tilde{F}_{\text{Obj}}(H)$ is the spatial Fourier transformation of the objective array factor F_{Obj} , which is defined in terms of the spatial variable H for each segment q_m of the M segments. Thus, the synthesis procedure to determine the unknown quantities of element location $\xi(q_m)$ and amplitude excitation current $A(q_m)$, should be associated with the observability window W_m obtained as:

$$W_m = \int_0^{\Delta\xi_w} \left| \tilde{F}_O(-H - \xi(q_{m-1})) \right| dH, \quad (57)$$

where $\Delta\xi_w$ is the aperture of W_m , which is computed as $\Delta\xi_w = (d_{\min}N)/(\lambda_0M)$ in terms of the minimal distance d_{\min} between the N antenna elements, where λ_0 is the free-space wavelength. Once the value of W_m has been determined, the second stage consists of computing the value of $A(q_m)$ as:

$$A(q_m) = \begin{cases} \frac{W_m}{\pi(q_m - q_{m-1})} - A(q_{m-1}) & \text{if } W_m \geq A_{\text{ref}}, \\ A_0 & \text{otherwise,} \end{cases} \quad (58)$$

where $A_{\text{ref}} = \pi(q_m - q_{m-1})(A(q_{m-1}) + A_0)$ and A_0 is the minimum power gain level to be operated in the array feeding network. A_0 can be set to the unit, as the authors suggest in Caratelli and Viganó (2011). However, in our experiments we find that when this parameter was relaxed to values greater than the unit, a better response was obtained. Also we found that this parameter has a strong influence on the calculation of the amplitude excitation current distribution.

In the third and last stage, the value of $\xi(q_m)$ is determined by means of an iterative process, where the initial value of ξ_0 is calculated as in Caratelli and Viganó (2011). The iterative process consists of increasing the integral upper limit until obtaining the right side equality in (56). During the solution process the Gauss-Kronrod quadrature integration formula was applied, as also suggested in Caratelli and Viganó (2011). However, to obtain an adequate amplitude excitation distribution $A(q)$ in our proposal, it was necessary to apply an envelope detector which can be readily implemented by means of a moving average filter, Hilbert transform or squaring and lowpass filtering. The latter was the one that we selected in our study, due that is a straightforward methodology to implement.

3.2 Phase optimization method to obtain the excitation phase

In Caratelli and Viganó (2011) the authors propose a phase synthesis $\alpha(q_m)$ by enforcing the point-matching condition at each node $H = -\xi(q_m)$, defined as $\alpha(q_m) =$

$\arg\{\tilde{F}_{\text{Obj}}(-\xi(q_m))\}$. However, since the properties of the required phase function $\alpha(q)$ essentially depend on the evenness of the amplitude excitation function $A(q)$ and the objective array factor F_{Obj} , the point-matching condition can be optimized in order to increase the fulfillment of beam pattern mask constraints over the sparse antenna arrays. Thereby, our proposal uses the Phase Optimization Method (POM) initially developed by Katsenelenbaum and Semenov (1967); Voitovich and Semenov (1968); Semenov (1969); Voitovich and Semenov (1970) for the multi-element phase field transformers and then transferred by Semenov (1972) to the antenna context. A complete description of this methodology is described below:

3.2.1 Phase optimization problems

Consider the following equation

$$|A\mu| = F, \quad (59)$$

where A is a linear bounded operator acting from the Hilbert space H_1 of L_2 -type into another space H_2 of the same type and F is a given non-negative function from H_2 . The following inner product is introduced, Bulatsyk *et al.* (2010):

$$(\mu_1, \mu_2)_1, \quad \mu_1, \mu_2 \in H_1, \quad (60a)$$

$$(f_1, f_2)_2, \quad f_1, f_2 \in H_2 \quad (60b)$$

in the spaces H_1 and H_2 denote the norms associated with them by

$$\|\mu\|_1^2 = (\mu, \mu)_1, \quad \|f\|_2^2 = (f, f)_1. \quad (61)$$

The problem is to find the function $\mu \in H_1$ which minimizes the functional

$$\sigma(\mu) = \||A\mu| - F\|_2^2. \quad (62)$$

The problem defined by (62) is reduced to a nonlinear Lagrange-Euler equation. Thus we must calculate the first variation of the functional, that is, the linear part $\delta\sigma$ of the perturbed functional

$$\sigma(\mu + \delta\mu) = \sigma(\mu) + \delta\sigma(\mu, \delta\mu) + o(\delta\mu), \quad (63)$$

caused by an arbitrary small perturbation $\delta\mu \in H_1$ of the function μ . It is convenient to write the functional $\sigma(\mu)$ in the form

$$\sigma(\mu) = (A\mu, A\mu)_2 - 2(|A\mu|, F)_2 + \|F\|_2^2 \quad (64)$$

and introduce the notation

$$f = A\mu. \quad (65)$$

Replacing μ by $\mu + \delta\mu$ in (64) and keeping the linear part of the perturbation, we obtain

$$\sigma(\mu + \delta\mu) = \sigma(\mu) + 2\text{Re}(\delta f, f)_2 - 2(\delta|f|, F)_2, \quad (66)$$

where

$$\delta f = A[\delta\mu], \quad (67)$$

$$\delta |f| = |f + \delta f| - |f|. \quad (68)$$

Multiplying the right-hand side of (68) by the unit factor $\frac{(|f+\delta f|+|f|)}{(|f+\delta f|+|f|)}$ and making simple derivations (dropping the values of higher order), we obtain:

$$\begin{aligned} \delta |f| &= \frac{|f + \delta f|^2 - |f|^2}{|f + \delta f| - |f|} = \frac{(f + \delta f)(\bar{f} + \bar{\delta f}) - f \cdot \bar{f}}{|f + \delta f| - |f|} \\ &= \frac{\delta f \cdot \bar{f} + \bar{\delta f} \cdot f}{2|f|} = \operatorname{Re}[\delta f \cdot \exp(-j \arg\{f\})]. \end{aligned} \quad (69)$$

Substituting (67), (69) into (66) and subtracting $\delta(\mu)$ from the result with using (65). we obtain

$$\delta\sigma(\mu, \delta\mu) = 2\operatorname{Re}((A[\delta\mu], A\mu)_2 - (A[\delta\mu] \cdot \exp[-j \arg\{A\mu\}], F)_2). \quad (70)$$

According to $(\mu_1 v, \mu_2) = (\mu_1, \mu_2 \bar{v})$ for any $\mu_1 \in H, \mu_2 \in H, |v| \leq C < \infty$ for the space H_2 ,

$$(A[\delta\mu] \cdot \exp[-j \arg\{A\mu\}], F)_2 = (A[\delta\mu], F \exp[j \arg\{A\mu\}])_2. \quad (71)$$

As a result, we obtain from (70)

$$\delta\sigma(\mu, \delta\mu) = 2\operatorname{Re}(\delta\mu, A^*[A\mu - F \exp(j \arg\{A\mu\})])_1, \quad (72)$$

where A^* is the adjoint operator to A , acting from H_2 to H_1 , that is, the operator

satisfying the identity

$$(A\mu_1, f_2)_2 = (\mu_1, A^* f_2)_1 \quad (73)$$

for any $\mu_1 \in H_1, f_2 \in H_2$. The Lagrange-Euler equation is obtained from the condition

$$\delta\sigma(\mu, \delta\mu) = 0, \quad \forall \delta\mu \in H_1. \quad (74)$$

In particular, if $\delta\mu$ is chosen as an arbitrary real function from H_1 , then (74) yields

$$\operatorname{Re}(A^* A\mu - A^* [F \exp(j \arg \{A\mu\})]) = 0. \quad (75)$$

Similarly, choosing $\delta\mu$ as an arbitrary imaginary function from H_1 , we obtain

$$\operatorname{Im}(A^* A\mu - A^* [F \exp(j \arg \{A\mu\})]) = 0. \quad (76)$$

These two equations together give the sought Lagrange-Euler equation

$$A^* A\mu = A^* [F \exp(j \arg \{A\mu\})] \quad (77)$$

for functional (63). Acting with the operator A on the both sides of (77), we have

$$AA^* f = AA^* [F \exp(j \arg \{f\})]. \quad (78)$$

This equation is equivalent to (77) if the kernel of A is empty, that is, if there are no functions $\mu \in H_1$ such that $A\mu = 0$. If (78) is solved, then the solution to (77) is calculated from the linear equation

$$A^* A\mu = A^* [F \exp(j \arg \{f\})], \quad (79)$$

which is a consequence of (77) and (66). Equation (78) is simpler than (77) both for analytical investigation and numerical solution.

3.2.2 The case for an isometric operator

A mapping U of a metric space (X, ρ_X) into a metric space (Y, ρ_Y) such that $\rho_X(x_1, x_2) = \rho_Y(Ux_1, Ux_2), \forall x_1, x_2 \in X$. If X and Y are real normed linear spaces, $U(X) = Y$ and $U(0) = 0$, then U is a linear operator. An isometric operator U maps X one-to-one onto $U(X)$, so that the inverse operator U^{-1} exists, and this is also an isometric operator, Akhiezer and Glazman (1981). If the operator A is isometric, that is,

$$(A\mu_1, A\mu_2)_2 = (\mu_1, \mu_2)_1 \quad (80)$$

for any $\mu_1, \mu_2 \in H_1$, then

$$(A[\delta\mu], A\mu)_2 = (\delta\mu, \mu)_1. \quad (81)$$

Substituting (81) into (71), we obtain the Lagrange-Euler equation

$$\mu = A^* [F \exp(j \arg \{f\})] \quad (82)$$

instead of (77), and the equivalent one

$$f = AA^* [F \exp(j \arg \{f\})] \quad (83)$$

instead of (78). Since the kernel of any isometric operator is empty, the equations (82) and (83) are equivalent. After (83) has been solved, the solution to (82) is calculated explicitly as

$$\mu = A^* [F \exp(j \arg \{f\})], \quad (84)$$

which is a consequence of (82) and (65).

3.2.3 The iterative method

The simplest iterative method can be proposed for solving (83). In each step of the method, a new approximation of the function f is calculated explicitly by the previous one as follows:

$$f_{p+1} = AA^* [F \exp(j \arg f_p)], \quad \forall p = 0, 1, 2, \dots \quad (85)$$

Form the methodical reasons, we divide each step of the method into two sub-steps and write its scheme shifted up by one substep, as

$$f_p = A\mu_p, \quad (86a)$$

$$\mu_{p+1} = A^* [F \exp(j \arg \{f_p\})]. \quad (86b)$$

We introduce the auxiliary functional related to the $(p + 1)$ -th step of the method:

$$\sigma_p(\mu) = \|A\mu - F \exp(j\psi_p)\|_2^2, \quad (87)$$

where $\psi_p = \arg \{f_p\}$. The function ψ_p is assumed to be given in (87). This functional

can be transformed in the following way:

$$\begin{aligned}\sigma_p(\mu) &= \|A\mu\|_2^2 - 2\operatorname{Re}(A\mu, F \exp(j\psi_p))_2 + \|F\|_2^2 \\ &= \|\mu\|_2^2 - 2\operatorname{Re}(A\mu, F \exp(j\psi_p))_2 + \|F\|_2^2.\end{aligned}\quad (88)$$

The Lagrange-Euler equation can be obtained for this functional. It has the form

$$\mu = A^* [F \exp(j\psi_p)]. \quad (89)$$

This is an explicit form of the function minimizing the functional $\sigma_p(\mu)$. Comparison of (89) with (86b) shows that the function μ coincides with μ_{p+1} . Calculate the difference

$$\begin{aligned}\sigma_p(\mu) - \sigma(\mu) &= 2(|f|, F)_2 - 2\operatorname{Re}(f, F \exp(j\psi_p))_2 \\ &= 2(\operatorname{Re}(f \{1 - \exp[j(\arg\{f\} - \psi_p)]\}), F)_2 \\ &= 2(|f| \{1 - \cos(\arg\{f\} - \psi_p)\}, F)_2 \geq 0.\end{aligned}\quad (90)$$

Here f is given by (66). Note that, in (90), the equality is reached if and only if $\arg\{f\}$ coincides with ψ_p or differ from it by π almost everywhere. The following chain of relations is valid:

$$\sigma(\mu_{p+1}) \leq \sigma_p(\mu_{p+1}) \leq \sigma_p(\mu_p) = \sigma(\mu_p). \quad (91)$$

Indeed, the first inequality follows from (90) applied to $\mu = \mu_{p+1}$, the second one follows from the fact that μ_{p+1} minimizes σ_p , and the third relation (equality) follows

from (90) applied to $\mu = \mu_p$. Consequently,

$$\sigma(\mu_{p+1}) \leq \sigma(\mu_p), \quad (92)$$

that is, each step of the iteration procedure (86a) (and its analogue (85)) does not increase the value of σ . Since σ is bounded from below ($\sigma(\mu) \geq 0$), the numeral sequence $\sigma(\mu_p)$ converges.

3.2.4 Phase optimization applied to the antenna arrays synthesis

Consider the case when the operator A describes the discrete Fourier transform of a finite-dimensional vector. In this perspective, Bulatsyk *et al.* (2010) define the following iterative process, integrating the objective array factor $F_{\text{Obj}}(\mu) \forall -1 \leq \mu \leq 1$:

$$f^{(p)}(\mu) = \sum_{n=1}^N [A_n \exp(j \arg \{w_n^{(p)}\} + jc\xi_n \mu)], \quad (93)$$

$$w_n^{(p+1)} = \int_{-1}^1 F_{\text{Obj}}(\mu) \exp(j \arg \{f^{(p)}(\mu)\} - jc\xi_n \mu) d\mu \quad (94)$$

in this formulation $c = 2\pi/\lambda$, the superscript (p) indicates the iteration number, $\mathbf{w} = \{\arg \{w_n\}\}$ is the vector of excitation current phases, $\mathbf{A} = \{A_n\}$ and $\mathbf{X} = \{\xi_n\}$ are the vectors of excitation current amplitudes and element locations, respectively. The amplitude excitation current values A_n and locations ξ_n can be calculated in a straightforward manner by uniformly sampling over the continuous function $A(q) = \{A(q_m)\}$ and $\xi(q) = \{\xi(q_m)\}$ presented in the previous section 3.1, as:

$$q_n = \text{Lim}_{\text{inf}} + \left[\frac{(\text{Lim}_{\text{sup}} - \text{Lim}_{\text{inf}})}{(N - 1)}(n - 1) \right] \quad (95)$$

where Lim_{inf} and Lim_{sup} are calculated using the bound points that define the sparseness region. A suitable methodology we have considered, to determine these bound points, consists of finding the abrupt changes or discontinuities around the amplitude response $A(q)$. The initial condition for w_n^0 , can be obtained using the expression defined in Bulatsyk *et al.* (2010) as:

$$w_n^0 = \int_{-1}^1 F_O(\mu) \cos(c\xi_n \mu) d\mu. \quad (96)$$

With this iterative procedure we can compute the optimal phase values $\alpha_n = \arg\{w_n\}$ for an objective array factor in a sparse context.

3.3 Numerical Analysis and Assessment

In this section, we assess the performance of our methodology in the synthesis of linear antenna arrays. We show three numerical experiments targeted to synthesize: a narrow-beam, a flat-top, and a square-cosecant beam pattern masks.

3.3.1 Narrow-Beam Pattern Synthesis

As a first numerical experiment, we applied a narrow-beam pattern mask like the one reported by Morabito *et al.* (2012). To achieve a fair comparison among our proposal and Caratelli's approach, we have chosen the number of antenna elements reported in Caratelli and Viganó (2011), for a similar beam pattern. The array factor mask consists in a peak side-lobe level equal to -25dB in the region defined between

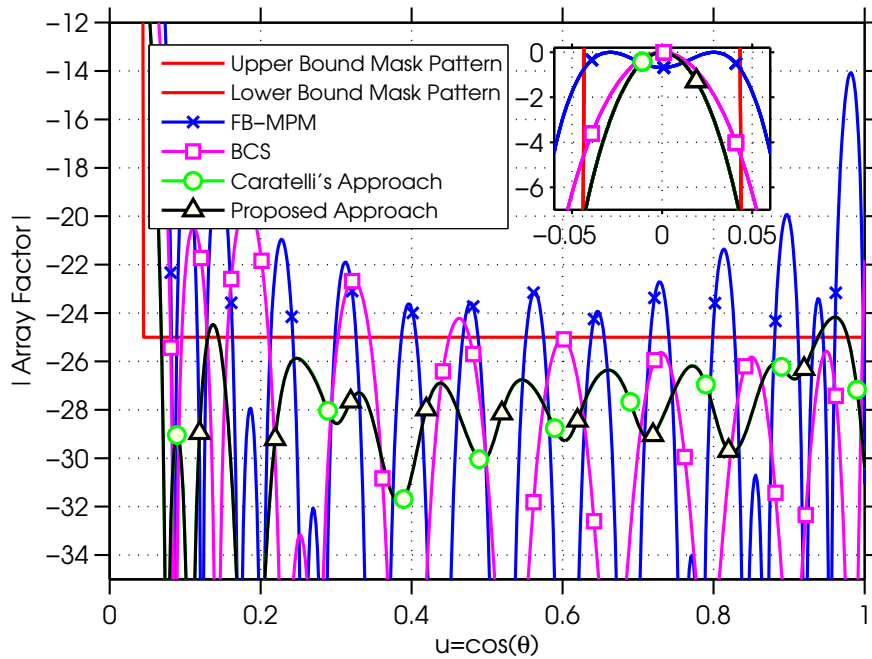


Figure 16. Narrow-beam pattern with 24 antenna elements for each of the evaluated techniques.

$|\theta| \geq 2.5^\circ$. Fig. 16 shows a narrow-beam pattern mask synthesized with 24 antenna elements, where our proposal is compared with the Forward-Backward Matrix Pencil Method (FB-MPM), Liu *et al.* (2010), Bayesian Compressive Sampling (BCS), Oliveri and Massa (2011) and the Caratelli approach Caratelli and Viganó (2011). These three reference methods have been implemented and validated with our computational tool built under the MATLAB[®] programming platform.

From Fig. 16 it can be seen that both the Caratelli's approach and our method are able to obtain better results than BCS and FB-MPM methods in terms of the achieved beam width. In fact, Caratelli's approach and ours produce the same radiation pattern in this scenario. The reason is due to the negligible impact of the excitation phase in the synthesis of narrow beam patterns with no beam steering, which makes

less critical the computation of optimized phase values. Of note is also that results presented for the Caratelli method does not consider the excitation phase component (i.e., the same phase is used for all antenna elements) since the applicability of the matching-point criteria specified in Caratelli and Viganó (2011) resulted always in poorer performance. The bounds of the sparseness region for this particular numerical experiment have been found to be $\text{Lim}_{\text{inf}} = 0.0380$ and $\text{Lim}_{\text{sup}} = 0.9250$.

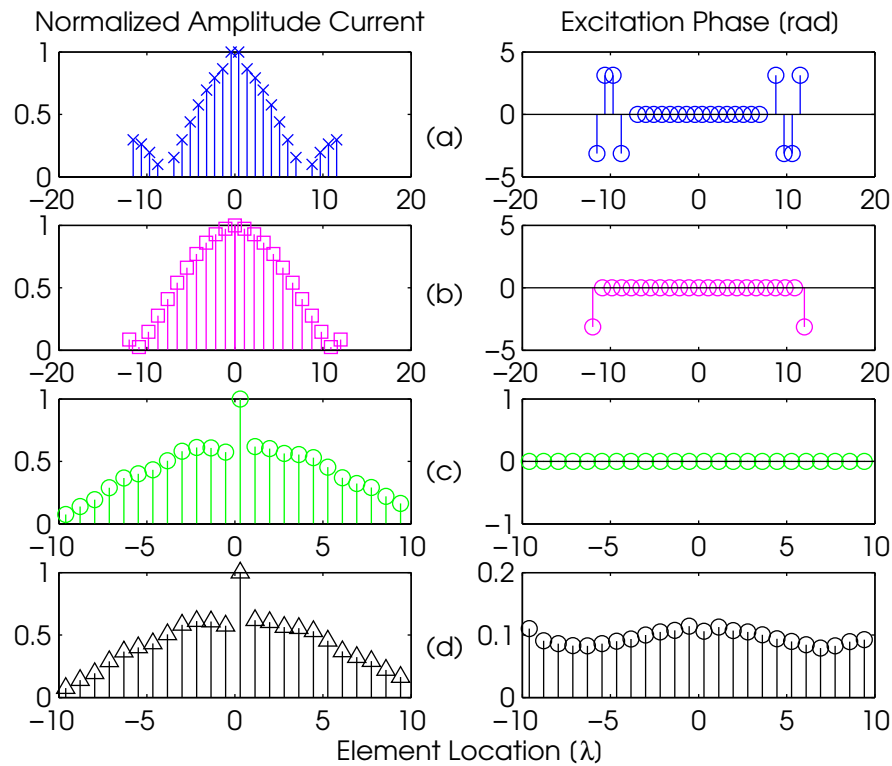


Figure 17. Graphical representation of the normalized amplitude current and excitation phase versus element locations for the narrow-beam pattern with 24 antenna elements, synthesized by means of (a) FB-MPM, (b) BCS, (c) Caratelli's Approach and (d) Proposed Approach.

To get further insight on the results achieved by each method, Fig. 17 shows the normalized amplitude and excitation phase versus the antenna element locations. We see that both Caratelli and our approach exhibit a decreased range of values for the antenna element locations regarding to the other methods. This decrease is

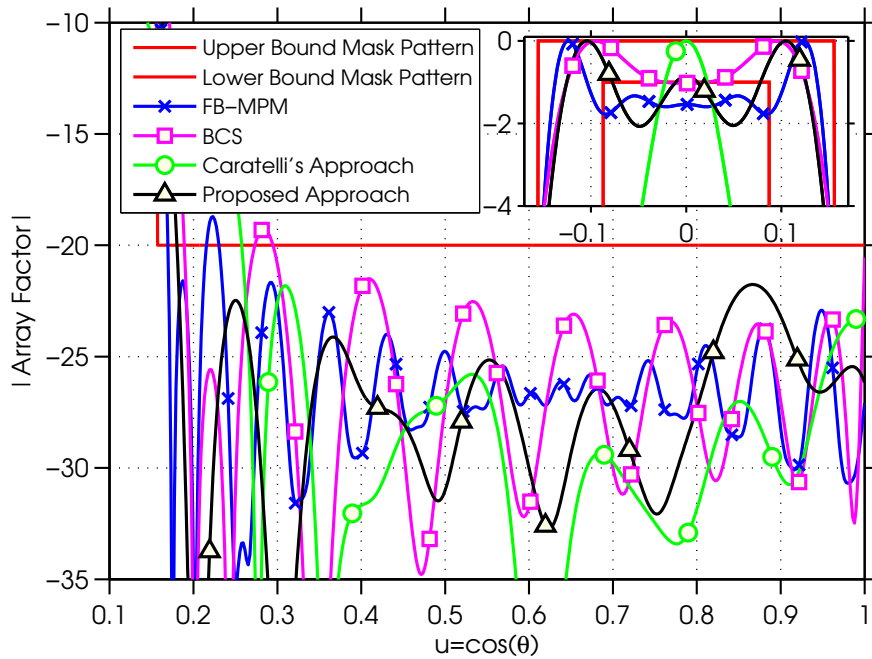


Figure 18. Flat-Top beam pattern synthesized with 22 antenna elements for each of the evaluated techniques.

achieved by the enforcement of the sparseness region bounds that also leads to a smoother fluctuation of the amplitude and phase values over the entire array. Fig. 17 also shows that the main difference among the Caratelli approach and our proposal is the obtained phase distribution.

3.3.2 Flat-Top Beam Pattern

In order to show the benefits to incorporate the phase procedure over Caratelli and Viganó (2011), we use the flat-top beam pattern mask reported by Bucci *et al.* (2013). The considered flat-top shape mask has a maximum ripple equal to ± 0.5 dB for $|\theta| \leq 5^\circ$ and a -20 dB peak side-lobe level for $|\theta| \geq 9^\circ$.

As it can be seen in Fig. 18, our proposal improves the FB-MPM response and outperforms the method proposed by Caratelli and Viganó (2011). Regarding to

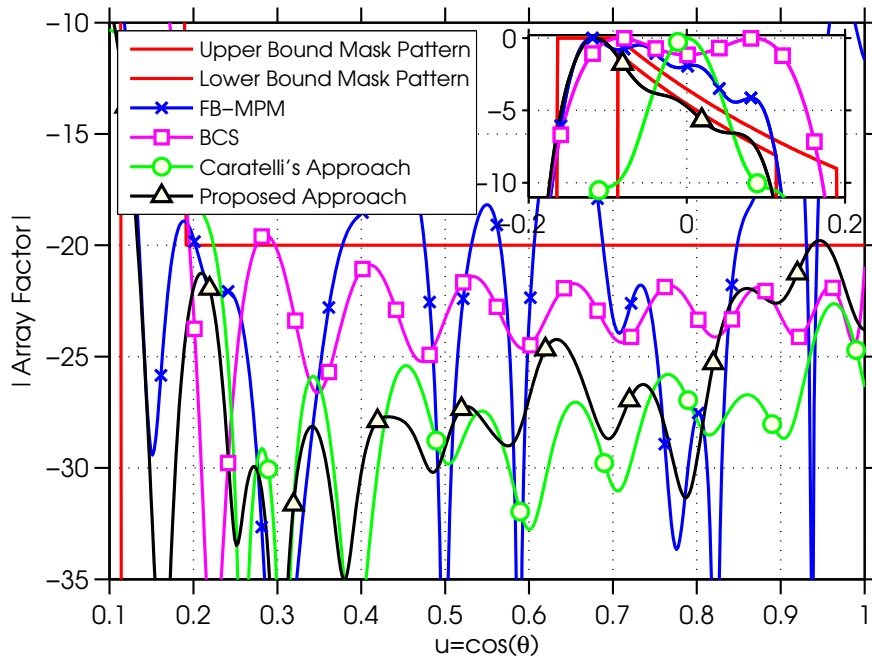


Figure 19. Square-Cosecant beam pattern synthesized with 29 antenna elements for each of the evaluated techniques.

BCS, this method fulfills the requirements on the main lobe region, but exhibits a slightly drawback over the side-lobe region. The array factor response achieved by our proposal has the same response with respect to BCS over the transition region, but in our case the side-lobe constraints was completely fulfilled. The bounds for the sparseness region were calculated as $\text{Lim}_{\text{inf}} = 0.0$ and $\text{Lim}_{\text{sup}} = 1.0$.

3.3.3 Square-Cosecant Beam Pattern

In our last numerical experiment, we use the square-cosecant beam pattern mask proposed in Bucci *et al.* (2013). The square-cosecant shape has a ± 0.5 dB ripple from $\theta = -5^\circ$ to $\theta = 6.5^\circ$, and enforces a peak side-lobe level equal to -20 dB outside the region from $\theta = -9.5^\circ$ to $\theta = 11^\circ$, as shown in Fig. 19.

The results achievable through our approach are able to preserve the peak side-lobe

level, as well as the square-cosecant shape on the mask constraints. As it can be seen, our proposal is able to match the beam pattern mask within the entire visible range, while the others accuracy decreases near the main-lobe and in the far side-lobes. In this numerical experiment, the FB-MPM, BCS, and Caratelli approach are not able to synthesize the desired response. The results achieved by these methods is dissimilar across the main- and side-lobe regions. In particular, inside the main-lobe region, our approach has a nearby behavior between the FB-MPM and BCS methodologies. On the other hand, in the side-lobe region, our approach achieves a suitable response that lies between the BCS and Caratelli approaches, ensuring that the side-lobe level is fulfilled. With this in mind, we conclude that our proposal is able to synthesize antenna arrays close-fitting to the radiation constraints required. The complex current and element locations associated with this array were calculated from the bounds in the sparse region defined as $\text{Lim}_{\text{inf}} = 0.0200$ and $\text{Lim}_{\text{sup}} = 0.9830$.

3.4 Hybrid sparse two-dimensional antenna array synthesis using independent compression regions

In this particular case, our proposed methodology is aimed to extend the hybrid synthesis technique that was developed in Yepes *et al.* (2014b) toward the design of two-dimensional antenna arrays. In addition, we assess our proposal making use of the advantages, that were obtained when the concept of ICR, that was applied to the synthesis of sparse 2D arrays based on the MPM and BCS methods. Our proposal can be described as follows.

1. As a first step, the reference arrays that are shown in Fig. 9 must be determined. We apply any of the sparse linear array synthesis methodologies, such

as MPM, BSC or HSLAS, over the beam pattern mask required for each one of the reference antenna array.

2. Once the product of both reference linear arrays is applied, as proposed in Yepes *et al.* (2013), the resultant planar antenna array response is decomposed into four independent regions, as is shown in Fig. 9. The boundaries for each region can be calculated from the singular value spectrum of each reference array pattern samples, as was reported in Yepes *et al.* (2013).
3. Finally, in order to reduce the reference antenna arrays associated with each independent region, the hybrid synthesis method is applied once again. The synthesized two-dimensional antenna array with sparseness characteristic is obtained from the sum of each independent region.

In order to assess the performance of our methodology in the synthesis of two-dimensional antenna arrays, we show two numerical experiments targeted to synthesize: Small 2-D Arrays and Shaped-Beam 2-D Arrays.

3.4.1 Small 2-D Arrays

The small 2-D array defined in Yepes *et al.* (2013), which has a setup of 10×10 planar array with $\lambda/2$ spacing, is considered. Initially we compressed the reference arrays using the HSLAS method, but we did not improve the results obtained by the MPM methodology. For this reason, the first step of compression was carried out with the MPM method. In a second step, the parameters P and Q were fixed to 5, as is proposed in Yepes *et al.* (2013).

Once the ICR was defined, the HSLAS was applied over each region, nevertheless the results show the same behavior that was reported in Yepes *et al.* (2013).

Table 4. Comparison between planar array specifications reported by Yepes *et al.* (2013) Vs. ICR Method based on HSLAS.

Specifications	Yepes <i>et al.</i> (2013)	ICR Method with HSLAS
MLW in -6 [dB]	0.236	0.234
PSLL in [dB]	-17.9	-17.5
Aperture	$22.29\lambda^2$	$22.29\lambda^2$
CTR	2.2	2.1
Number of Elements	46	46

Whereby, at the sceneries where the phase current does not represent a strong influence about the antenna array response, such as narrow-beam patterns without steering, both the techniques MPM and HSLAS are able to synthesize sparse linear array with similar performance. To support this fact, Table 4 shows the performance among the techniques MPM and HSLAS with respect to the specifications of main-lobe width (MLW), peak side-lobe level (PSLL), aperture, current taper ratio (CTR)

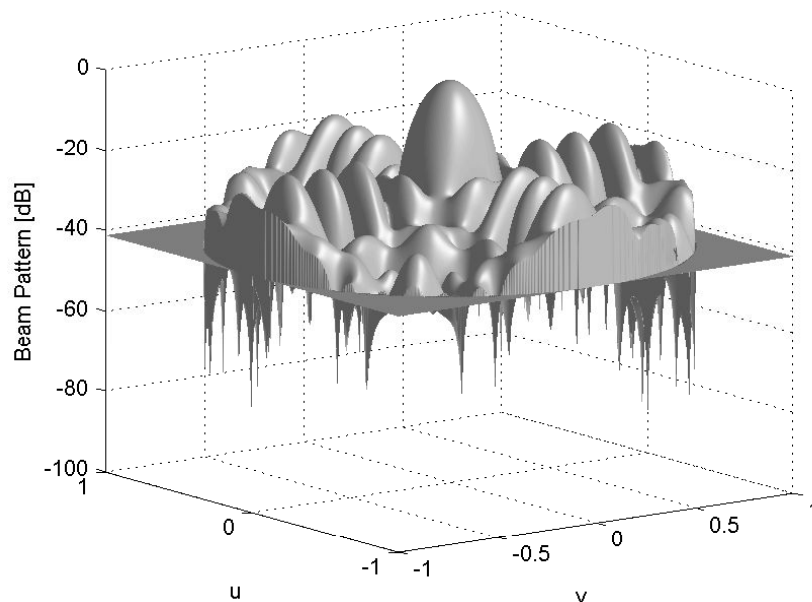


Figure 20. Beam pattern with 46 elements using the ICR method based on HSLAS. The PSLL= -17.5 dB and the MLW = 0.234.

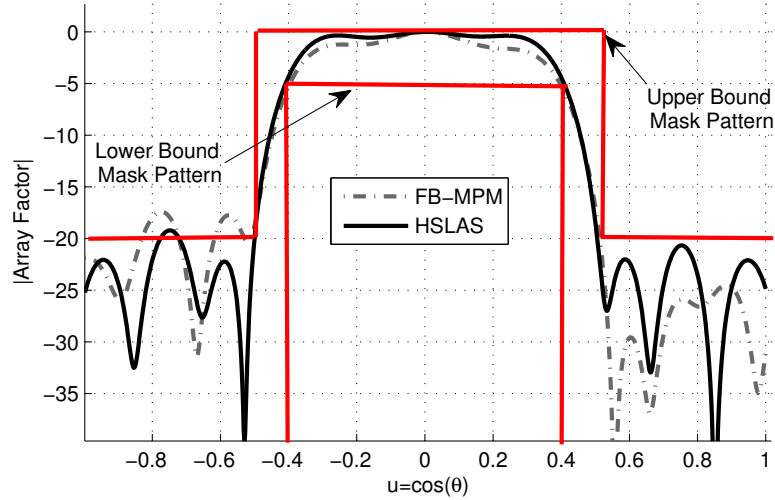


Figure 21. Shaped-beam pattern synthesized with 24 antenna elements for each of the evaluated techniques.

and number of elements. In addition, a graphical representation of the resultant array factor is shown in Fig. 20.

3.4.2 Shaped-Beam 2-D Large Arrays

In order to show the benefits of incorporating the HSLAS technique over the synthesis of shaped-beam 2-D large arrays, we use the flat-top beam pattern mask reported by Bucci *et al.* (2013). The considered flat-top shape mask has a maximum ripple equal to ± 0.5 dB for $|\theta| \leq 5^\circ$ and a -20 dB peak sidelobe level for $|\theta| \geq 9^\circ$.

As it can be seen in Fig. 21, the HSLAS approach improves the other comparable techniques. Accordingly, the HSLAS method was applied at the first procedural step, then, once the singular value spectrum was applied, the boundaries P and Q were calculated with values of 8 and 9, respectively. In order to demonstrate the robust phase compromise of this realization, Fig. 22 shows that the HSLAS method

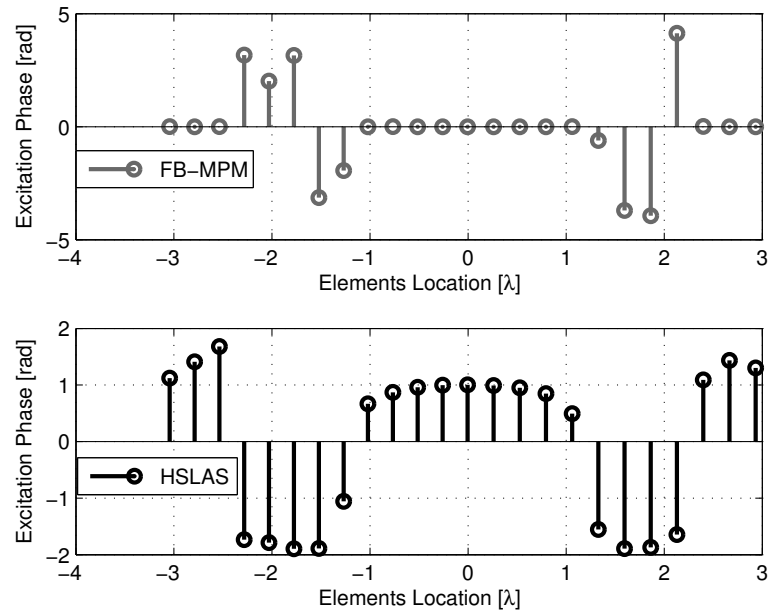


Figure 22. Graphical representation of the excitation phase versus element locations for the shaped-beam pattern with 24 antenna elements, synthesized by means of FB-MPM and HSLAS.

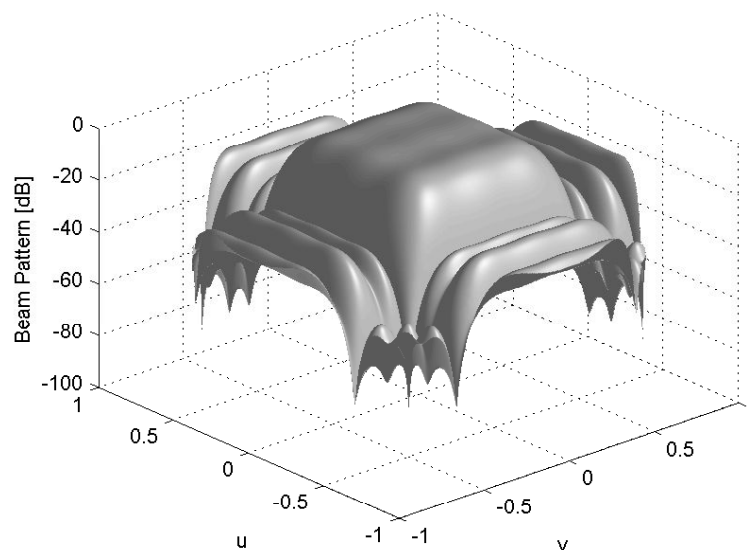


Figure 23. Beam pattern with 224 elements using the ICR method for shaped-beam pattern synthesis. The PSLL = -20 dB and the MLW = 0.856.

has non-zero values over the phase of each element, which allows to fulfill the mask pattern requirements, compared with the phase synthesized by the MPM method. During the final step, in order to increase even more the compression level about the antenna elements number, we applied the FB-MPM method over the region D. In this way, we manage to combine the HSLAS and MPM methods in order to fulfill the sparseness purpose, thanks to the use of the ICR concept. The array factor response is shown in Fig. 23.

3.5 Conclusions

We have presented in this chapter a new hybrid methodology aimed to synthesize linear antenna arrays. The proposed procedure is able to synthesize an objective antenna beam pattern mask when a sparseness characteristic is applied to the number of antenna elements. Moreover, we have carried out three numerical experiments that demonstrated the feasibility of applying our proposal with respect to other procedures that are used for the similar purpose, and were evaluated using the same sparse number of elements. Another contribution has been the definition of the concept of a sparseness region on the array response, as well as the phase optimization with respect to this region, allowing us to enhance the fulfillment of constraints over the antenna beam pattern regarding the method originally proposed in Caratelli and Viganó (2011).

On the other hand, the hybrid sparse methodology was extended to synthesize two-dimensional antenna arrays. The proposed procedure allows to explode the phase optimization provided by the Hybrid Sparse Linear Array Synthesis (HSLAS) method and the versatility of the Independent Compression Regions (ICR) technique, in or-

der to increase the sparseness over the number of the antenna elements. Therefore, we have conducted two numerical experiments where we demonstrated the feasibility of applying our proposal, with respect to other procedures that are used for the similar purpose. Thus, our procedure is able to increase the sparseness when synthesis procedure required a strong phase compromise, such as shaped-beam antenna patterns. Furthermore, we show how the HSLAS and MPM techniques can be simultaneously combined in order to increase even further the overall compression level, thanks to the use of the ICR procedure, achieving in this way a compression level of up to 61.12%.

As seen so far, we can say that we have concluded the first part of this thesis, associated with the antenna array design methodologies with sparseness characteristics, which are aimed to reduced the number of antenna array elements; thus, a minor electric consumption is achieved. In the next two chapters, an additional contribution of this research work is displayed, aimed to the inter-cell interference management. First, in chapter 4 we introduce the coordinate multi-point transmission-reception concept from the coordinated beamforming approach. So, what will be presented in chapter 5 will allow to realize the interconnection of chapters 4, 2 and 3, all through the the energy efficiency optimization criteria.

PART II

INTERFERENCE MANAGEMENT

Coordinated multi-point (CoMP) transmission-reception via coordinated beamforming (CB)

In this chapter, we introduce the second part of this thesis, which is focused on the interference management using Coordinated Multi-point Transmission-Reception (CoMP) scheme. Although the term CoMP may refer to a multitude of schemes, all of them have in common that intra- or inter-cell interference is somehow taken into account, or even exploited to enhance data rates and/or fairness. However, in this chapter is shown an analysis of the state-of-the-art regarding to the theoretical aspects that involves the coordinated beamforming (CB) scheme. To this end, we aims to identify the models and mathematical formulation that we allowing substantiate the analisis that is addressed in the chapter 5.

4.1 Coordinated multi-point (CoMP) transmission-reception schemes and target scenarios

Interference is a major issue limiting the performance in wireless networks. Specifically, as 4G cellular systems densify their cell deployment, co-channel interference becomes a major source of obstacles to cell throughput improvement. In addition, cell edge users suffer more from co-channel interference, which may govern end users experiences, and therefore, schemes for efficient interference management are indispensable.

Base station cooperation concepts (CoMP) are especially attractive since they improve the cell-edge data rate and average data rate, and they are suitable to increase spectral efficiency (and hence capacity) for much more dense network deployments in urban areas and capacity hotspots, Li *et al.* (2014). As we will see later in this chapter, this increase in access capacity with CoMP concepts comes at the cost of more backhaul capacity, i.e. more communication bandwidth between base stations, Marsch and Fettweis (2011).

4.1.1 Mobile cellular scenarios to be analyzed

In order to define the mobile cellular network scenarios to be analyzed, a large cellular system is depicted in Fig 24. Here, a large number of mobile terminals, or user equipments (UE's), is distributed over a set of cells, where we assume that each cell is served by exactly one base station (BS). As this is the case for most currently deployed cellular systems, we further assume that multiple BSs are grouped into a so-called cluster. The term cluster is used to indicate a set of cells between which

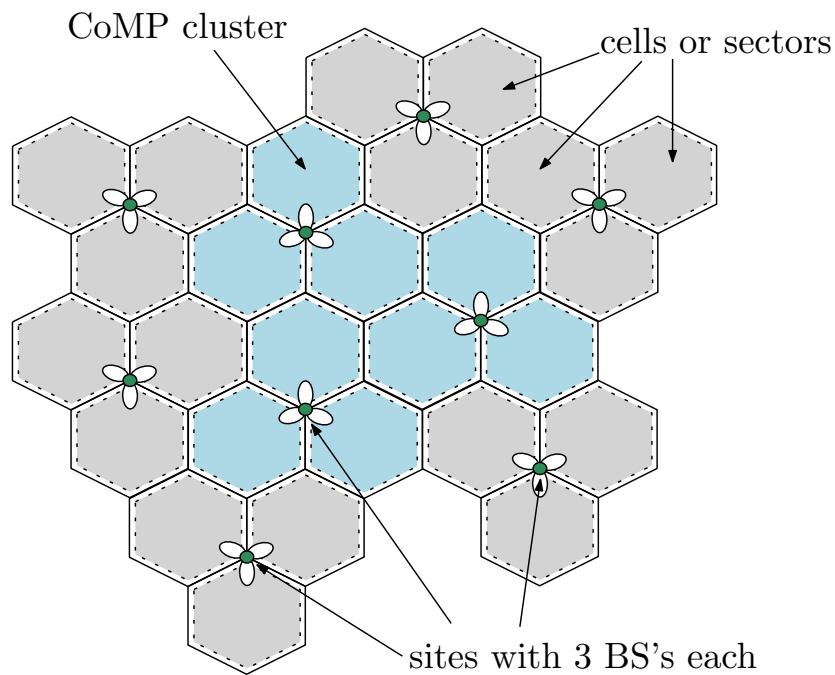


Figure 24. Mobile cellular system considered and the definition of CoMP cluster, Marsch and Fettweis (2011).

some form of CoMP may take place (e.g., joint transmission, coordinated scheduling and coordinated beamforming). As the number of UE's is typically significantly larger than the number of cells, UE's have to be scheduled to resources. In our analysis, we assume that orthogonal frequency division multiple access (OFDMA) is employed as a multiple access technique, which allows each UE to be assigned to resources that are orthogonal in time and frequency, in this way, we simplify most of the analytical models and derivations obtained.

To start our analysis, we introduce a CoMP schemes where no, or little information, is exchanged between cooperating base stations. Initially, we analyze a non-cooperative downlink transmission scheme, where each base station performs individual intra-cell beamforming, while the terminals are able to mitigate inter-cell inter-

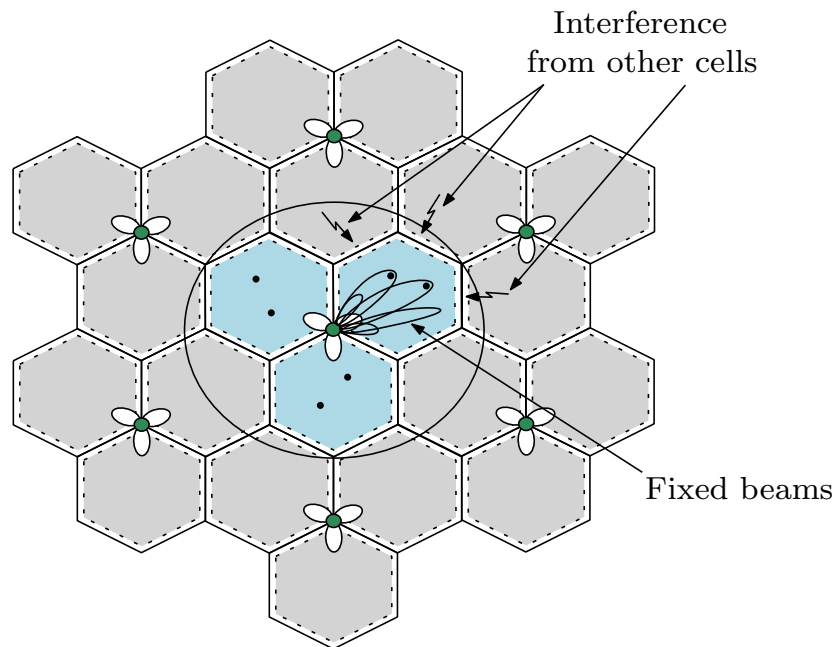


Figure 25. Concept of intra-cell beamforming, Marsch and Fettweis (2011).

ference to a certain extent through a particular interference estimation and rejection concept. Then, the level of base station cooperation is increased and the multi-cell coordinated beamforming is investigated.

4.2 Downlink multi-user beamforming with interference Rejection combining

This approach based on proposal of Thiele *et al.* (2009), analyzes a non-cooperative downlink transmission scheme, i.e. where no explicit cooperation takes place between base stations (BSs), but where interference-aware transmission and reception is performed within cells. The base stations perform intra-cell precoding based on limited feedback information from the user equipments (UEs), in conjunction with interference-aware scheduling and interference rejection combining (IRC) at the terminal side.

The key to success, in this approach, is a predictable interference scenario at the receiver side, which also helps to improve the link adaptation process. Thus, we consider using fixed beams (i.e., fixed sets of possible vectors to be chosen) for transmission as depicted in Fig. 25. In particular, terminals are assumed to report their preferred precoding matrix indicators (PMIs) in combination with corresponding post-equalization signal-to-interference-noise ratios (SINR) via a low-rate feedback channel. The PMI allows the UE to indicate to eNB which precoding matrix should be used for downlink transmission which is determined by Rank Indicator (RI), in which the UE indicates to eNB, the number of layers that should be used for downlink transmission to the UE. RI and PMI can be configured to support MIMO operation (closed loop and open loop spatial multiplexing). These both transmission modes use precoding from a well defined codebook (the lookup table of cross coupling factors used for precoding shared between UE and eNB) to form the transmission layers. In case of transmit diversity PMI and RI need not to be reported to eNB. Another important indicator is the CQI (Channel Quality Indicator), reported by UE to eNB. UE indicates modulation scheme and coding scheme to eNB. To predict the downlink channel condition, CQI feedback by the UE is an input. CQI reporting can be based on PMI and RI. Higher the CQI value (from 0 to 15) reported by UE, higher the modulation scheme (from QPSK to 64QAM) and higher the coding rate will be used by eNB to achieve higher efficiency. Dahlman *et al.* (2011). For the equalization at the UE, comprehensive channel knowledge on the radio system is required, which may be obtained by multi-cell channel estimation based on pilot symbols. Therefore, downlink transmission has to be synchronized.

4.2.1 Downlink system model

We define an OFDMA transmission on a single sub-carrier from M BSs to K UEs that are scheduled to the same resource in time and frequency. The BSs and UEs are equipped with N_{bs} and N_{ue} antennas, respectively, leading to an overall number of $N_{\text{BS}} = MN_{\text{bs}}$ transmit antennas and $N_{\text{UE}} = KN_{\text{ue}}$ receive antennas. This implies that each BS may transmit up to N_{bs} streams simultaneously on the same resource, while each UE may receive up to N_{ue} such streams simultaneously. In the downlink, the precoding, transmission and equalization of each OFDM symbol on a single sub-carrier can be established as

$$\bar{\mathbf{x}} = \mathbf{G}^H \mathbf{y} = \begin{bmatrix} \mathbf{G}_1^H & & \mathbf{0} \\ & \ddots & \\ \mathbf{0} & & \mathbf{G}_K^H \end{bmatrix} (\mathbf{H}^H \mathbf{W} d\{\mathbf{x}\} + \mathbf{n}) \quad (97)$$

where $\mathbf{x} \in \mathbb{C}^{[N_{\text{UE}} \times 1]}$ are the symbols to be transmitted to the UEs, and $d\{\cdot\}$ can be any arbitrary manipulation of these symbols performed by the BS. $\mathbf{W} \in \mathbb{C}^{[N_{\text{BS}} \times N_{\text{UE}}]}$ is a precoding matrix applied at the BS side. The transmit covariance¹ is now given as

$$\Phi_{ss} = E \left\{ \mathbf{W} d\{\mathbf{x}\} (d\{\mathbf{x}\})^H \mathbf{W}^H \right\}, \quad (98)$$

which is typically subject to either a sum, per-BS or per-antenna power constraint.

$\mathbf{H} \in \mathbb{C}^{[N_{\text{BS}} \times N_{\text{UE}}]}$ is the channel matrix. $\mathbf{G} \in \mathbb{C}^{[N_{\text{BS}} \times N_{\text{UE}}]}$ is a matrix containing the UE-side receive filters, which is block-diagonal, this is an true assumption, if and only if,

¹The transmit covariance matrix among various transmission-receptions points, is used to determine, under certain assumptions, the relative gain amounts of different transmission-reception points that the coordinated scheme should or are predicted to choose to hold in a diversity context. Cover and Thomas (1991)

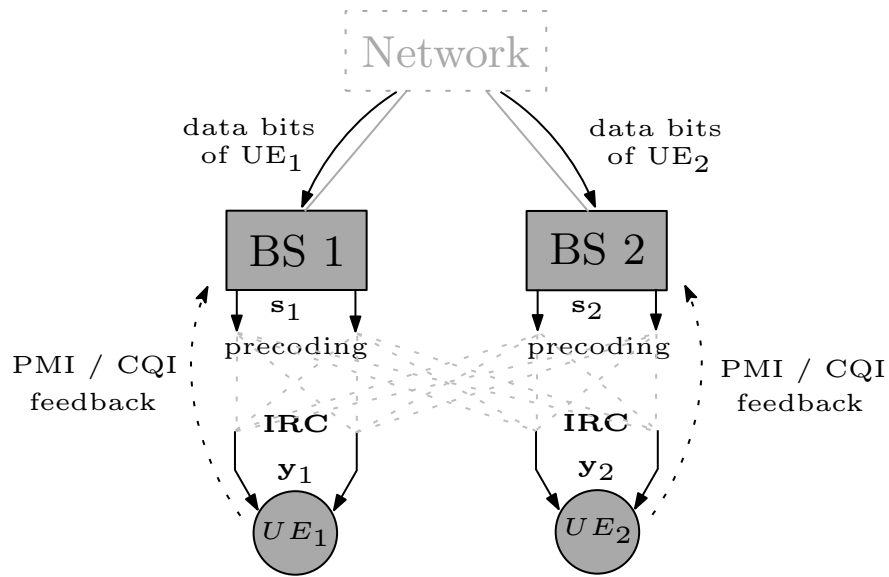


Figure 26. Non-cooperative transmission and PMI/CQI feedback concept considered, Marsch and Fettweis (2011).

when a noncooperation takes place between UEs, $\mathbf{n} \in \mathbb{C}^{[N_{UE} \times 1]}$ is the thermal noise and background interference present at the receive antennas of the UEs, which we assume zero-mean Gaussian with covariance $E\{\mathbf{nn}^H\} = \sigma^2 \mathbf{I}$. Each UE finally obtains estimates $\bar{\mathbf{x}} \in \mathbb{C}^{[N_{UE} \times 1]}$ of the originally transmitted symbols \mathbf{x} .

As we are observing non-cooperative downlink transmission, this means that each stream may only be transmitted from one BS, as illustrated for a setup with $M = K = 2$ in Fig. 26. Consequently, the overall precoding matrix $\mathbf{W} \in \mathbb{C}^{[N_{BS} \times N_{UE}]}$ is sparse, as each column connected to one UE and one stream may only have non-zero entries connected to the antennas of one BS. In the sequel, let us observe one UE k which is served by BS $m = k$. While set \mathcal{K} captures all K UEs, we denote as \mathcal{K}_m the set of all UEs served by BS m simultaneously on the same resource, which is obviously limited to the number of BS transmit antennas, e.g. $|\mathcal{K}_m| \leq N_{bs}$. All received signals of our observed UE k can be expressed as

$$\mathbf{y}_k = \underbrace{(\mathbf{H}_k^m)^H \mathbf{W}_k^m}_{\bar{\mathbf{H}}_k} \mathbf{x}_k + \underbrace{\sum_{j \in \{\mathcal{K}_m \setminus k\}} (\mathbf{H}_k^m)^H \mathbf{W}_j^m \mathbf{x}_j}_{\text{Intra-cell interf. } \zeta_k} + \underbrace{\sum_{j \in \{\mathcal{K} \setminus \mathcal{K}_m\}} (\mathbf{H}_k)^H \mathbf{W}_j \mathbf{x}_j}_{\text{Inter-cell interf. } \mathbf{z}_k} + \mathbf{n}_k, \quad (99)$$

where \mathbf{H}_k is the channel between UE k and all BSs, \mathbf{W}_k is the compound precoding vector used to serve UE k , and \mathbf{H}_k^m and \mathbf{W}_k^m are the sub-portions of these matrices or vectors connected to BS m . We denote as $\bar{\mathbf{H}}_k$ the effective channel between UE k and its serving BS after precoding, which consists of one column for each of the N_{ue} streams the UE may potentially receive, i.e. $\bar{\mathbf{H}}_k = [\bar{\mathbf{H}}_{k,1} \cdots \bar{\mathbf{H}}_{k,N_{\text{bs}}}]$. The corresponding potential data streams stacked in \mathbf{x}_k with $\mathbf{x} \sim \mathcal{N}_{\mathbb{C}}(\mathbf{0}, \mathbf{I})$ are distorted by the intra-cell, inter-cell interference and noise aggregated in ζ_k and \mathbf{z}_k , respectively. Each BS m may select a limited number, $Q_m \leq N_{\text{bs}}$, of active beams to serve one user with multiple beams or multiple users simultaneously. This is done by choosing the corresponding columns of BS m -related precoding matrix \mathbf{W}^m from the columns of a pre-defined beam set Ω_i^m . In the case of $N_{\text{bs}} = 2$, beam set size $\omega = 2$ and discrete Fourier transform (DFT)-based precoding, this can be either

$$\Omega_1^m = \frac{1}{\sqrt{2}} \begin{bmatrix} 1 & 1 \\ j & -j \end{bmatrix} \text{ or } \Omega_2^m = \frac{1}{\sqrt{2}} \begin{bmatrix} 1 & 1 \\ 1 & -1 \end{bmatrix}. \quad (100)$$

Columns in \mathbf{W}^m representing streams that are not used, then, they are simply filled with zeros. Note that \mathbf{W}^m has to be scaled depending on the choice of Q_m in order to fulfill a per-base station power constraint, i.e. $\text{tr} \{ \mathbf{W}^m (\mathbf{W}^m)^H \} \leq P_m$. If only one beam is active, i.e. $Q_m = 1$, we name as single stream (SS) mode, while for $Q_m > 1$, we refer to it as multiple stream (MS) mode.

SINR calculation for linear receivers as a performance metric

In information theory and telecommunication engineering, the signal-to-interference-plus-noise ratio (SINR) (also known as the signal-to-noise-plus-interference ratio (SNIR)) is a quantity used to give theoretical upper bounds on channel capacity (or the rate of information transfer) in wireless communication systems such as networks. Analogous to the SNR used often in wired communications systems, the SINR is defined as the power of a certain signal of interest divided by the sum of the interference power (from all the other interfering signals) and the power of some background noise. If the power of noise term is zero, then the SINR reduces to the signal-to-interference ratio (SIR). Conversely, zero interference reduces the SINR to the signal-to-noise ratio (SNR), which is used less often when developing mathematical models of wireless networks such as cellular networks, Andrews *et al.* (2010).

Assuming that a linear equalizer $\mathbf{g}_{k,u}$ is employed to extract the useful signal from \mathbf{y}_k connected to stream u , this yields a post-equalization SINR given by

$$\text{SINR}_{k,u} = \frac{\mathbf{g}_{k,u}^H \bar{\mathbf{h}}_{k,u} \bar{\mathbf{h}}_{k,u}^H \mathbf{g}_{k,u}}{\mathbf{g}_{k,u}^H \mathbf{Z}_{k,u} \mathbf{g}_{k,u}}, \quad (101)$$

where $\mathbf{Z}_{k,u}$ is the covariance matrix of the streams received by UE k (except stream u) and the interfering signals and noise aggregated in ζ_k and \mathbf{z}_k , i.e. $\mathbf{Z}_{k,u} = \sum_{v \neq u} \bar{\mathbf{h}}_{k,v} (\bar{\mathbf{h}}_{k,v})^H + E \left\{ (\zeta_k + \mathbf{z}_k) (\zeta_k + \mathbf{z}_k)^H \right\}$. For IRC, Winters (1984), the interference-aware minimum mean square error (MMSE) receiver is used, i.e.

$$\mathbf{g}_{k,u}^{\text{MMSE}} = \mathbf{R}_{yy,k}^{-1} \bar{\mathbf{h}}_{k,u}, \quad (102)$$

where $\mathbf{R}_{yy,k}$ denotes the covariance matrix of the received signal \mathbf{y}_k , i.e.

$$\mathbf{R}_{yy,k} = E \left\{ \mathbf{y}_k (\mathbf{y}_k)^H \right\} = \bar{\mathbf{H}}_k \bar{\mathbf{H}}_k^H + E \left\{ (\zeta_k + \mathbf{z}_k) (\zeta_k + \mathbf{z}_k)^H \right\}. \quad (103)$$

The derivation of the MMSE receiver is addressed by Winters (1984), Marsch and Fettweis (2011), they obtain that the MMSE receiver yields a post-equalization SINR

$$\text{SINR}_{k,u}^{\text{MMSE}} = \bar{\mathbf{h}}_{k,u}^H \mathbf{Z}_{k,u}^{-1} \bar{\mathbf{h}}_{k,u}. \quad (104)$$

Based on this SINR, the achievable spectral efficiency can be estimated in an down-link OFDMA multi-cellular simulation environment. Another approach, based on maximum ratio combining (MRC), Winters (1984), can be implemented in order to compare the MMSE receiver performance. The MRC receiver is defined as

$$\mathbf{g}_{k,u}^{\text{MRC}} = \bar{\mathbf{h}}_{k,u} \quad (105)$$

yielding a post-equalization SINR

$$\text{SINR}_{k,u}^{\text{MRC}} = \frac{\|\bar{\mathbf{h}}_{k,u}^H \bar{\mathbf{h}}_{k,u}\|^2}{\bar{\mathbf{h}}_{k,u}^H \mathbf{Z}_{k,u} \bar{\mathbf{h}}_{k,u}}. \quad (106)$$

4.2.2 Imperfect radio channel estimation

The evaluation of the performance metric defined above, only can be assessed if a radio channel matrix (\mathbf{H}) is estimated. For theoretical investigations, full channel state information at the receiver (CSIR) may be assumed. In wireless communications, channel state information (CSI) refers to known channel properties of a communication link. This information describes how a signal propagates from the

transmitter to the receiver and represents the combined effect of, for example, scattering, fading, and power decay with distance. The CSI makes it possible to adapt transmissions to current channel conditions, which is crucial for achieving reliable communication with high data rates in multi-antenna systems. CSI needs to be estimated at the receiver and usually quantized and fed back to the transmitter (although reverse-link estimation is possible in TDD systems). Therefore, the transmitter and receiver can have different CSI. The CSI at the transmitter and the CSI at the receiver are sometimes referred to as CSIT and CSIR, respectively, Dahlman *et al.* (2011).

In order to obtain the achievable data rate in a practical system, different channel estimation models have been developed in the literature. In Thiele *et al.* (2008), the IRC methodology was evaluated and it has shown to be highly sensitive to the estimation errors, since the spatial structure of the interference covariance matrix is utilized for equalization. Therefore, we assume quasi-static channel conditions over the observation interval. Besides, we assume perfect synchronization between UEs and their serving BSs and a sufficiently large cyclic prefix, which alleviates the effect of inter-symbol interference (ISI).

From the radio channel theory, we distinguish between the following radio channel cases:

- **Non-synchronization BSs**, i.e. BSs are not synchronized to each other with respect to the carrier frequencies and frame start. Therefore, we introduce channel estimation errors according to

$$\hat{\mathbf{h}}_{k,u} = \bar{\mathbf{h}}_{k,u} + \delta_{k,u}. \quad (107)$$

Where the term $\hat{\mathbf{h}}_{k,u}$ denotes the biased estimate of variable $\bar{\mathbf{h}}_{k,u}$, and $\delta_{k,u}$ denotes the zero-mean Gaussian distributed error with variance μ . For SINR estimation, we consider knowledge on frequency-flat and frequency-selective independently and identically distributed (i.i.d) interference power σ_{IF}^2 according to the following expressions:

- **Frequency-flat i.i.d interference power** σ_{IF}^2

$$\hat{\mathbf{Z}}_{k,u} = \left[E_q \left\{ \left(\sum_{\forall j,v} |\bar{\mathbf{h}}_{j,v}(q)|^2 \right) - |\hat{\mathbf{h}}_{k,u}(q)|^2 \right\} + \sigma^2 \right] \cdot \mathbf{I} \quad (108)$$

- **Frequency-selective i.i.d interference power** σ_{IF}^2

$$\hat{\mathbf{Z}}_{k,u}(q) = \left[\left(\sum_{\forall j,v} |\bar{\mathbf{h}}_{j,v}(q)|^2 \right) - |\hat{\mathbf{h}}_{k,u}(q)|^2 + \sigma^2 \right] \cdot \mathbf{I} \quad (109)$$

- **Frequency-selective covariance** $\mathbf{Z}_{k,u}$

$$\hat{\mathbf{Z}}_{k,u}(q) = E_n \{ \mathbf{y}_k(q, n) \mathbf{y}_k(q, n)^H \} - \hat{\mathbf{h}}_{k,u}(q) \hat{\mathbf{h}}_{k,u}(q)^H. \quad (110)$$

- **Synchronized Bss**, using multi-cell channel estimation based on virtual pilot sequences $c_{k,u}(n)$, Thiele *et al.* (2008). These sequences are block-orthogonal and defined over time-domain. For channel estimation, the receiver uses a simple correlator. For simplicity, we drop the subcarrier index q in the sequel. According to Thiele *et al.* (2008), we use pilot sequences $c_{k,u}(n)$ which are derived from Hadamard matrices. Hence, the multi-cell channel knowledge

degrades with increasing mobility of the UE, and we state

$$\hat{\mathbf{h}}_{k,u} = \frac{1}{N} \sum_{n=0}^{N-1} c_{k,u}^*(n) \mathbf{y}_k(n) \quad (111)$$

$$\hat{\mathbf{Z}}_{k,u} = \sum_{\forall j,v} \hat{\mathbf{h}}_{j,v} \hat{\mathbf{h}}_{j,v}^H - \hat{\mathbf{h}}_{k,u} \hat{\mathbf{h}}_{k,u}^H. \quad (112)$$

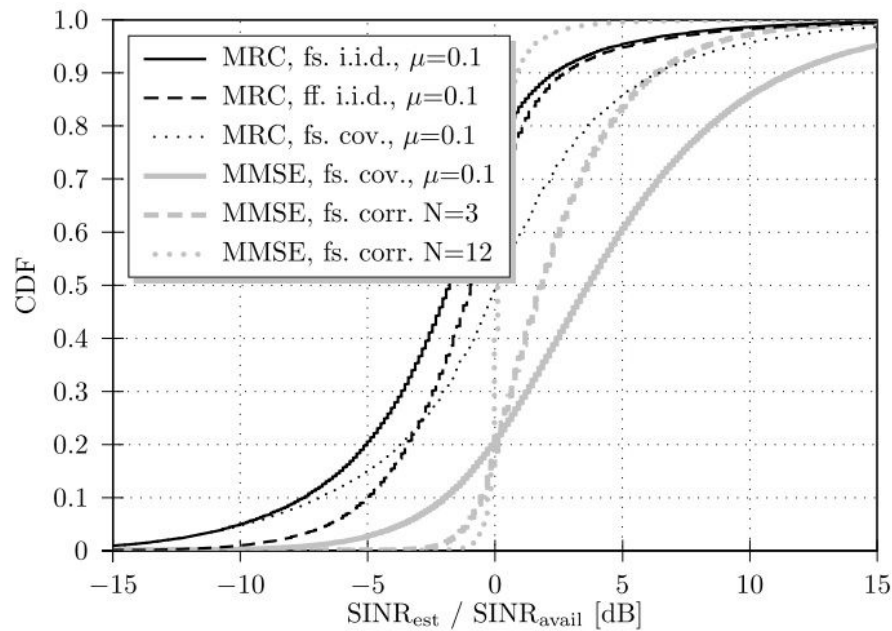
4.2.3 Performance assessment under multi-cell environment with imperfect CSI

In order to analyze the performance of this approach, it is carried out for a triple-sectorized hexagonal cellular network with $M = 57$ BSs in total, i.e. 19 sites of 3 cells/sectors each, forming two circular tiers of interfering sites around a central site used as reference. Simulation parameters are given in Table 5. Fig 27 indicates the estimation error of the single-stream SINR at the terminal. We compare the ratio of the estimated SINR_{est} to the achievable $\text{SINR}_{\text{avail}}$ under perfect CSIR and estimated equalization weights conditions. Employing either MRC in an asynchronous network or IRC in a synchronized network, one of them leads to significantly different estimation errors.

For MRC based on (109), the estimation suffer in two ways: There is a median shift of -1.9 dB, i.e. SINR_{est} is systematically too low. In addition, the estimation error has a considerable variance. With overestimated SINR conditions, the channel may be overloaded, i.e. the reported channel quality indicator (CQI) and the supported MCS do not match, which results in a substantial performance degradation and an increased block error rate (BLER). Assuming that strong channel codes, as well as

Table 5. Simulation assumptions to analyze a multi-cell environment with imperfect CSI.

Parameter	Value
channel model	3GPP Spatial Channel Model
scenario	urban-macro with scenario-mix
traffic model	full buffer
carrier frequency f_c	2 GHz, frequency reuse 1
system bandwidth	18 MHz, 100 PRBs
inter-site distance (ISD)	500 m
number of sites	19 having 3 cells each
N_{bs} ; antenna spacing	1, 2, 4; 4λ
transmit power	46 dBm
sectorization	triple, with FWHM of 68°
BS height	32 m
N_{ue} ; antenna spacing	1, 2, 4; $\lambda/2$
UE height	2 m
CQI granularity	1 Resource Block
feedback delay	0 ms

**Figure 27. SINR estimation error reported by Thiele *et al.* (2009).**

hybrid automatic repeat request (HARQ) mechanisms are able to correct errors if 10% of the resources are overloaded, we have to ensure that the 90th percentile of

$\frac{\text{SINR}_{\text{est}}}{\text{SINR}_{\text{avail}}}$ is below 0 dB. This can be achieved by introducing a safety factor $S < 1$, shifting all SINR_{est} correspondingly. Besides, we can estimate S to be 2.3 dB from Fig. 27. Focusing on the median value, there is an overall penalty (offset) of approx. $\text{SINR}_{\text{pen}} = 4.2$ dB at the multiple access channel (MAC) compared to $\text{SINR}_{\text{avail}}$. Averaging the interference power σ_{IF}^2 over the entire frequency band, i.e. using (108), reduces the penalty to $\text{SINR}_{\text{pen}} = 3.7$ dB. Covariance estimation, i.e. (110), leads to unbiased SINR_{est} , but the S -factor is higher due to the larger variance, resulting in $\text{SINR}_{\text{pen}} = 6.3$ dB. Concentrating on asynchronous downlink transmission, we conclude that an interference estimation scheme assuming a frequency-flat i.i.d. with σ_{IF}^2 results in the highest performance.

The penalties can be further reduced if the interference is estimated more precisely, e.g. in a synchronous system using an MMSE receiver and the correlation approach as given in (111) and (112). For a correlation window spanning $N = 3$ pilot symbols, we assume to be able to distinguish between the channels belonging to 3 out of 57 sectors or cells. Hence, interference cannot be separated sufficiently, and thus SINR is systematically overestimated. However, already with a correlation window spanning $N = 12$ pilot symbols, 12 sectors and thus more interferers can be identified, and the SINR is determined more precisely, Thiele *et al.* (2009). The safety factor is then $S = 0.9$ dB, and the median shift becomes negligible.

4.3 CoMP using downlink coordinated beamforming (CB)

In this section, we consider downlink interference coordination schemes where base stations (BSs) exchange channel state information (CSI) in order to adjust their trans-

mission strategies, so that the generated extent of inter-cell interference is reduced. The term coordinated beamforming was introduced by the 3GPP LTE-A literature, which offer a fair balance between ensuring a reasonable load on the backhaul links, and attaining the performance gains using cooperation. The shared CSI is used by BSs to design individual precoding matrices (or beamforming vectors for single-stream transmission) to transmit exclusively to users within their own cell, Ekbal and Cioffi (2005).

There are several distributed approaches for coordinated beamforming. For example, Ekbal and Cioffi (2005) propose an iterative algorithm to minimize transmit power, which does not necessarily maximize sum-rates. Lee *et al.* (2009), proposes a non-iterative distributed solution to design precoding matrices for multi-cell systems, which will maximize the sum-rates for only a two-cell system at high signal-to-noise ratio (SNR), using a per base station power constraint. Another important partial cooperation-based transmit strategy is inter-cell interference nulling (ICIN), Zhang and Andrews (2010), in which each BS transmit in the null-space of the interference is causing to neighboring cells. Although, all above approaches provide different points of view about coordinated beamforming, we will focus in a proposed developed by Qiang *et al.* (2010), where the signal-to-leakage information² to other cells is exploited, in order to design the precoding vector that reduce the inter-cell interference.

²The leakage term refers to the interference caused by the signal intended for a desired user on the remaining users. That is, leakage is a measure of how much signal power leaks into the other users. The performance criterion for choosing the beamforming coefficients will be based on maximizing the signal-to-leakage-and-noise ratio (SLNR) for all users simultaneously. Sadek *et al.* (2007b)

4.3.1 Coordinated beamforming description and system model

The proposed coordinated beamforming scheme, developed by Qiang *et al.* (2010), has an explicit feedback which denote the full channel state information. This scheme is based on the idea of signal-to-leakage-plus noise ratio (SLNR), Sadek *et al.* (2007a), which maximize the sum of the achievable rate through minimizing the leakage to other UEs, and the precoding metric takes the same form as SLNR. But the SLNR precoding is independently developed for the multi-user downlink channel in a single cell environment. In this way, the proposed scheme provides a solution for selecting a UE at each cell to maximize the total achievable rate, which considers not only the desired signal power in the serving cell, but also the signal broadcasting to the other UEs in adjacent cells as interference.

Considering the downlink CoMP-CB mode comprised of L cells in intra-eNodeB scenario, it is assumed that a single UE uniformly distributed at the edge of each cell is selected by the user scheduler of its serving cell. The UE and the access point (AP) are configured with N_r receive antennas and N_t transmit antennas, respectively. We restrict ourselves to one data stream per UE. The signal received by user k can be represented as

$$\mathbf{y}_k = \mathbf{H}_k^{(k)} \mathbf{w}^{(k)} x_k + \sum_{i=1, i \neq k}^L \mathbf{H}_k^{(i)} \mathbf{w}^{(i)} x_i + \mathbf{n}_k \quad (113)$$

where $\mathbf{H}_k^{(i)}$ denotes the $N_r \times N_t$ channel matrix from i -th cell (i -th AP) to the k -th UE. $\mathbf{w}^{(i)}$ is a $N_t \times 1$ linear precoding vector in the i -th cell, $\|\mathbf{w}^{(i)}\|^2 = 1$, $\forall i = 1, 2, \dots, L$. \mathbf{n}_k denotes the $N_r \times 1$ additive white Gaussian noise (AWGN) vector with

zero mean and universal variance σ^2 . x_i is the signal data information for the i -UE and the total power constraint is imposed by $E\{\|x\|^2\} = P_t$. The second term on the right hand side in (113) is the interference from the other adjacent cells. The signal-to-interference-plus-noise ratio (SINR) at the input of the receive of user k is given by

$$\text{SINR}_k = \frac{P_t \left\| \mathbf{H}_k^{(k)} \mathbf{w}^{(k)} \right\|^2}{N_0 + \sum_{i=1, i \neq k}^L P_t \left\| \mathbf{H}_k^{(i)} \mathbf{w}^{(i)} \right\|^2} \quad (114)$$

where N_0 is the power of the noise. We assume that, the UEs belonged to different cells in the CoMP set feedback the channel state information, through reverse channel link under TDD mode. All the APs share the channel state information under the control of the same eNodeB. From the receive signal expression (113), the capacity of k -th cell can be expressed as Lee *et al.* (2009)

$$C^{(k)} = \log_2 \det \left\{ \mathbf{I} + P_t \left(\mathbf{H}_k^{(k)} \mathbf{w}^{(k)} \right) \left(\mathbf{H}_k^{(k)} \mathbf{w}^{(k)} \right)^H \left(\Psi^{(k)} \right)^{-1} \right\} \quad (115)$$

where $\Psi^{(k)}$ is the covariance matrix of the noise and interference at the UE,

$$\Psi^{(k)} = \sum_{i=1, i \neq k}^L P_t \left(\mathbf{H}_k^{(i)} \mathbf{w}^{(i)} \right) \left(\mathbf{H}_k^{(i)} \mathbf{w}^{(i)} \right)^H + N_0 \mathbf{I} \quad (116)$$

An optimization problem represents to find the precoding vectors for maximizing the total system capacity including the L cells, which can be further denoted as

$$\left(\mathbf{w}_{\text{opt}}^{(1)}, \dots, \mathbf{w}_{\text{opt}}^{(L)} \right) = \arg \max_{(\mathbf{w}^{(1)}, \dots, \mathbf{w}^{(L)})} \left[\sum_{i=1}^L C^{(i)} \right]. \quad (117)$$

In order to simplify the optimization problem in (117), we take $L = 2$ cells as an

example to derive the coordinated beamforming vector. We have referred to the derivation in Sadek *et al.* (2007a)

$$\begin{aligned}
(\mathbf{w}_{\text{opt}}^{(1)}, \mathbf{w}_{\text{opt}}^{(2)}) &= \arg \max_{(\mathbf{w}^{(1)}, \mathbf{w}^{(2)})} \left[\sum_{i=1}^2 C^{(i)} \right] \\
&= \arg \max_{(\mathbf{w}^{(1)}, \mathbf{w}^{(2)})} \left[\log_2 \left(1 + \text{SINR}^{(1)} \right) + \log_2 \left(1 + \text{SINR}^{(2)} \right) \right] \quad (118) \\
&= \arg \max_{(\mathbf{w}^{(1)}, \mathbf{w}^{(2)})} \left[\log_2 \left(1 + \frac{P_t \|\mathbf{H}_1^{(1)} \mathbf{w}^{(1)}\|^2}{N_0 + P_t \|\mathbf{H}_1^{(2)} \mathbf{w}^{(2)}\|^2} \right) + \right. \\
&\quad \left. \log_2 \left(1 + \frac{P_t \|\mathbf{H}_2^{(2)} \mathbf{w}^{(2)}\|^2}{N_0 + P_t \|\mathbf{H}_2^{(1)} \mathbf{w}^{(1)}\|^2} \right) \right].
\end{aligned}$$

Assuming $\text{SINR} \gg 1$, then we can make a close approximation that $\log_2 \left(1 + \text{SINR}^{(i)} \right) \approx \log_2 \left(\text{SINR}^{(i)} \right)$, $\forall i = 1, 2$. Expression (118) will turn into

$$\begin{aligned}
(\mathbf{w}_{\text{opt}}^{(1)}, \mathbf{w}_{\text{opt}}^{(2)}) &\approx \arg \max_{(\mathbf{w}^{(1)}, \mathbf{w}^{(2)})} \left[\log_2 \left(\text{SINR}^{(1)} \right) + \log_2 \left(\text{SINR}^{(2)} \right) \right] \quad (119) \\
&= \arg \max_{(\mathbf{w}^{(1)}, \mathbf{w}^{(2)})} \left[\log_2 \left(\frac{P_t \|\mathbf{H}_1^{(1)} \mathbf{w}^{(1)}\|^2}{N_0 + P_t \|\mathbf{H}_1^{(2)} \mathbf{w}^{(2)}\|^2} \right) + \right. \\
&\quad \left. \log_2 \left(\frac{P_t \|\mathbf{H}_2^{(2)} \mathbf{w}^{(2)}\|^2}{N_0 + P_t \|\mathbf{H}_2^{(1)} \mathbf{w}^{(1)}\|^2} \right) \right] \\
&= \arg \max_{(\mathbf{w}^{(1)}, \mathbf{w}^{(2)})} \left[\log_2 \left\{ \left(\frac{P_t \|\mathbf{H}_1^{(1)} \mathbf{w}^{(1)}\|^2}{N_0 + P_t \|\mathbf{H}_1^{(2)} \mathbf{w}^{(2)}\|^2} \right) \left(\frac{P_t \|\mathbf{H}_2^{(2)} \mathbf{w}^{(2)}\|^2}{N_0 + P_t \|\mathbf{H}_2^{(1)} \mathbf{w}^{(1)}\|^2} \right) \right\} \right] \\
&= \arg \max_{(\mathbf{w}^{(1)}, \mathbf{w}^{(2)})} \left[\log_2 \left\{ \left(\frac{P_t \|\mathbf{H}_1^{(1)} \mathbf{w}^{(1)}\|^2}{N_0 + P_t \|\mathbf{H}_2^{(1)} \mathbf{w}^{(1)}\|^2} \right) \left(\frac{P_t \|\mathbf{H}_2^{(2)} \mathbf{w}^{(2)}\|^2}{N_0 + P_t \|\mathbf{H}_1^{(2)} \mathbf{w}^{(2)}\|^2} \right) \right\} \right].
\end{aligned}$$

Then we get

$$\mathbf{w}_{\text{opt}}^{(1)} = \arg \max_{\mathbf{w}^{(1)}} \left[\frac{P_t \left\| \mathbf{H}_1^{(1)} \mathbf{w}^{(1)} \right\|^2}{N_0 + P_t \left\| \mathbf{H}_2^{(1)} \mathbf{w}^{(1)} \right\|^2} \right] \quad (120)$$

$$\mathbf{w}_{\text{opt}}^{(2)} = \arg \max_{\mathbf{w}^{(2)}} \left[\frac{P_t \left\| \mathbf{H}_2^{(2)} \mathbf{w}^{(2)} \right\|^2}{N_0 + P_t \left\| \mathbf{H}_1^{(2)} \mathbf{w}^{(2)} \right\|^2} \right]. \quad (121)$$

Then, the expression (120) and (121) take the same form as SLNR metric, and the numerator denotes the signal to the serving UE, the denominator refers to the noise plus interference caused by the signal intended for a desired UE on the other UEs in adjacent cells. So we can directly use the SLNR solution, Sadek *et al.* (2007a), to get the optimal precoding vector.

$$\mathbf{w}_{\text{opt}}^{(i)} \propto \text{max eigenvector} \left\{ \left[N_0 \mathbf{I} + \left(\tilde{\mathbf{H}}^{(i)} \right)^H \tilde{\mathbf{H}}^{(i)} \right]^{-1} \left(\mathbf{H}^{(i)} \right)^H \mathbf{H}^{(i)} \right\} \quad (122)$$

where

$$\tilde{\mathbf{H}}^{(i)} = \left[\mathbf{H}_1^{(i)} \cdots \mathbf{H}_{l-1}^{(i)} \mathbf{H}_{l+1}^{(i)} \cdots \mathbf{H}_L^{(i)} \right]^T, \in \mathbb{C}^{LN_r \times N_t}. \quad (123)$$

It is shown that the optimal solution is given by (122) in terms of the eigenvector corresponding to the largest eigenvalue of the matrix $\left\{ \left[N_0 \mathbf{I} + \left(\tilde{\mathbf{H}}^{(i)} \right)^H \tilde{\mathbf{H}}^{(i)} \right]^{-1} \left(\mathbf{H}^{(i)} \right)^H \mathbf{H}^{(i)} \right\}$.

The norm of $\left\| \mathbf{w}_{\text{opt}}^{(i)} \right\|^2 = 1$.

Although this scheme is derived under the case $L = 2$, it can be extended to arbitrary number of cells by adding the channels between the serving cell and the UEs in other cells in (123). The scheme proposed in (122) is sub-optimal in terms of SINR

maximization, yet simple enough that one can find the best linear precoding solution, which has the same identity with SLNR scheme. For CoMP-CB mode, some schemes with limited feedback are under discussion. As we mentioned before, the UE estimates the channel matrices and finds the best-matching precoder from the codebook knowing to both the AP and UE. Then, the UE feeds back the best PMI index of the serving cell, and the least interfering PMI of the neighboring cell to implement coordination. By PMI feedback, beam collision can be avoided. However, the performance is limited for the implicit feedback. And it is complex for the eNodeB to schedule different APs to choose the proper PMIs when the number of APs is increasing.

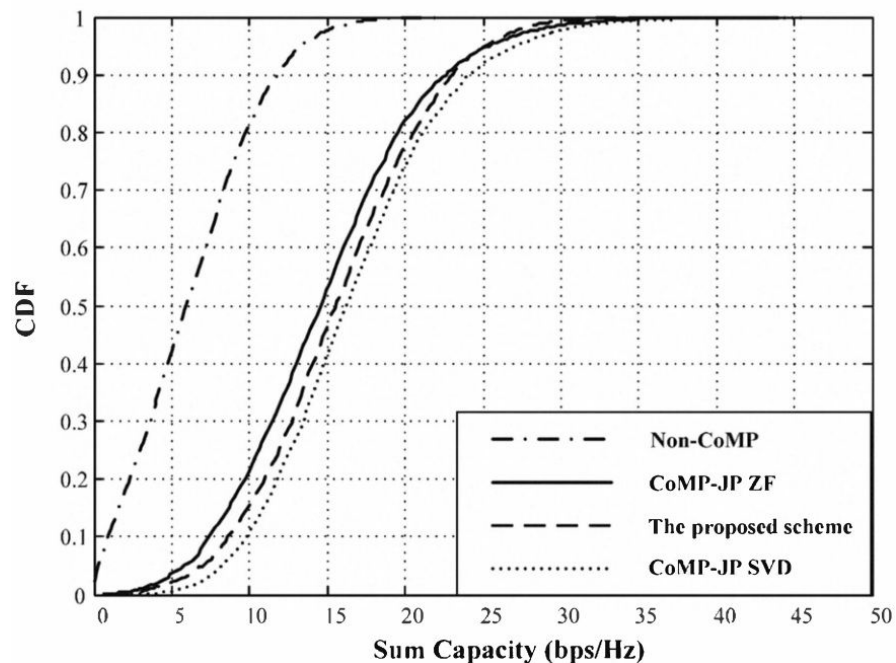
4.3.2 Numerical assessment

In this section, we present the results reported by Qiang *et al.* (2010). The setup of this simulation is listed in Table 6, where is consider that each cell has selected one UE with $L = 2$ APs' coordination.

Fig. 28 shows the cumulative distribution function (CDF) results of the sum system capacity. Each AP is configured with $N_t = 2$ antennas. As a reference, we give the non-CoMP scheme, that means there is no coordination among APs and each UE will suffer from severe interference from other cells. The CoMP joint processing (JP) scheme is also evaluated, in which a zero-forcing (ZF) or singular value decomposition (SVD) procedures was applied in order to obtain the precoder vector to transmit two data streams to a single UE with equal power allocation, which is across two APs' coordination under the control of the same eNodeB.

Table 6. Simulation assumptions to analyze a CoMP-CB based on the SLNR metric.

Parameters	Value
Layout	Hexagonal grid, 3 cells sites, 3 sectors per site
Inter-site distance	500 [m]
Channel model	SCM, urban macro, 1 path
Users per cell	1, dropped uniformly
Minimum distance between UE and cell	≥ 35 [m]
Number of antennas (N_t, N_r)	(4/2, 2)
Antennas separation in wavelength (N_t, N_r)	(10, 0.5) [λ]
Distance-dependent path loss shadowing standard deviation	$L = 34.5 + 35 \log_{10}(R)$, R in [m] 8 [dB]
Bandwidth	10 [MHz]
Carrier Frequency	2 [GHz]
UE speed	3 [Km/h]
Receiver processing	MMSE
Channel estimation error	Ideal estimation
AP transmit power	46 [dBm]
Noise density	-174 [dBm/Hz]

Figure 28. CDF of system sum capacity reported by Qiang *et al.* (2010).

From such results, we can see that the CoMP-JP mode or the CoMP-CB mode are better than Non-CoMP scheme, which confirms that the CoMP technique is a very useful and promising scheme to improve the cell edge capacity. The scheme proposed by Qiang *et al.* (2010), outperforms the CoMP-JP ZF scheme and it is closed to the CoMP-JP SVD scheme. SVD is an optimal linear precoding scheme for the single UE when it applies in ComP-JP mode. Compared with CoMP-JP mode, the Comp-CB mode only requires the channel information exchange which reduces a heavy overhead on the network.

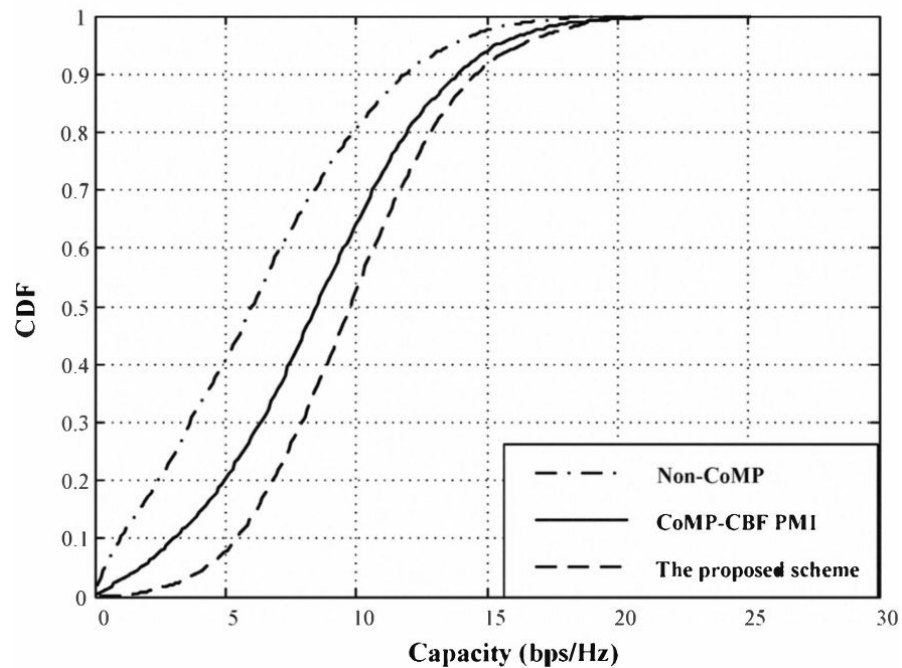


Figure 29. Cumulative distribution function of capacity in one cell reported by Qiang *et al.* (2010).

In Fig. 29, the CDF results of capacity in one cell are given. In this case, one UE is chosen, which denotes the capacity of its cell to analyze the performance gain, each AP has $N_t = 4$ antennas. The codebook is the DFT codebook with the size of

(16, 4), the quantization vectors are 16 and each vector has a dimension of 4. The UE feeds back $B = 4$ bits index PMI. Each AP sends only one data stream to one UE in all schemes. Because of the severe interference without coordination, Non-CoMP scheme performs worst. It can be seen that the SLNR scheme performs much better than the CoMP-CB scheme with PMIs feedback and shows an obvious gain.

4.4 Conclusions

We have conducted two different cases in order to introduce the CoMP schemes where no, or small information, was exchanged between cooperating base stations. First, a non-cooperative downlink transmission scheme was introduced, in which was assumed that the UE terminals are able to estimate their dedicated and a certain number of interfering channel coefficients. Thus, we can conclude two important observations: Efficient MU-MIMO transmission can be achieved by using a fixed unitary precoding, i.e. without the requirement of full channel knowledge. Further, proper application of the MU-MIMO mode, enables to conveniently serve even users with multiple streams, who experience relatively poor SNR conditions. In addition, it was shown that knowledge on the interference channels yields a more precise estimation of the achievable SINR compared to the traditional approach, where the interference is assumed white.

On the other hand, the proposed coordinated beamforming scheme in downlink CoMP system, reported by Qiang *et al.* (2010), only required the channel state information to further reduce the overhead on the network, and it has provided a considerable performance with respect to counterpart Comp-JP scheme. This scheme

has utilized the signal leakage information to other cells to design the precoding vector to mitigate the multi-cell interference. The simulation results have shown that this scheme shows a much higher performance gain even outperforms zero-forcing scheme in CoMP-JP mode. The CoMP-CB mode has started to attract much attention for future research work, because of the low overhead and good performance. In general, CoMP-CB mode is the trend for CoMP technique to be deployed into the practice, which can meet the requirements set by LTE-A.

The next chapter, introduces a new tendency for CoMP-CB technologies, in which is incorporated the energy efficiency metric to the wireless systems in order to reduce the impact on the global carbon footprint. This new approach of CoMP, establishes the state-of-the-art regarding to the concept of the green networks.

Energy efficiency optimization applied to CoMP-CB

The energy efficiency optimization of wireless systems has become urgently important due to its impact on the global carbon footprint. In this chapter, we assess the design of energy efficient multi-cell multi-user precoding (or beamforming), developed by He *et al.* (2014), where a new criterion of weighted sum energy efficiency was considered, which is defined as the weighted sum of the energy efficiencies of multiple-cells, and also can satisfy heterogeneous requirements from different kinds of cells. Besides, we have conducted an entire matlab script in order to obtain and analyze the most relevant results achieved by He *et al.* (2014). In this way, we have contributed with a flexible platform to analyze coordinated base station schemes.

5.1 Coordinated Beamforming formulation under the energy efficiency criterion

With the rapid and radical evolution of the information and communications technology, energy consumption is also growing at a staggering rate, Han *et al.* (2011), and Feng *et al.* (2013). Low energy efficiency in wireless communications may result a negative impact on the environment and increase costs. For high throughput downlink cellular networks, energy efficiency can be defined as the ratio of the sum rate to the total power consumption of the network, which involves transmit power and circuit power, Li *et al.* (2014). It has been recognized that the well-explored transmission schemes designed toward high spectral efficiency do not necessarily provide high energy efficiency, Xu *et al.* (2013). To improve the energy efficiency, we should increase the spectral efficiency and meanwhile decrease the total power consumption.

Inter-cell interference (ICI) is the major limiting factor for improving the spectral efficiency of the full frequency reuse cellular networks. When the base stations with multiple antennas can share some form of information related to channel, coordinated beamforming can effectively alleviate the impact of ICI, which has been optimized from different perspectives, as it has been shown on previous chapter.

5.1.1 System model for CoMP-CB with energy efficiency criterion

Consider a K -cell multi-user MIMO (MU-MIMO) downlink system where each cell includes one multiple antenna base station (BS) and a plurality of multiple antenna users. We denote the k -the user in cell j as User- (j, k) and the BS in cell m as Bs- m . Bs j is equipped with M_j transmit antennas and serves I_j users in cell j .

User- (j, k) is equipped with $N_{j,k}$ antennas. The received signal of User- (j, k) is then expressed as

$$\mathbf{y}_{j,k} = \sum_{m=1}^K \mathbf{H}_{m,j,k} \sum_{n=1}^{I_m} \mathbf{W}_{m,n} \mathbf{x}_{m,n} + \mathbf{z}_{j,k} \quad (124)$$

where $\mathbf{H}_{m,j,k} \in \mathbb{C}^{N_{j,k} \times M_m}$ denotes the flat fading channel coefficient between BS- m and User- (j, k) , including both the large scale fading and the small scale fading, $\mathbf{W}_{j,k} \in \mathbb{C}^{M_j \times d_{j,k}}$ denotes the beamforming matrix for User- (j, k) , $d_{j,k}$ denotes the number of data streams for User- (j, k) , $\mathbf{x}_{j,k} \in \mathbb{C}^{d_{j,k} \times 1}$ denotes the information signal intended for User- (j, k) with pdf $p(\mathbf{x}_{j,k}) = \mathcal{CN}(\mathbf{0}, \mathbf{I})$, and $\mathbf{z}_{j,k} \in \mathbb{C}^{N_{j,k} \times 1}$ denotes the additive white Gaussian noise with distribution $\mathcal{CN}(\mathbf{0}, \sigma_{j,k}^2 \mathbf{I})$. We assume that the signals for different users are independent from each other and the receiver noise.

In order to incorporate the energy efficiency criterion, we will define the energy efficiency measure for each cell, which is defined as the ratio of the weighted sum rate to the per-cell power consumption, given by

$$f_j(\mathbf{W}) = \frac{\sum_{k=1}^{I_j} \bar{\omega}_{j,k} r_{j,k}}{\vartheta_j \sum_{k=1}^{I_j} \text{Tr}(\mathbf{W}_{j,k} \mathbf{W}_{j,k}^H) + M_j P_c + P_0}, \quad \forall j \quad (125)$$

where P_c is the constant circuit power consumption per antenna including power dissipations in the transmit filter, mixer, frequency synthesizer, and digital-to-analog converter, which are independent of the actual transmitted power, P_0 is the basic power consumed at the BS and is independent of the number of transmit antennas, $\vartheta_j \geq 1$ is a constant which accounts for the inefficiency of the power amplifier, Ng *et al.* (2012), the weight $\bar{\omega}_{j,k}$ is used to represent the priority of User- (j, k) , giving a larger value to the user with a higher rate requirement, and $r_{j,k}$ denotes the instan-

taneous rate of User- (j, k) and is calculated as

$$r_{j,k} = \log_2 \left| \mathbf{I} + \mathbf{H}_{j,j,k} \mathbf{W}_{j,k} \mathbf{W}_{j,k}^H \mathbf{H}_{j,j,k}^H \mathbf{R}_{j,k}^{-1} \right| \quad (126)$$

where $\mathbf{R}_{j,k}$ denotes the interference-plus-noise which includes the inter-user interference, the inter-cell interference and the additive Gaussian white noise, given by

$$\mathbf{R}_{j,k} = \sum_{(m,n) \neq (j,k)} \mathbf{H}_{m,j,k} \mathbf{W}_{m,n} \mathbf{W}_{m,n}^H \mathbf{H}_{m,j,k}^H + \sigma_{j,k}^2 \mathbf{I}. \quad (127)$$

For notational convenience, let $\mathbf{W}_j = \{\mathbf{W}_{j,1}, \dots, \mathbf{W}_{j,I_j}\}$ denote the multi-user precoder set of BS j and let $\mathbf{W} = \{\mathbf{W}_1, \dots, \mathbf{W}_K\}$ denote the collection of all the precoders. In order to obtain a trade-off between the sum rate and the total power consumption, we adopt a new energy efficiency optimization criterion defined as, He *et al.* (2014)

$$\begin{aligned} & \max_{\mathbf{W}} \sum_j \alpha_j f_j(\mathbf{W}) \\ \text{s.t. } & \sum_{k=1}^{I_j} \text{Tr}(\mathbf{W}_{j,k} \mathbf{W}_{j,k}^H) \leq P_j, \quad \forall j \end{aligned} \quad (128)$$

where P_j is power constraint of BS- j , α_j is used to satisfy heterogeneous requirements from different cells, for instance the macro cell and small cell in heterogeneous network usually have different energy efficiency priorities. In order to further investigate the relationship between the spectral efficiency maximization and the energy efficiency maximization, the conventional weighted sum rate optimization problem is also considered, given as

$$\begin{aligned}
& \max_{\mathbf{W}} \sum_j \bar{\omega}_{j,k} r_{j,k} \\
\text{s.t. } & \sum_{k=1}^{I_j} \text{Tr}(\mathbf{W}_{j,k} \mathbf{W}_{j,k}^H) \leq P_j, \quad \forall j
\end{aligned} \tag{129}$$

Note that the coupling of the optimization variables leads problems (128) and (129) non-convex and they are therefore difficult to solve directly, which is the main drawback for beamforming algorithm design. Moreover, the sum-f-ratio form in the objective function (128) makes the problem more intractable. In the rest of this chapter, we will focus on finding solutions to the optimization problems in (128) and (129).

5.1.2 Multi-cell multi-user precoding optimization

In order to address the problem (128), we rewrite the numerator expression of its objective function into a quadratic form using a method similar to that used in Wang and Zhang (2010). Based on this, the weighted sum energy efficiency optimization problem can be transformed into parameterized linear optimization through the classical fractional programming approach. Then, an alternating optimization algorithm is developed by He *et al.* (2014) to solve the problem (128), and they prove that the convergence of this proposed iterative algorithm is guaranteed.

Equivalent problem transformation

The function $\log(\cdot)$ in the user rate is nonlinear, which makes problem (128) hard to solve. In what follows, the nonlinear user rate is first transformed into a quadratic form by using some existing methods. According to Lemma 13.8.1 in Cover and Thomas (1991), the achievable rate $r_{j,k}$ of User- (j, k) can be expressed as

$$r_{j,k} = I(\mathbf{y}_{j,k}; \mathbf{x}_{j,k}) = \max_{q(\mathbf{x}_{j,k}|\mathbf{y}_{j,k})} \mathbb{E} \left[\log_2 \frac{q(\mathbf{x}_{j,k}|\mathbf{y}_{j,k})}{p(\mathbf{x}_{j,k})} \right], \quad (130)$$

where $I(\mathbf{y}_{j,k}; \mathbf{x}_{j,k})$ is the mutual information between $\mathbf{y}_{j,k}$ and $\mathbf{x}_{j,k}$; $q(\mathbf{x}_{j,k}|\mathbf{y}_{j,k})$ is the test posterior probability. It was revealed from Wang and Zhang (2010), for fixed beamforming matrix \mathbf{W} , that the optimal test posterior probability $q^{\text{opt}}(\mathbf{x}_{j,k}|\mathbf{y}_{j,k})$ for (130) is the posterior probability $p(\mathbf{x}_{j,k})$, i.e.,

$$\begin{aligned} q^{\text{opt}}(\mathbf{x}_{j,k}|\mathbf{y}_{j,k}) &= p(\mathbf{x}_{j,k}) \\ &= \mathcal{CN}(\mathbf{U}_{\mathbf{x}_{j,k}|\mathbf{y}_{j,k}}\mathbf{y}_{j,k}, \Sigma_{\mathbf{x}_{j,k}|\mathbf{y}_{j,k}}) \end{aligned} \quad (131)$$

where $\mathbf{U}_{j,k}$ and $\Sigma_{j,k}$ are defined as the receiver weight matrix and positive definite covariance matrix of User- (j, k) , respectively. For notational convenience, let $\mathbf{U}_j = \{\mathbf{U}_{j,1}, \dots, \mathbf{U}_{j,I_j}\}$, $\mathbf{U} = \{\mathbf{U}_1, \dots, \mathbf{U}_K\}$, $\Sigma_j = \{\Sigma_{j,1}, \dots, \Sigma_{j,I_j}\}$ and $\Sigma = \{\Sigma_1, \dots, \Sigma_K\}$, respectively. Obviously, $q^{\text{opt}}(\mathbf{x}_{j,k}|\mathbf{y}_{j,k})$ is in the Gaussian family of the form $\mathcal{CN}(\mathbf{U}_{j,k}\mathbf{y}_{j,k}, \Sigma_{j,k})$. Recalling that $p(\mathbf{x}_{j,k}) = \mathcal{CN}(\mathbf{0}, \mathbf{I})$, we have an alternative form of (130), given by

$$\begin{aligned} r_{j,k} &= \max_{\mathbf{U}_{j,k}, \Sigma_{j,k}} \mathbb{E} \left[\log_2 \frac{\mathcal{CN}(\mathbf{U}_{j,k}\mathbf{y}_{j,k}, \Sigma_{j,k})}{\mathcal{CN}(\mathbf{0}, \mathbf{I})} \right] \\ &= \max_{\mathbf{U}_{j,k}, \Sigma_{j,k}} \epsilon_{j,k}(\mathbf{W}, \mathbf{U}, \Sigma), \end{aligned} \quad (132)$$

where

$$\begin{aligned}
\epsilon_{j,k}(\mathbf{W}, \mathbf{U}, \boldsymbol{\Sigma}) &= \mathbb{E} \left[\log_2 \frac{\mathcal{CN}(\mathbf{U}_{j,k} \mathbf{Y}_{j,k}, \boldsymbol{\Sigma}_{j,k})}{\mathcal{CN}(\mathbf{0}, \mathbf{I})} \right] \\
&= \mathbb{E} \left[\log_2 \frac{\frac{1}{\Pi^{d_{j,k}} |\boldsymbol{\Sigma}_{j,k}|} \exp \left[-(\mathbf{x}_{j,k} - \mathbf{U}_{j,k} \mathbf{Y}_{j,k})^H \boldsymbol{\Sigma}_{j,k}^{-1} (\mathbf{x}_{j,k} - \mathbf{U}_{j,k} \mathbf{Y}_{j,k}) \right]}{\frac{1}{\Pi^{d_{j,k}} |\mathbf{I}_{d_{j,k}}|} \exp(-\mathbf{x}_{j,k}^H \mathbf{x}_{j,k})} \right] \\
&= \mathbb{E} \left[-(\mathbf{x}_{j,k} - \mathbf{U}_{j,k} \mathbf{Y}_{j,k})^H \boldsymbol{\Sigma}_{j,k}^{-1} (\mathbf{x}_{j,k} - \mathbf{U}_{j,k} \mathbf{Y}_{j,k}) \right] - \log_2 |\boldsymbol{\Sigma}_{j,k}| + d_{j,k} \\
&= -\text{Tr}(\mathbf{U}_{j,k}^H \boldsymbol{\Sigma}_{j,k}^{-1} \mathbf{U}_{j,k} \mathbf{J}_{j,k}) - \text{Tr}(\boldsymbol{\Sigma}_{j,k}^{-1}) + 2\text{Re} \{ \text{Tr}(\boldsymbol{\Sigma}_{j,k}^{-1} \mathbf{U}_{j,k} \mathbf{H}_{j,j,k} \mathbf{W}_{j,k}) \} \\
&\quad - \log_2 |\boldsymbol{\Sigma}_{j,k}| + d_{j,k} \tag{133}
\end{aligned}$$

where $\mathbf{J}_{j,k} = \mathbf{R}_{j,k} + \mathbf{H}_{j,j,k} \mathbf{W}_{j,k} \mathbf{W}_{j,k}^H \mathbf{H}_{j,j,k}^H$. It is easily known that $\epsilon_{j,k}$ is convex in each of the optimization variables \mathbf{W} , \mathbf{U} , and $\boldsymbol{\Sigma}$, Christensen *et al.* (2008) and Shi *et al.* (2011). Based on (133), we can easily obtain the optimal solutions to (132), given by

$$\mathbf{U}_{j,k}^{\text{opt}} = \mathbf{U}_{\mathbf{x}_{j,k}|\mathbf{y}_{j,k}} = \mathbf{W}_{j,k}^H \mathbf{H}_{j,j,k}^H \mathbf{J}_{j,k}^{-1}, \tag{134}$$

and

$$\boldsymbol{\Sigma}_{j,k}^{\text{opt}} = \boldsymbol{\Sigma}_{\mathbf{x}_{j,k}|\mathbf{y}_{j,k}} = \mathbf{I}_{d_{j,k}} - \mathbf{U}_{\mathbf{x}_{j,k}|\mathbf{y}_{j,k}} \mathbf{H}_{j,j,k} \mathbf{W}_{j,k}. \tag{135}$$

By substituting (132) into (125), the optimization problem (128) can be reformulated as

$$\begin{aligned}
&\max_{\mathbf{W}, \mathbf{U}, \boldsymbol{\Sigma}} \sum_j \alpha_j \frac{h_j(\mathbf{W}, \mathbf{U}, \boldsymbol{\Sigma})}{g_j(\mathbf{W})} \\
&\text{s.t.} \quad \sum_{k=1}^{I_j} \text{Tr}(\mathbf{W}_{j,k} \mathbf{W}_{j,k}^H) \leq P_j, \quad \forall j, \tag{136}
\end{aligned}$$

where

$$h_j(\mathbf{W}, \mathbf{U}, \mathbf{\Sigma}) = \sum_{k=1}^{I_j} \bar{\omega}_{j,k} \epsilon_{j,k}(\mathbf{W}, \mathbf{U}, \mathbf{\Sigma}), \quad (137a)$$

$$g_j(\mathbf{W}) = \vartheta_j \sum_{k=1}^{I_j} \text{Tr}(\mathbf{W}_{j,k} \mathbf{W}_{j,k}^H) + M_j P_c + P_0. \quad (137b)$$

In contrast to the original objective function in problem (128), the equivalent objective function in problem (136) has a more tractable form. Furthermore, for a given \mathbf{W} , it is easily shown that the optimal solutions of $\mathbf{U}_{j,k}$ and $\mathbf{\Sigma}_{j,k}$ are given by (134) and (135), respectively. Moreover, for a given \mathbf{U} and $\mathbf{\Sigma}$, the functions $h_j(\mathbf{W}, \mathbf{U}, \mathbf{\Sigma})$ and $g_j(\mathbf{W})$ are all convex functions with respect to the variable \mathbf{W} . In what follow, we show how the problem (136) has been solved by exploiting the powerful fractional programming approach. To proceed, He *et al.* (2014) has proposed that the problem (136) be rewritten into an equivalent form, given by

$$\begin{aligned} & \max_{\mathbf{W}, \mathbf{U}, \mathbf{\Sigma}, \beta} \sum_j \alpha_j \beta_j \\ \text{s.t. } & \frac{h_j(\mathbf{W}, \mathbf{U}, \mathbf{\Sigma})}{g_j(\mathbf{W})} \leq \beta_j, \quad \forall j, \\ & \sum_{k=1}^{I_j} \text{Tr}(\mathbf{W}_{j,k} \mathbf{W}_{j,k}^H) \leq P_j, \quad \forall j \end{aligned} \quad (138)$$

where $\beta = \{\beta_1, \dots, \beta_K\}$, the first inequality set denotes energy efficiency constraints, and the second inequality set denotes transmit power constraints.

Theorem 1 - If $(\bar{\mathbf{W}}, \bar{\mathbf{U}}, \bar{\mathbf{\Sigma}}, \bar{\beta})$ is the solution of problem (138), then there

exist $\bar{\lambda}$, such that $(\bar{\mathbf{W}}, \bar{\mathbf{U}}, \bar{\Sigma})$ satisfies the Karush-Kuhn-Tucker (KKT) of the following problem for $\lambda = \bar{\lambda}$ and $\beta = \bar{\beta}$.

$$\begin{aligned} \max_{\mathbf{W}, \mathbf{U}, \Sigma} \quad & \sum_{j=1}^K \lambda_j (h_j(\mathbf{W}, \mathbf{U}, \Sigma) - \beta_j g_j(\mathbf{W})) \\ \text{s.t.} \quad & \sum_{k=1}^{I_j} \text{Tr}(\mathbf{W}_{j,k} \mathbf{W}_{j,k}^H) \leq P_j, \quad \forall j, \end{aligned} \quad (139)$$

and $(\bar{\mathbf{W}}, \bar{\mathbf{U}}, \bar{\Sigma})$ also satisfies the following system equations for $\lambda = \bar{\lambda}$ and $\beta = \bar{\beta}$.

$$\lambda_j = \frac{\alpha_j}{g_j(\mathbf{W})}, \quad \forall j, \quad (140a)$$

$$\beta_j = \frac{h_j(\mathbf{W}, \mathbf{U}, \Sigma)}{g_j(\mathbf{W})}, \quad \forall j. \quad (140b)$$

On the contrary, if $(\bar{\mathbf{W}}, \bar{\mathbf{U}}, \bar{\Sigma})$ is a solution of problem (139) and satisfies system equation (140) for $\lambda = \bar{\lambda}$ and $\beta = \bar{\beta}$, $(\bar{\mathbf{W}}, \bar{\mathbf{U}}, \bar{\Sigma}, \bar{\beta})$ also satisfies the KKT conditions of problem (138) for Lagrange multiples $\lambda = \bar{\lambda}$ associated with energy efficiency constraints.

The proof of the theorem 1 is shown in appendix B. Theorem 1 means that the solution of problem (135) can be obtained by finding those solutions satisfying system equation (140) among the solutions of problem (139). Furthermore, if such a solution is unique, the solution is just the global solution of problem (135). The parameterized non-fractional form of problem (139) facilitates the solution development with an

effective approach.

5.1.3 Energy Efficient Maximization Algorithm

An iterative algorithm to solve the problem (139) is introduced in this subsection. We started investigating the solution of the problem (139) for fixed λ and β . Since the cost function of (139) is convex with respect to each of the optimization variables \mathbf{W} , \mathbf{U} , Σ , He *et al.* (2014) proposed to use the block coordinate monotonic method to solve it. Specifically, they maximize the cost function by sequentially fixing two of these three variables \mathbf{W} , \mathbf{U} , Σ and updating the third. Based on the above analysis, it is reasonable to update \mathbf{U} and Σ through their closed-form expressions given by (134) and (135), respectively. The remaining key step in finding the solution to problem (139) is the update of the beamforming matrices \mathbf{W} for fixed λ , β , \mathbf{U} and Σ . By substituting (127) and (137) into (139), the objective of (139) can be rewritten as

$$\begin{aligned}
& \sum_j \lambda_j [h_j(\mathbf{W}, \mathbf{U}, \Sigma) - \beta_j g_j(\mathbf{W})] \\
= & - \sum_{j,k} \lambda_j \bar{\omega}_{j,k} \sum_{m,n} \text{Tr}(\mathbf{W}_{m,n}^H \mathbf{H}_{m,j,k}^H \mathbf{U}_{j,k}^H \Sigma_{j,k}^{-1} \mathbf{U}_{j,k} \mathbf{H}_{m,j,k} \mathbf{W}_{m,n}) \\
& + \sum_j \lambda_j \delta_j + \sum_{j,k} \lambda_j \times [2\bar{\omega}_{j,k} \text{Re}\{\text{Tr}(\Sigma_{j,k}^{-1} \mathbf{U}_{j,k} \mathbf{H}_{j,j,k} \mathbf{W}_{j,k})\} - \beta_j \vartheta_j \text{Tr}(\mathbf{W}_{j,k} \mathbf{W}_{j,k}^H)] \\
= & \sum_{j,k} [-\text{Tr}(\mathbf{W}_{j,k}^H \Xi_j \mathbf{W}_{j,k}) - \lambda_j \beta_j \vartheta_j \text{Tr}(\mathbf{W}_{j,k} \mathbf{W}_{j,k}^H)] \\
& \times \sum_{j,k} 2\lambda_j \bar{\omega}_{j,k} \text{Re}\{\text{Tr}(\Sigma_{j,k}^{-1} \mathbf{U}_{j,k} \mathbf{H}_{j,j,k} \mathbf{W}_{j,k})\} + \sum_j \lambda_j \delta_j \tag{141}
\end{aligned}$$

where Ξ_j is calculated as

$$\Xi_j = \sum_{m,n} \lambda_m \bar{\omega}_{m,n} \mathbf{H}_{j,m,n}^H \mathbf{U}_{m,n}^H \Sigma_{m,n}^{-1} \mathbf{U}_{m,n} \mathbf{H}_{j,m}, \quad (142)$$

and δ_j is a constant and is given by

$$\begin{aligned} \delta_j = & - \sum_{k=1}^{I_j} \bar{\omega}_{j,k} \sigma_{j,k} \text{Tr} (\mathbf{U}_{j,k}^H \Sigma_{j,k}^{-1} \mathbf{U}_{j,k}) + \sum_{k=1}^{I_j} \bar{\omega}_{j,k} [-\text{Tr} (\Sigma_{j,k}^{-1}) - \log_2 |\Sigma_{j,k}| + d_{j,k}] \\ & - \beta_j (M_j P_c + P_0). \end{aligned} \quad (143)$$

It is easily known from (141) that the update of the beamforming matrix $\mathbf{W}_{j,k}$ for all User- (j, k) can be decoupled into K independent subproblems across transmitters, given by

$$\begin{aligned} \min_{\mathbf{W}_j} \sum_{k=1}^{I_j} & [\text{Tr} (\mathbf{W}_{j,k}^H \Xi_j \mathbf{W}_{j,k}) + \lambda_j \beta_j \vartheta_j \text{Tr} (\mathbf{W}_{j,k} \mathbf{W}_{j,k}^H)] \\ & - 2 \sum_{k=1}^{I_j} \lambda_j \bar{\omega}_{j,k} \text{Re} \{ \text{Tr} (\Sigma_{j,k}^{-1} \mathbf{U}_{j,k} \mathbf{H}_{j,j,k} \mathbf{W}_{j,k}) \} \\ \text{s.t.} \quad & \sum_{k=1}^{I_j} \text{Tr} (\mathbf{W}_{j,k} \mathbf{W}_{j,k}^H) \leq P_j, \quad \forall j. \end{aligned} \quad (144)$$

Introducing a Lagrange multiplier v_j to the power budget constraint of BS- j , we obtain the following Lagrange function

$$\begin{aligned} \mathcal{L}(\mathbf{W}_j, v_j) = & \sum_{k=1}^{I_j} \text{Tr} (\mathbf{W}_{j,k}^H \Xi_j \mathbf{W}_{j,k}) - 2 \sum_{k=1}^{I_j} \lambda_j \bar{\omega}_{j,k} \text{Re} \{ \text{Tr} (\Sigma_{j,k}^{-1} \mathbf{U}_{j,k} \mathbf{H}_{j,j,k} \mathbf{W}_{j,k}) \} \\ & + \sum_{k=1}^{I_j} \lambda_j \beta_j \vartheta_j \text{Tr} (\mathbf{W}_{j,k} \mathbf{W}_{j,k}^H) + v_j \left[\sum_{k=1}^{I_j} \text{Tr} (\mathbf{W}_{j,k} \mathbf{W}_{j,k}^H) - P_j \right]. \end{aligned} \quad (145)$$

The first-order optimality condition of $\mathcal{L}(\mathbf{W}_j, v_j)$ with respect to each $\mathbf{W}_{j,k}$ yields

$$\mathbf{W}_{j,k}^{\text{opt}}(v_j) = \lambda_j \bar{\omega}_{j,k} (\mathbf{\Xi}_j + \lambda_j \beta_j \vartheta_j \mathbf{I} + v_j \mathbf{I})^{-1} \mathbf{H}_{j,j,k}^H \mathbf{U}_{j,k}^H \mathbf{\Sigma}_{j,k}^{-1} \quad (146)$$

where v_j should be chosen such that the complementarity slackness condition of the power constraint is satisfied. If $\sum_{k=1}^{I_j} \text{Tr} \left[\mathbf{W}_{j,k}^{\text{opt}}(0) (\mathbf{W}_{j,k}^{\text{opt}}(0))^H \right] \leq P_j$ holds, then $\mathbf{W}_{j,k}^{\text{opt}}(0)$ is the optimal beamforming matrix. Otherwise, let $\mathbf{\Psi}_j \mathbf{\Lambda}_j \mathbf{\Psi}_j^H$ be the eigendecomposition of the matrix $\mathbf{\Xi}_j + \lambda_j \beta_j \vartheta_j \mathbf{I}$, then we have

$$\sum_{k=1}^{I_j} \text{Tr} \left[\mathbf{W}_{j,k}^{\text{opt}}(v_j) (\mathbf{W}_{j,k}^{\text{opt}}(v_j))^H \right] = \text{Tr} \left[(\mathbf{\Lambda}_j + v_j \mathbf{I})^{-2} \mathbf{\Phi}_j \right] = \sum_{n=1}^{M_j} \frac{[\mathbf{\Phi}_j]_{n,n}}{([\mathbf{\Lambda}]_{n,n} + v_j)^2} \quad (147)$$

where $\mathbf{\Phi}_j = \lambda_j^2 \mathbf{\Psi}_j^H \left(\sum_{k=1}^{I_j} \bar{\omega}_{j,k}^2 \mathbf{H}_{j,j,k}^H \mathbf{U}_{j,k}^H \mathbf{\Sigma}_{j,k}^{-2} \mathbf{U}_{j,k} \mathbf{H}_{j,j,k} \right) \mathbf{\Psi}_j$. We also note that the left-hand side of (147) is a non-increasing function in v_j for $v_j > 0$. Therefore, (147) can be easily solved by a finite-interval one-dimension search, such as bisection method, in the range of $\left[0, \sqrt{\frac{M_j \mathbf{\Phi}_j^{\max}}{P_j}} \right]$ where $\mathbf{\Phi}_j^{\max}$ is the maximum of the diagonal elements of matrix $\mathbf{\Phi}_j$. Once the optimal v_j^{opt} is obtained, the optimum beamforming matrix $\mathbf{W}_{j,k}^{\text{opt}}(v_j^{\text{opt}})$ is also attained.

Based on the above analysis, a two-layer alternating optimization algorithm is proposed to solve problem (136). In the outer layer, the auxiliary variables λ and β are updated using a Newton-like method. In the inner layer, the variables \mathbf{W} , \mathbf{U} and $\mathbf{\Sigma}$ are updated through (146), (134) and (135), respectively. The detailed steps are summarized in the Algorithm 1 where

$$\psi_j(\lambda_j) = \lambda_j g_j(\mathbf{W}) - \alpha_j, \quad \forall j, \quad (148a)$$

$$\varphi(\beta_j) = \beta_j g_j(\mathbf{W}) - h_j(\mathbf{W}, \mathbf{U}, \boldsymbol{\Sigma}), \quad \forall j, \quad (148b)$$

$$\chi_j = \frac{1}{g_j(\mathbf{W})}, \quad \forall j. \quad (148c)$$

and ρ denotes the objective value of (139).

5.1.4 Algorithm Analysis - Computational complexity analysis

It is obvious that the main computational complexity of the Algorithm 1 involves steps 2-5. Assume that $M_j = M$, $N_{j,k} = N$, $I_j = I$, $d_{j,k} = d, \forall j, k, d \leq N$ and $Id \leq \min(IN, M)$. We count the floating point operations (flops) to indicate the complexity. A flop corresponds to a real floating-point operation. Therefore a real addition, multiplication, or division is counted as one flop while a complex addition and multiplication have two flops and six flops, respectively. Similar to Golub and Loan (1996), Zhang and Lee (2008), the complexity of some basic matrix calculations are approximately counted as follows:

Multiplication of two $m \times p$ and $p \times q$ complex matrices involves $8mpq$ flops; inversion of an $m \times m$ Hermite matrix involves $\frac{4m^3}{3}$ flops; inversion of an $m \times m$ real matrix involves $\frac{2m^3}{3}$ flops; inversion of an $m \times m$ real symmetric matrix involves $\frac{m^3}{3}$ flops. Based on these references, the computational required for each active User- (j, k) is a follows:

- Inversion of $\Xi_j + \lambda_j \beta_j \vartheta_j \mathbf{I} + \nu_j \mathbf{I}$ needs about $\frac{4M^3}{3} + \frac{4d^3}{3} + 8dMKI(M + N)$ flops.

Therefore, the update of beamforming matrix $\mathbf{W}_{j,k}$ needs about $\frac{4M^3}{3} + \frac{4d^3}{3} +$

Algorithm 1 Energy Efficiency Optimization.

1: Let $n = 0$, choose $\forall \xi \in (0, 1)$, $\forall \epsilon \in (0, 1)$ and choose arbitrarily $\mathbf{W}^{(n)}$ such that it satisfies the power constraints, and compute $\mathbf{U}^{(n)}$ and $\Sigma^{(n)}$, $\rho^{(n)} = 0$. Let

$$\lambda_j^{(n)} = \frac{\alpha_j}{g_j(\mathbf{W}^{(n)})}, \forall j \quad (149a)$$

$$\beta_j^{(n)} = \frac{h_j(\mathbf{W}^{(n)}, \mathbf{U}^{(n)}, \Sigma^{(n)})}{g_j(\mathbf{W}^{(n)})}, \forall j \quad (149b)$$

2: Update \mathbf{W} with (146), $\mathbf{U}^{(n)}$, $\Sigma^{(n)}$, $\lambda^{(n)}$, and $\beta^{(n)}$, then obtain \mathbf{W}^* .

3: Update \mathbf{U} with (134) and $\mathbf{W}^{(*)}$, then obtain $\mathbf{U}^{(*)}$.

4: Update Σ with (135), $\mathbf{W}^{(*)}$, and $\mathbf{U}^{(*)}$, then obtain $\Sigma^{(*)}$.

5: Compute $\rho^{(*)}$ with $\mathbf{W}^{(*)}$, $\mathbf{U}^{(*)}$, $\Sigma^{(*)}$, $\lambda^{(n)}$, and $\beta^{(n)}$. If $|\rho^{(*)} - \rho^{(n)}| \leq \eta$, where η is a predefined threshold, then let $\mathbf{W}^{(n+1)} = \mathbf{W}^{(*)}$, $\mathbf{U}^{(n+1)} = \mathbf{U}^{(*)}$, $\Sigma^{(n+1)} = \Sigma^{(*)}$, $\rho^{(n+1)} = \rho^{(*)}$ and go to step 6, Otherwise, let $\mathbf{W}^{(n)} = \mathbf{W}^{(*)}$, $\mathbf{U}^{(n)} = \mathbf{U}^{(*)}$, $\Sigma^{(n)} = \Sigma^{(*)}$, $\rho^{(n)} = \rho^{(*)}$, and go to step 2.

6: If the following conditions are satisfied,

$$\lambda_j^{(n)} g_j(\mathbf{W}^{(n+1)}) - \alpha_j = 0, \forall j \quad (150a)$$

$$h_j(\mathbf{W}^{(n+1)}, \mathbf{U}^{(n+1)}, \Sigma^{(n+1)}) - \beta_j^{(n)} g_j(\mathbf{W}^{(n+1)}) = 0, \forall j \quad (150b)$$

then output the optimal solutions $\mathbf{W}^{(n+1)}$, $\mathbf{U}^{(n+1)}$ and $\Sigma^{(n+1)}$, and stop the algorithm. Otherwise, let $i^{(n)}$ denote the smallest integer among $i \in \{0, 1, 2, \dots\}$ satisfying

$$\begin{aligned} \sum_j \left| \psi_j \left(\lambda_j^{(n)} - \xi^i \chi_j \psi_j \left(\lambda_j^{(n)} \right) \right) \right|^2 + \sum_j \left| \varphi_j \left(\beta_j^{(n)} - \xi^i \chi_j \varphi_j \left(\beta_j^{(n)} \right) \right) \right|^2 \\ \leq (1 - \epsilon \xi^i)^2 \sum_j \left[\left| \psi_j \left(\lambda_j^{(n)} \right) \right|^2 + \left| \varphi_j \left(\beta_j^{(n)} \right) \right|^2 \right] \end{aligned} \quad (151)$$

with $\mathbf{W}^{(n+1)}$, $\mathbf{U}^{(n+1)}$, and $\Sigma^{(n+1)}$, then let $n = n + 1$ and

$$\lambda_j^{(n)} = \lambda_j^{(n-1)} - \xi^{i^{(n)}} \chi_j \psi_j \left(\lambda_j^{(n-1)} \right), \forall j \quad (152a)$$

$$\beta_j^{(n)} = \beta_j^{(n-1)} - \xi^{i^{(n)}} \chi_j \varphi_j \left(\beta_j^{(n-1)} \right), \forall j \quad (152b)$$

with $\mathbf{W}^{(n)}$, $\mathbf{U}^{(n)}$, $\Sigma^{(n)}$, and go to step 2.

$8dM(KIM + KIN + d)$ flops. We also note that matrix Ξ_j can be calculated only once for all beamforming $\mathbf{W}_{j,k}, \forall k$.

- The calculation of $\mathbf{R}_{j,k}^{-1}$ needs about $\frac{4N^3}{3} + 8dNKI(M + N)$ flops. Therefore, the calculation of $\mathbf{U}_{j,k}$ needs about $\frac{4N^3}{3} + 8dNKI(M + N) + 8dN^2$ flops.
- The calculation of $\Sigma_{j,k}$ needs about $8d^2N$ flops.
- The objective value calculation needs about $\frac{4d^3}{3} + 8dN(KIM + KIN + 3d + N)$ flops.

Therefore, one execution of steps 2-5 in Algorithm 1 takes approximately $\frac{4}{3}KI(M^3 + N^3 + d^3) + 8dK^2I^2(M + N)(M + 2N) + 8dKI(Md + 2N^2 + 3Nd) = O(37K^2I^2\tau^3)$ flops, where $\tau = \max(M, N)$.

5.1.5 Numerical analysis and assessment

The performance of the multi-cell beamforming scheme proposed by He *et al.* (2014) is investigated via numerical simulations, which we have conducted using a Matlab script that was developed in order to provide a flexible platform to assess the coordinated base station schemes. We consider a cooperative cluster of $K = 3$ hexagonal adjacent cells each consisting of one BS and multiple users. In cell j , BS j is equipped with M_j transmit antennas and serves I_j users each equipped with $N_{j,k}$ receive antennas. The cell radius is set to 500 [m] and all users are randomly distributed in the cooperative region as shown in Fig. 30. The circuit power per antenna is $P_c = 30$ [dBm], and the basic power consumed at the BS is $P_0 = 40$ [dBm], Ng *et al.* (2012). The flat fading channel matrix $\mathbf{H}_{m,j,k}$ from BS- m to User- (j, k) is generated based on the follows formulation:

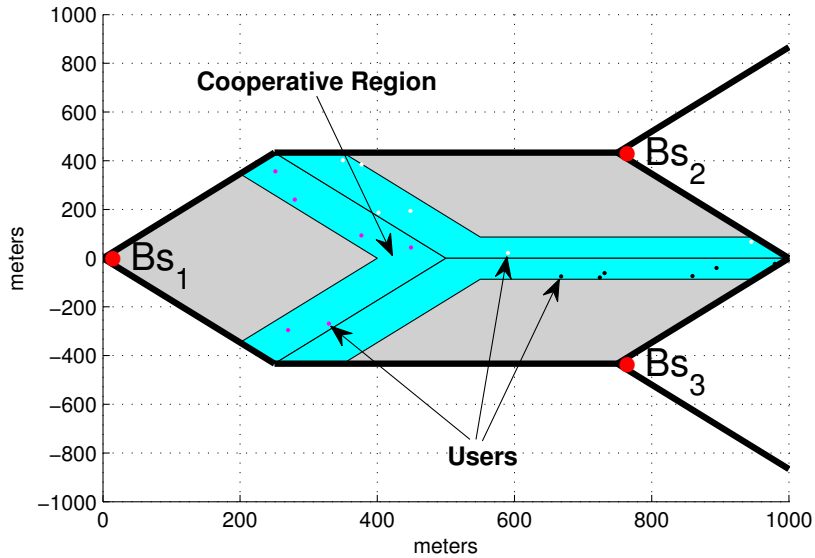


Figure 30. Simulation platform to assessment a coordinated base station scheme, with $K = 3$.

$$\mathbf{H}_{m,j,k} \triangleq \sqrt{\theta_{m,j,k}} \mathbf{H}_{m,j,k}^w \quad (153)$$

where $\mathbf{H}_{m,j,k}^w$ denotes the small scale fading channel matrix whose entries follow independently and identically Gaussian distribution with zero mean and unit covariance, $\theta_{m,j,k}$ denotes the large scale fading factor which in decibels is given by:

$$10 \log_{10} (\theta_{m,j,k}) = -38 \log_{10} (D_{m,j,k}) - 34.5 + \eta_{m,j,k} \quad (154)$$

where $D_{m,j,k}$ is the distance between the BS j associated with the cell m and the user k , and $\eta_{m,j,k}$ represents the log-normal shadow fading with zero mean and standard deviation 8 dB. The noise figure at each user terminal is 9 [dBm]. The transmit power budget is set to P for each BS and the SNR in the figures is defined as the transmit power in decibels, i.e., $\text{SNR} = 10 \log_{10}(P)$. The weighted factors $\bar{\omega}_{j,k}$, α_j and ϑ_j are unity for any j and k . The convergence threshold η is set to be 10^{-3} .

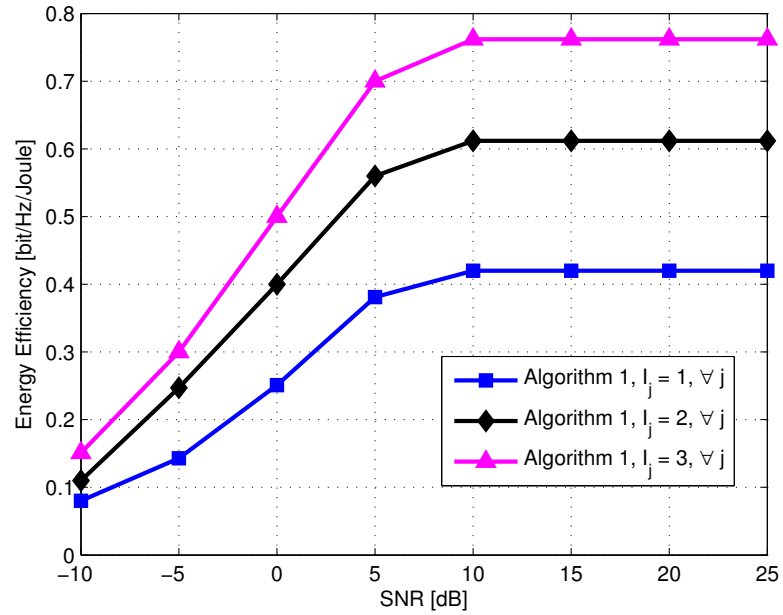


Figure 31. Energy efficiency performance of Algorithm 1, for $M_j = 4, N_{j,k} = 2, d_{j,k} = 1, \forall j, k$.

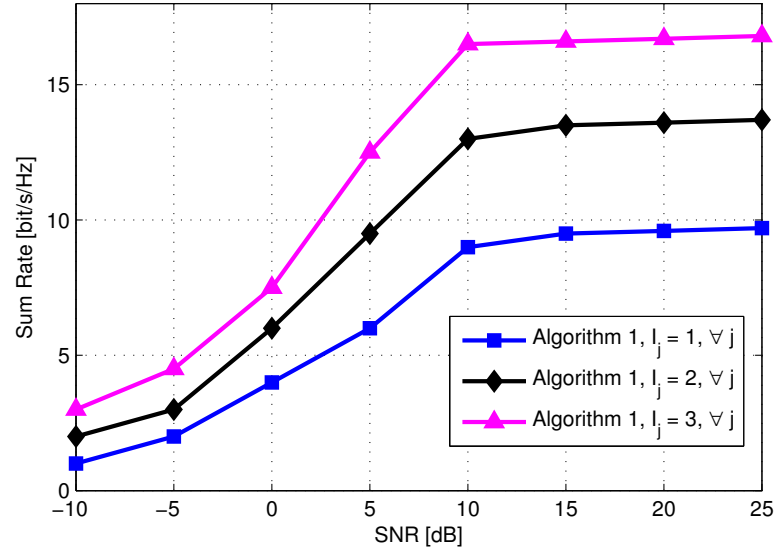


Figure 32. Sum rate performance of Algorithm 1, for $M_j = 4, N_{j,k} = 2, d_{j,k} = 1, \forall j, k$.

Fig. 31 illustrates the average energy efficiency of Algorithm 1 with different number of users, over 10000 random channel realizations. Numerical results exhibit two

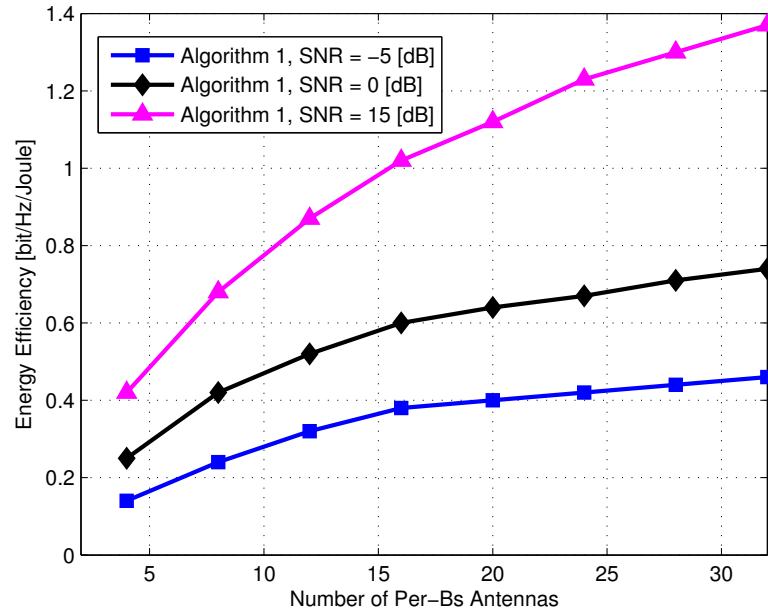


Figure 33. Energy efficiency performance of Algorithm 1, for $N_{j,k} = 2, d_{j,k} = 1, \forall j, k$.

different regions associated with the SNR levels. The first region in the low SNR regimen such as $-10 \sim 5$ [dB], in which is displayed an increasing regards to the energy efficiency, and the slope of this increase is proportional with the number of users I_j that were served. Moreover, the second or high transmit power region, shown how is remained the maximum optimal average energy efficiency, even though the SNR level is increasing. Therefore, the energy efficiency optimization algorithm is able to preserve the optimal energy consumption, but at the expense of reduce the sum rate over the entire system, as shown in Fig. 32. For this reason, is adequate establish a compromise between energy consumption and the bit rate served.

Fig. 33 shows the average energy efficiency of Algorithm 1 varying with the number of transmit antennas over 2000 random channel realizations, where the number of the served users at each BS is configured to increase with the number of transmit antennas according to a fixed ratio which is set to 1 : 4 in our simulation setting.

Numerical results corroborate that the energy efficiency increase with the number of transmit antennas. It is interesting to note that these observations are similar to the results obtained in Ngo *et al.* (2013), i.e., multiplexing to many users rather than beamforming to a single user and increasing the number of service antennas can simultaneously benefit both the spectral efficiency and the energy efficiency.

5.2 Conclusions

In this chapter, we investigated the multi-cell multi-user precoding design problem aiming at maximizing the weighted sum energy efficiency. In order to solve the non-convex problem with sum-of-ratio form, the user rate was first written into a linear optimization problem where the test conditional probabilities need to be optimized, such that the energy efficient optimization problem was transformed into a parameterized linear optimization problem, by which the solution was achieved through two-layer optimization. The effectiveness of the proposed energy efficient scheme, developed by He *et al.* (2014), was finally validated via numerical results, in which it was shown that the optimal energy efficiency and spectral efficiency can be achieved simultaneously in the low SNR region; while in the middle-high SNR region, the maximization of spectral efficiency usually cannot bring optimal energy efficiency at the same time and vice-versa. Besides, we have conducted a flexible platform to assess a future improvement to the coordinated base station proposals.

The next and final chapter is aimed to highlight the most relevant aspects regarding to the entire research thesis topics, and also defined new research horizons that involves the continuity of this work.

Conclusions and future work

This chapter is aimed to expose the highlighting contributions and conclusions of this research work, and also proposes some directions for future work.

6.1 Summary of main contributions and conclusions

The summary of contributions and conclusions is divided in two parts. First, the main contributions of antenna array design methodologies are exposed. Then, the most relevant contributions and conclusions of the interference management are shown.

6.1.1 Antenna array design

In this initial thematic, the main motivation was to explore the new paradigms to synthesis antenna arrays, specially, the antenna array design based on the antenna elements number reduction. This approach was essential to define the main objective to this research work, which is aimed to reduce the carbon footprint on the mobile cellular systems.

The most relevant conclusions associated with this part of the thesis, can be summarized as follow:

- The synthesis of antenna arrays with sparseness characteristics opens up a new line of research on the antenna design field, allowing to achieve a significant reduction on cost, size and energy consumption that involve the entire radiation system chain, own of the wireless communications systems. This three reduction factors, are able to extend their benefits to the promising massive MIMO and 3D MIMO systems, which are intended to support the highest requirements, such as the use of high number of base station antennas and the incorporation of beamformers both in elevation and azimuthal angles, to the present and future cellular systems (4G and Beyond).
- In order to contribute into the state-of-the-art on the antenna array design, our initial analysis about this thematic led us to propose a new procedure that allows to use the methodologies to synthesize linear antenna arrays with sparseness characteristics, in the synthesis of planar or two-dimensional antenna arrays. In this way, we achieved a better performance in terms of the level of reduction of the antenna elements numbers for this kind of radiation structures.
- Following with this research pathway, we try to resolve several drawbacks that involve the use of the existing methodologies, such as the complex values on the location of antenna arrays that not allows build the antenna array, which led us to develop a new methodology to synthesize antenna arrays, called hybrid sparse linear array synthesis (HSLAS). With this new methodology, we achieve to synthesize antenna arrays with antenna elements located with a purely real values. Besides, we managed to improve the current phase behavior to increase the level of sparseness.
- Although, the aforementioned proposals allows a better sparseness behavior

over the antenna array structure, the deterministic FB-MPM methodology and the Bayesian compressive sampling procedure, represent a suitable initial approach to consider when a sparse antenna array should be designed.

- Product of our numerical experiments, when the sparseness is achieved using tapering functions over the continuous excitation current function, such a Doyle-Skolnik, we have concluded that it is necessary to avoid aliasing over the excitation current for each antenna array geometry, due that the current cumulative function is sensible to this issues.

6.1.2 Interference management

The second part of this research work, was aimed to design an interference management strategy which will allowed to incorporated a energy efficiency metric on the entire cellular network. In this way, we were able to measure and control the impact of the LTE-Advanced mobile cellular networks over the global carbon footprint.

The summary of conclusions related to the interference management strategy are shown below:

- Coordinated multi-point (CoMP) transmission-reception is a promissory strategy to achieve the current cellular networks requirements. Specifically, the CoMP scheme based on coordinated beamforming (CB), allows to implement a flexible solution to both the inter-cellular interference management as well as on the maximization of the energy efficiency on the entire mobile cellular system.
- The CoMP-CB scheme has started to attract much attention due that allows the compromise between low overhead and good performance over the cellular

network.

- An important result, was the importance to define a compromise between the energy efficiency maximization and the spectral efficiency maximization, given that the latter can not be achieved when the energy constraints are imposed.
- The most relevant aspect associated with the interference management part of this thesis, represents the fact that we were able to reproduce the complete results reported by He *et al.* (2014), and we found with the primordial parameters to analyze the performance at LTE-Advanced cellular network, and the considerations to have into account for a suitable release. Besides, we have contributed with a flexible platform to assessment a future improves to the coordinated base station proposals.

As a retrospective aspect, with the concatenation of these two thesis parts, we have achieved to fulfill with the primal aim of this thesis, which was focused on the design and assessment of a coordinated precoder to manage the inter-cell interference with an approach aimed to the reduction of the energy consumption on the entire cellular network, specially, when a sparse antenna array is present at the base station.

6.2 Future research work and recommendations

After to concluding the aforementioned research activities, we have been identified several lines of future research, which are described follows:

- As a first research topic, it is proposed evaluate different geometries to synthesize antenna array with sparseness characteristics, such as circular and fractal

structures. Besides, it is necessary to define new mechanisms to compute an optimal sparse representation over this geometries.

- Another important performance metric to be considered in the next research activities, is the evaluation of mutual coupling among antenna elements.
- In order to measure the level of energy consumption over the antenna array system, is proposed a testbed able to evaluate the energy consumption per each antenna array located over the base station.
- Due that the inter-cellular interference is a relevant factor on the mobile cellular system spectral efficiency, we propose relaxed operators over the convex optimization carried out to compute the precoders that improve both, the spectral efficiency, and the energy efficiency, and in turn, they are capable of improve the time of algorithmic convergence, which is a necessary research activity.
- The level of cooperation between base stations, although not is a parameter considered in this research, opens the possibility to reduce the bandwidth required within backhaul network. For this reason, another future research is the impact evaluation of the level of cooperation between base stations over the spectral and energy efficiencies.

List of References

- Akhiezer, N. and Glazman, I. (1981). *Theory of Linear Operators in Hilbert Space*, Vol. I. Frederick Ungar Publishing Co, pages 1–36.
- Amador, L. E., Conte, R., and Covarrubias, D. H. (2009). Performance evaluation of planar antenna arrays onboard low earth orbit satellites. *International Journal of Electronics and Communications*, 64: p. 377–382.
- Andrews, J., Ganti, R., Haenggi, M., Jindal, N., and Weber, S. (2010). A primer on spatial modeling and analysis in wireless networks. *IEEE Communications Magazine*, 48(11): p. 156–163.
- Arce, A., Yepes, L. F., Covarrubias, D. H., and Panduro, M. A. (2012). A new approach in the simplification of a multiple-beam forming network based on corps using compressive arrays. *International Journal of Antennas and Propagation*, 2012: p. 8.
- Ares, F. and Moreno, E. (1990). The convolution applied on the synthesis shaped beam. *Microwave Conference, 1990. 20th European*, 2: p. 1491–1494.
- Astely, D., Dahlman, E., Fodor, G., Parkvall, S., and Sachs, J. (2013). Lte release 12 and beyond. *IEEE Communications Magazine*, 51(7): p. 154–160.
- Bae, J.-H., Kim, K.-T., and Pyo, C.-S. (2005). Design of steerable linear and planar array geometry with non-uniform spacing for side-lobe reduction. *IEICE Trans. Comm.*, E88-B(1): p. 345–357.
- Balanis, C. A. (1997). *Antenna Theory Analysis and Design*. Jhon Wiley and Sons, Inc., second edition, pages 1–941.
- Borwein, J. and Lewis, A. (2006). *Convex Analysis and Nonlinear Optimization: Theory and Examples*. Springer Verlag, New York, NY, USA, pages 1–308.
- Bucci, O. M., Isernia, T., and Morabito, A. F. (2013). An effective deterministic procedure for the synthesis of shaped beams by means of uniform-amplitude linear

- sparse arrays. *IEEE Transactions on Antennas and Propagation*, 61(1): p. 169–175.
- Bulatsyk, O. O., Katsenelenbaum, B. Z., Topolyuk, Y. P., and Voitovich, N. N. (2010). *Phase Optimization Problems: Applications in Wave Field Theory*. Wiley-VCH Verlag GmbH & Co. KGaA, pages 1–309.
- Caratelli, D. and Viganó, M. C. (2011). A novel deterministic synthesis technique for constrained sparse array design problems. *IEEE Transactions on Antennas and Propagation*, 59(11): p. 4085–4093.
- Chen, K., He, Z., and Han, C. (2006). A modified real ga for the sparse linear array synthesis with multiple constraints. *IEEE Transactions on Antennas and Propagation*, 54(7): p. 2169–2173.
- Chen, K., Yun, X., He, Z., and Han, C. (2007). Synthesis of sparse planar arrays using modified real genetic algorithm. *IEEE Transactions on Antennas and Propagation*, 55(4): p. 1067–1073.
- Christensen, S., Agrawal, R., Carvalho, E., and Cioffi, J. (2008). Weighted sum rate maximization using weighted mmse for mimo-bc beamforming design. *IEEE Transactions on Wireless Communications*, 7(12): p. 4792–4799.
- Collin, R. E. and Zucker, F. J. (1969). *Antenna Theory*. McGraw-Hill Inc.,US, pages 1–672.
- Cover, T. and Thomas, J. (1991). *Elements of Information Theory*. Wiley, New York, NY, pages 1–776.
- Dahlman, E., Parkvall, S., and Skold, J. (2011). *4G LTE/LTE-Advanced for Mobile Broadband*. Elsevier, Academic Press, pages 1–431.
- Ekbal, A. and Cioffi, J. (2005). Distributed transmit beamforming in cellular networks - a convex optimization perspective. In *IEEE International Conference on Communications (ICC'05)*.
- Elliot, R. S. (2003). *Antenna Theory & Design*. Wiley, first edition, pages 1–619.
- Feng, D., Jiang, C., Lim, G., Jr., L. C., Feng, G., and Li, G. (2013). A survey of energy-efficient wireless communications. *IEEE Communications Surveys and Tutorials*, 15(1): p. 167–178.
- Golub, G. and Loan, C. V. (1996). *Matrix Computations*. The John Hopkins University Press, Baltimore, MD, USA, pages 1–694.

- Han, C., Harrold, T., Armour, S., Krikidis, I., Videv, S. S., Grant, P., Haas, H., Thompson, J., Ku, I., Wang, C., Le, T., Nakhai, M., Zhang, J., and Hanzo, L. (2011). Green radio: Radio techniques to enable energy-efficient wireless networks. *IEEE Communications Magazine*, 49: p. 46–54.
- He, S., Huang, Y., Yang, L., and Ottersten, B. (2014). Coordinated multicell multiuser precoding for maximizing weighted sum energy efficiency. *IEEE Transactions on Signal Processing*, 62(3): p. 741–751.
- ITU (2014). Recovered of <http://www.itu.int/es/publications/pages/default.aspx>. Periodical report.
- Katsenelenbaum, B. Z. and Semenov, V. V. (1967). Synthesis of phase correctors shaping a specified field. *Radio Eng. and Electron. Phys.*, 12: p. 223–231.
- Kim, T. M., Sun, F., and Paulraj, A. J. (2013). Low-complexity mmse precoding for coordinated multipoint with per-antenna power constraint. *IEEE Signal Processing Letters*, 20(4): p. 395–398.
- Kummer, W. H. (1992). Basic array theory. *Proceedings of the IEEE*, 80(1): p. 127–140.
- Lee, B., Je, H., Shin, O., and Lee, K. (2009). A novel uplink mimo transmission scheme in a multicell environment. *IEEE Transactions on Wireless Communications*, 8(10): p. 4981–4987.
- Li, Y., Tian, Y., and Yang, C. (2014). Energy-efficient coordinated beamforming under minimal data rate constraint of each user. *IEEE Transactions on Vehicular Technology*, In Press.
- Liu, Y., Nie, Z., and Liu, Q. H. (2008). Reducing the number of elements in a linear antenna array by the matrix pencil method. *IEEE Transactions on Antennas and Propagation*, 56(9): p. 2955–2962.
- Liu, Y., Liu, Q. H., and Nie, Z. (2010). Reducing the number of elements in the synthesis of shaped-beam patterns by the forward-backward matrix pencil method. *IEEE Transactions on Antennas and Propagation*, 58(2): p. 604–608.
- Marcano, D. and Durán, F. (2000). Synthesis of antenna arrays using genetic algorithms. *IEEE Antennas and Propagation Magazine*, 42(3): p. 12–20.
- Marsch, P. and Fettweis, G. P. (2011). *Coordinated Multi-Point in Mobile Communications from Theory to practice*. Cambridge University Press, pages 1–508.
- Morabito, A., Massa, A., Rocca, P., and Isernia, T. (2012). An effective approach to the synthesis of phase-only reconfigurable linear arrays. *IEEE Transactions on Antennas and Propagation*, 60(8): p. 3622–3631.

- Ng, D., Lo, E., and Schiber, R. (2012). Energy-efficient resource allocation in ofdma systems with large numbers of base station antennas. *IEEE Transactions on Wireless Communications*, 11(9): p. 3292–3304.
- Ngo, H., Larsson, E., and Marzetta, T. (2013). Energy and spectral efficiency of very large multiuser mimo systems. *IEEE Transactions on Communication*, 61(4): p. 1436–1449.
- Oliveri, G. and Massa, A. (2011). Bayesian compressive sampling for pattern synthesis with maximally sparse non-uniform linear arrays. *IEEE Transactions on Antennas and Propagation*, 59(2): p. 467–481.
- Oliveri, G., Carlin, M., and Massa, A. (2012). Complex-weight sparse linear array synthesis by bayesian compressive sampling. *IEEE Transactions on Antennas and Propagation*, 60(5): p. 2309–2326.
- Panduro, M., Brizuela, C., Covarrubias, D. H., and López, C. (2006). A trade-off curve computation for linear antenna arrays using an evolutionary multi-objective approach. *Soft Computing Journal, Editorial Springer-Verlag*, pages 125–131.
- Prisco, G. and D’Urso, M. (2011). An effective approach for sparse arrays design with the minimum number of sensors. *Antennas and Propagation (EUCAP), Proceedings of the 5th European Conference on*, pages 1277 – 1278.
- Qiang, L., Yang, Y., Shu, F., and Gang, W. (2010). Coordinated beamforming in downlink comp transmission system. *2010 5th International ICST Conference on Communications and Networking in China (CHINACOM)*, pages 1–5.
- Rocha Alicano, C. R., Covarrubias Rosales, D. H., Brizuela Rodriguez, C. A., and Panduro Mendoza, M. A. (2007). Differential evolution algorithm applied to side-lobe level reduction on a planar array. *AEU International Journal of Electronic and Communications.*, pages 286–290.
- Sadek, M., Tarighat, A., and Sayed, A. H. (2007a). Active antenna selection in multi-user mimo communications. *IEEE Transactions on Signal Processing*, 55(4): p. 1498–1510.
- Sadek, M., Tarighat, A., and Sayed, A. H. (2007b). A leakage-based precoding scheme for downlink multi-user mimo channels. *IEEE Transactions on Wireless Communications*, 6(5): p. 1711–1721.
- Semenov, V. V. (1969). Calculation method of multilens system forming of given field. *Radiotekhnika i Elektronika*, 14: p. 1321–1323.
- Semenov, V. V. (1972). Two problems in antenna synthesis theory. *Radio Eng. and Electron. Phys.*, 17: p. 18–24.

- Shi, Q., Razaviyayn, M., Luo, Z., and He, C. (2011). An iteratively weighted mmse approach to distributed sum-utility maximization for a mimo interfering broadcast channel. *IEEE Transactions on Signal Processing*, 59(9): p. 4331–4340.
- Thiele, L., Schellmann, M., Wirth, T., and Jungnickel, V. (2008). On the value of synchronous downlink mimo-ofdma systems with linear equalizers. In *IEEE Int. Symp. on Wireless Communications Systems (ISWCS'08)*.
- Thiele, L., Schellmann, M., Wirth, T., and Jungnickel, V. (2009). Interference-aware scheduling in the synchronous cellular multi-antenna downlink. In *Vehicular Technology Conference, 2009. VTC Spring 2009. IEEE 69th*, pages 1–6, Barcelona.
- Tipping, M. E. and Faul, A. C. (2003). Fast marginal likelihood maximization for sparse bayesian models. In C. Bishop and B. Frey, editors, *Proc. 9th Int. Workshop Artificial Intelligence and Statistics*.
- Trees, H. L. V. (2002). *Optimum Array Processing Part IV of Detection, Estimation, and Modulation Theory*. Wiley-Interscience, pages 1–1472.
- Trucco, A. (1999). Thinning and weighting of large planar arrays by simulated annealing. *IEEE Transactions on Ultrasonics, ferroelectrics and Frequency control*, 46(2): p. 347–355.
- Vereecken, W., Heddeghrm, W. V., Deruyck, M., Pupe, B., Lannoo, B., Jpseph, W., Colle, D., Martens, L., and Pickavet, M. (2011). Power consumption in telecommunication networks: Overview and reduction strategies. *IEEE Communications Magazine*, 49(6): p. 62–69.
- Voitovich, N. N. and Semenov, V. V. (1968). Forming a field of prescribed structure. *Radiotekhnika i Elektronika*, 13: p. 1213–1221.
- Voitovich, N. N. and Semenov, V. V. (1970). Quasioptical lines as feeders. *Radiotekhnika i Elektronika*, 15: p. 697–704.
- Wang, X. and Zhang, X. (2010). Linear transmission for rate optimization in mimo broadcast channels. *IEEE Transactions on Wireless Communications*, 9(10): p. 3247–3257.
- Winters, J. (1984). Optimum combining in digital mobile radio with cochannel interference. *IEEE Journal on Selected Areas in Communications*, 2(4): p. 528–539.
- Xu, Z., Yang, C., Li, G. Y., Zhang, S., Chen, T., and Xu, S. (2013). Energy-efficient configuration of spatial and frequency resources in mimo-ofdma systems. *IEEE Transactions on Communication*, 61(2): p. 564–575.
- Yang, K., Zhao, Z., and Liu, Y. (2011). Synthesis of sparse planar arrays with matrix pencil method. *Computational Problem-Solving (ICCP), 2011 International Conference on*, pages 82–85.

- Yepes, L. F., Covarrubias, D. H., Alonso, M. A., and Arceo, J. G. (2013). Synthesis of two-dimensional antenna array using independent compression regions. *IEEE Transactions on Antennas and Propagation*, 61(1): p. 449–453.
- Yepes, L. F., Covarrubias, D. H., Alonso, M. A., and Arceo, J. G. (2014a). Corrections to synthesis of two-dimensional antenna array using independent compression regions. *IEEE Transactions on Antennas and Propagation*, 62(8): p. 4436.
- Yepes, L. F., Covarrubias, D. H., Alonso, M. A., and Ferrus, R. (2014b). Hybrid sparse linear array synthesis applied to phased antenna arrays. *IEEE Antennas and Wireless Propagation Letters*, 13: p. 185–188.
- Yepes, L. F., Covarrubias, D. H., Alonso, M. A., and Ferrus, R. (2014c). Hybrid sparse two-dimensional antenna array synthesis using independent compression regions. In *2014 Loughborough Antennas and Propagation Conference (LAPC)*, Burleigh Court International Conference Centre, Loughborough University, United Kingdom.
- Zhang, H., Venturino, L., Prasad, N., Li, P., Rangarajan, S., and Wang, X. (2011). Weighted sum-rate maximization in multi-cell networks via coordinated scheduling and discrete power control. *IEEE Journal on Selected Areas in Communications*, 29(6): p. 1214–1224.
- Zhang, J. and Andrews, J. (2010). Adaptive spatial intercell interference cancellation in multicell wireless networks. *IEEE Journal on Selected Areas in Communications, Special issue on Cooperative Communications in MIMO Cellular Networks*, 28: p. 1455–1468.
- Zhang, X. and Lee, J. (2008). Low complexity mimo scheduling with channel decomposition using capacity upperbound. *IEEE Transactions on Communication*, 56: p. 871–876.

Appendix A

First appendix

A.1 Sequential solver for the Maximization of $\mathcal{L}(\mathbf{a}, \sigma^2)$

The marginal likelihood maximization algorithm proposed in Tipping and Faul (2003) is hereinafter customized to deal with user-defined pattern matching problems. Starting from the knowledge of \mathbf{E}_{Ref} and Ψ , the following sequence is iteratively (r being the iteration index) applied:

1. **Initialization** ($r = 0$)– Set $[\sigma^2]^{(r)} = [\mathbf{E}_{\text{extrmRef}}] \times \sigma_0^2$ and the n -th entry of the diagonal matrix $A^{(r)} \triangleq (a_1^{(r)}, \dots, a_N^{(r)})$ as follows

$$a_n^{(r)} = \frac{\|\psi_n\|^4}{\|\psi_n^T \mathbf{E}_{\text{Ref}}\|^2 - [\sigma^2]^{(r)} \|\psi_n\|^2} \quad (155)$$

if $n = \hat{n}$ and $a_n^{(r)} = \infty$ otherwise, \hat{n} and ψ_n being randomly picked integers within $[1, N]$ and the n -th column of Ψ , respectively;

2. **Update**– Evaluate $\Sigma^{(r)} = \Sigma(A^{(r)}, [\text{sigma}^2]^{(r)})$ and $\mu^{(r)} = \mu(A^{(r)}, [\text{sigma}^2]^{(r)})$ to compute the sparsity factors $s_n^{(r)} = \psi_n^T C_{-n}^{-1} \psi_n, \forall n = 1, \dots, N$ and quality factors $z_n^{(r)} = \psi_n^T C_{-n}^{-1} \mathbf{E}_{\text{Ref}}, \forall n = 1, \dots, N$ where $C_{-n} = C - a_n^{-1} \psi_n \psi_n^T$;

3. **Candidate Basis Vector Evaluation**– Select the r –th candidate basis vector¹ ψ_n , $n = r$, and compute $\Theta_n^{(r)} = \left(z_n^{(r)}\right)^2 - s_n^{(r)}$. If $\Theta_n^{(r)} > 0$, then update the value of $a_n^{(r)}$ by means of (155), otherwise set $a_n^{(r)} = \infty$;
4. **Convergence Check**– Compute the value of $\Theta_n^{(r)} \forall n \in [1, \dots, N]$. If $\Theta_n^{(r)} \leq \tau \forall n$ (τ being the tolerance factor usually set to 10^{-8}), then terminate. Otherwise, update the iteration index ($r \leftarrow r + 1$) and go to step 2.

¹Please refer to Tipping and Faul (2003) for a review of the strategies for candidate selection.

Appendix B

Second Appendix

B.1 Proof of Theorem 1, introduced in section 5.1.3 for the energy efficiency maximization algorithm.

Introducing Lagrange multipliers $\lambda = \{\lambda_1, \dots, \lambda_K\}$ associated with energy efficiency constraint and $\zeta = \{\zeta_1, \dots, \zeta_K\}$ associated with the transmit power constraint, respectively. Thus, the Lagrange function of problem (138) is given by

$$\begin{aligned} \mathcal{L}(\mathbf{W}, \mathbf{U}, \Sigma, \beta, \lambda, \zeta) = & \sum_{j=1}^K \alpha_j \beta_j + \sum_{j=1}^K \lambda_j [h_j(\mathbf{W}, \mathbf{U}, \Sigma) - \beta_j g_j(\mathbf{W})] \\ & - \sum_{j=1}^K \zeta_j \left[\sum_{k=1}^{I_j} \text{Tr}(\mathbf{W}_{j,k} \mathbf{W}_{j,k}^H) - P_j \right]. \end{aligned} \quad (156)$$

As $(\bar{\mathbf{W}}, \bar{\mathbf{U}}, \bar{\Sigma}, \bar{\beta})$ is the solution of problem (138), there exist $\bar{\lambda}$ and $\bar{\zeta}$ such that the corresponding Karush-Kuhn-Tucker (KKT) conditions, Borwein and Lewis (2006), of problem (138) are as follows

$$\begin{aligned} \frac{\partial \mathcal{L}}{\partial \mathbf{W}} &= \sum_{j=1}^K \lambda_j [\nabla h_j(\bar{\mathbf{W}}, \bar{\mathbf{U}}, \bar{\mathbf{\Sigma}}) - \bar{\beta}_j \nabla g_j(\mathbf{W})] \\ &\quad - \sum_{j=1}^K \bar{\zeta}_j \nabla \left[\sum_{k=1}^{I_j} \text{Tr}(\bar{\mathbf{W}}_{j,k} \bar{\mathbf{W}}_{j,k}^H) - P_j \right] = 0, \end{aligned} \quad (157a)$$

$$\frac{\partial \mathcal{L}}{\partial \bar{\mathbf{U}}} = \sum_{j=1}^K \bar{\lambda}_j [\nabla h_j(\bar{\mathbf{W}}, \bar{\mathbf{U}}, \bar{\mathbf{\Sigma}}) - \bar{\beta}_j \nabla g_j(\bar{\mathbf{W}})] = 0, \quad (157b)$$

$$\frac{\partial \mathcal{L}}{\partial \bar{\mathbf{\Sigma}}} = \sum_{j=1}^K \bar{\lambda}_j [\nabla h_j(\bar{\mathbf{W}}, \bar{\mathbf{U}}, \bar{\mathbf{\Sigma}}) - \bar{\beta}_j \nabla g_j(\bar{\mathbf{W}})] = 0, \quad (157c)$$

$$\frac{\partial \mathcal{L}}{\partial \beta_j} = \alpha_j - \bar{\lambda}_j g_j(\bar{\mathbf{W}}) = 0, \quad (158)$$

$$\lambda_j \frac{\partial \mathcal{L}}{\partial \lambda_j} = \bar{\lambda}_j (h_j(\bar{\mathbf{W}}, \bar{\mathbf{U}}, \bar{\mathbf{\Sigma}}) - \bar{\beta}_j g_j(\bar{\mathbf{W}})) = 0, \quad (159)$$

$$\bar{\zeta}_j \frac{\partial \mathcal{L}}{\partial \zeta_j} = \bar{\zeta}_j \left[\sum_{k=1}^{I_j} \text{Tr}(\bar{\mathbf{W}}_{j,k} \bar{\mathbf{W}}_{j,k}^H) - P_j \right] = 0, \quad (160)$$

$$\sum_{k=1}^{I_j} \text{Tr}(\mathbf{W}_{j,k} \mathbf{W}_{j,k}^H) \leq P_j, \quad \lambda_j \geq 0, \zeta_j \geq 0, \forall j. \quad (161)$$

Since $g_j(\mathbf{W}) > 0, \forall j$ for arbitrary \mathbf{W} , (158) is equivalent to

$$\bar{\lambda}_j = \frac{\alpha_j}{g_j(\bar{\mathbf{W}})}, \quad (162)$$

and (159) is equivalent to

$$\bar{\beta}_j = \frac{h_j(\bar{\mathbf{W}}, \bar{\mathbf{U}}, \bar{\mathbf{\Sigma}})}{g_j(\bar{\mathbf{W}})}. \quad (163)$$

Moreover, the system equations (157),(160), and (161) are just the KKT conditions of the following problem for parameters $\lambda = \bar{\lambda}$ and $\beta = \bar{\beta}$.

$$\begin{aligned} & \max_{\mathbf{W}, \mathbf{U}, \Sigma} \sum_j \lambda_j [h_j(\mathbf{W}, \mathbf{U}, \Sigma) - \beta_j g_j(\mathbf{W})] \\ & \text{s.t.} \quad \sum_{k=1}^{I_j} \text{Tr}(\mathbf{W}_{j,k} \mathbf{W}_{j,k}^H) \leq P_j, \quad \forall j. \end{aligned} \quad (164)$$

Therefore, the first conclusion in Theorem 1 holds. Following a similar procedure, it is easy to prove that the contrary conclusion also holds. ■